

ALMA MATER STUDIORUM · UNIVERSITÀ DI BOLOGNA

---

SCUOLA DI INGEGNERIA E ARCHITETTURA  
Corso di Laurea in Ingegneria Aerospaziale

**Pulsed Plasma Thruster  
Ignition System:  
Investigation, Test Design and Results**

Tesi di Laurea in Sistemi Di Propulsione Avanzati LM

Relatore:  
Chiar.mo Prof.  
FABRIZIO PONTI

Presentata da:  
FEDERICO ROMEI

Correlatore:  
Chiar.mo Prof.  
STEVE GABRIEL

III Sessione  
Anno Accademico 2012/2013



*“Don't Panic.”*

– Douglas Adams, *The Hitchhiker's Guide to the Galaxy*



# Abstract

*What stops the breakdown?*

This is the question. What stops the Pulsed Plasma Thruster, PPT, Spark Plug breakdown? What is a PPT? How does the PPT spark plug work? These are the first questions to which this MSc thesis work tries to answer. Several are the parameters involved in such questions, for examples materials, spark plug geometry, erosion and deposition mechanisms on its surface exposed in the PPT discharge chamber, ignition circuit and ignition energy.

This MSc thesis is divided into three parts. In the first one, the result of a literature review on the Pulsed Plasma Thruster spark plug lifetime is exposed. Then, the basics concepts of vacuum arc science are summarized.

The second part of the work concerns the design of a test facility to investigate on some parameters which are involved in the spark plug lifetime problem. The test design includes both the electronics and the spark plug. In particular, the electronics has been the focal point of the work, trying to understand how the electronics influences the spark plug breakdown and *vice versa*. To do so, two types of ignition, or trigger, circuit have been designed, manufactured and tested. The former is the classic configuration using a switching device and a step-up coaxial pulse transformer to achieve an high voltage trigger pulse. The other one, is a transformer-less MOSFETs series circuit.

The last part shows the manufactured electronics and spark plugs. Then the spark plugs and the designed ignition circuits are tested, in air and in vacuum. The data acquired during the tests are the breakdown voltage, measured on the spark plug interior electrode with respect to the ground,

and the current, measured by means of a Rogowski coil. From these results some conclusions and future work are suggested.

# Contents

<b>Abstract</b>	<b>i</b>
<b>I Study of the Spark Plug Lifetime Problem</b>	<b>1</b>
<b>1 PPT Spark Plug Lifetime</b>	<b>3</b>
1.1 Introduction . . . . .	3
1.2 Selection of the Spark Plug Structure . . . . .	5
1.3 The Performance of Spark Plug . . . . .	7
1.3.1 Characteristic parameters . . . . .	7
1.3.2 Performance Requirements . . . . .	8
1.4 Coupling Element . . . . .	10
1.4.1 Coupling Resistance . . . . .	10
1.4.2 Coupling Inductor . . . . .	13
1.4.3 Conclusions . . . . .	13
1.5 Ignition Circuit . . . . .	14
1.6 Current Interactions . . . . .	15
1.7 Spark Plug Erosion . . . . .	15
1.8 Spark Plug Lifetime . . . . .	16
<b>2 Vacuum Arc Physics Background</b>	<b>17</b>
2.1 Plasmas and Arc Discharges . . . . .	19
2.2 Arc Ignition . . . . .	20
2.3 Cathode Spots . . . . .	22

<b>II</b>	<b>Test Design</b>	<b>25</b>
<b>3</b>	<b>Foreword</b>	<b>27</b>
<b>4</b>	<b>Spark Plug Design</b>	<b>29</b>
<b>5</b>	<b>Ignition Circuit Design</b>	<b>33</b>
5.1	Investigation of High Voltage Pulse Generators . . . . .	36
5.1.1	MOSFET Circuit . . . . .	37
5.1.2	PPT Ignition Circuit examples . . . . .	41
5.2	Ignition Circuit Design . . . . .	44
5.2.1	MOSFETs Ignition Circuit . . . . .	46
<b>III</b>	<b>Manufacturing, Testing and Modeling</b>	<b>49</b>
<b>6</b>	<b>Test Devices Manufacturing</b>	<b>51</b>
6.1	Spark Plugs . . . . .	51
6.2	MOSFETs Ignition Circuit . . . . .	53
6.3	Coaxial Transformer . . . . .	58
<b>7</b>	<b>Tests</b>	<b>63</b>
7.1	Breadboard Preliminary Tests . . . . .	63
7.2	MOSFETs Ignition Circuit - Air Tests . . . . .	68
7.2.1	MIC Attempt 1 . . . . .	68
7.2.2	MIC Attempt 2 . . . . .	72
7.2.3	MIC Attempt 3 . . . . .	74
7.3	Transformer Ignition Circuit - Air and Vacuum Tests . . . . .	80
7.3.1	MSL Spark Plug Test . . . . .	82
7.3.2	Manufactured Spark Plugs Tests . . . . .	86
<b>8</b>	<b>Semi-empirical Breakdown Model</b>	<b>95</b>
8.1	Foreword . . . . .	95
8.2	Statistical Data . . . . .	95
8.2.1	MOSFET Ignition Circuit statistics . . . . .	95
8.2.2	Transformer Ignition Circuit statistics . . . . .	96

---

8.3 RLC Series Circuit Semi-empirical Model for MIC . . . . .	99
<b>Summary and Conclusions</b>	<b>107</b>
<b>A Experimental Data and RLC Series Model</b>	<b>111</b>
A.1 Experimental Data . . . . .	111
A.2 RLC Series Modeling Examples . . . . .	142
<b>B Spark Plug Design</b>	<b>153</b>
<b>C MOSFETs Ignition Circuit Design</b>	<b>155</b>
<b>Bibliography</b>	<b>157</b>



# List of Figures

1.1	Solid propellant Pulsed Plasma Thruster configuration . . . . .	4
1.2	Typical transformer circuit configuration of a PPT ignition circuit . . . . .	9
1.3	1 – <i>mlb</i> pulsed plasma thruster discharge chamber component locations [3] . . . . .	11
1.4	Semiconductor spark plug resistance variation varying the coupling resistor value [3] . . . . .	12
1.5	Coupling current comparison [3] . . . . .	13
1.6	Effect of different closing switch device on the trigger current pulse [3] . . . . .	14
2.1	General structure of a Multi-Cathode Spot vacuum arc [5] . . . . .	18
2.2	1- <i>mlb</i> ignitor plug semiconductor [3] . . . . .	21
2.3	Hydride type trigger for ignition of vacuum arcs in a three terminal device [5] . . . . .	21
2.4	Typical Paschen curves, log-log plot, showing gas breakdown voltage versus the product of pressure and gap length, $p \cdot d$ [5] . . . . .	22
2.5	Evolution of the cathode spot process and macro particle formation as a result of plasma pressure on the liquid cathode material [14] . . . . .	23
4.1	Paschen curve to forecast the air breakdown voltage of two types of the spark plugs manufactured . . . . .	31

5.1	High peak power delivering to a resistive load, $R_L$ , with a capacitive energy storage system. The current limited high voltage source charges the capacitor over a relatively long time interval. Activating the closing switch device, the energy is quickly delivered to the load [5] . . . . .	34
5.2	Parallel-MOSFET pulse generator circuit diagram [11] . . . . .	38
5.3	Zener diodes in back-to-back configuration . . . . .	38
5.4	Series-MOSFET pulse generator circuit diagram [11] . . . . .	39
5.5	Methodology for reliable operation of stacked power MOS-FETs [8] . . . . .	40
5.6	Alternative topology for reliable operation of stacked power MOSFETs [8] . . . . .	42
5.7	Ignition circuit schematic of MDT-2A [1] . . . . .	43
5.8	EO-1 PPT Ground schematics diagram [4] . . . . .	45
5.9	Former design of a single PCB including MOSFETs Ignition Circuit and MOSFET Driver Circuit . . . . .	47
5.10	Separated MOSFETs Ignition Circuit adopted . . . . .	47
6.1	Big size spark plug manufactured SP1 . . . . .	51
6.2	Big size spark plug manufactured SP2 . . . . .	52
6.3	Big size spark plug manufactured SP3 . . . . .	52
6.4	Big size spark plug manufactured SP4 . . . . .	52
6.5	Small size spark plug manufactured SP5 . . . . .	53
6.6	Optocoupler with PCB socket . . . . .	53
6.7	MOSFET Driver Circuit PCB track . . . . .	54
6.8	MOSFET Driver Circuit PCB completed with components . . . . .	54
6.9	Sketch of spark plug crocodiles positioning on PCB . . . . .	55
6.10	Power MOSFET high voltage PCB tracks . . . . .	55
6.11	High voltage banana connectors . . . . .	56
6.12	Power MOSFETs soldered and heatsinks mounted . . . . .	56
6.13	Crocodiles connectors to ensure the SP on the PCB . . . . .	57
6.14	Coaxial transformer disassembled . . . . .	59
6.15	Secondary winding wire SWG30 . . . . .	59
6.16	Primary winding wire SWG24 . . . . .	60

6.17	Primary winding mounted over the insulated secondary winding	60
6.18	Pulse transformer completed with outer Kapton insulation . . .	61
7.1	Mosfet Driver Circuit OrCAD schematic . . . . .	63
7.2	MDC breadboard test with one STW9N150 Power MOSFET	65
7.3	MOSFET Ignition Circuit breadboard . . . . .	66
7.4	SP1 with graphite breadboard experiment . . . . .	66
7.5	SP1 surface with graphite on the Macor insulator . . . . .	67
7.6	Power MOSFET breadboard copper tracks detail . . . . .	67
7.7	MIC Experiment setup for high voltage breakdown experi- ments at TDHVL . . . . .	68
7.8	MDC output signal with: $V_1 = 23V$ , $p_w = 100ns$ and $V_{pulse} =$ $4V$ . BLUE:MDC output, ORANGE: optocoupler out . . . . .	69
7.9	Single STW9N150 Power MOSFET output signal with $HV =$ $34V$ . BLUE: HV pulse, ORANGE: MDC output . . . . .	69
7.10	5-STW9N150 Power MOSFETs output signal with $HV =$ $34V$ . BLUE:HV pulse, ORANGE: Pulse Generator . . . . .	70
7.11	MOSFET Ignition Circuit schematics . . . . .	73
7.12	MIC attempt 3 schematic . . . . .	75
7.13	DPO7254 oscilloscope <i>FastFrame</i> setup window to set the pulse width of MDC . . . . .	76
7.14	HV probes comparison on the MOSFETs Circuit output sig- nal. CH1: $V_{GS1}$ , CH2: P5122 probe, CH3: P6015A probe . .	77
7.15	SP1 breakdown with period $T = 2s$ , $HV = 3kV$ , $C_2 = 150pF$ and $p_w = 200ns$ . . . . .	78
7.16	SP2 breakdown with period $T = 2s$ , $HV = 3kV$ , $C_2 = 150pF$ and $p_w = 200ns$ . . . . .	79
7.17	MIC3 test: $HV = 3500V$ , SP2, $C'_2 = 150pF$ , $p_w = 150ns$ and $C_{13} = 0.33nF$ leading to a maximum energy $E_{max} \approx 2mJ$ . .	80
7.18	Transformer Ignition Circuit schematic . . . . .	81
7.19	Vacuum chamber used for tests (location: <i>Delta v micro HV</i> <i>4-5</i> at TDHVL) . . . . .	82
7.20	Transformer Ignition Circuit, air experiment setup. Energy storage capacitor bank of $1.2\mu F$ . . . . .	83

7.21	Transformer Ignition Circuit, vacuum experiment setup. Energy storage capacitor bank of $1.2\mu F$ . . . . .	84
7.22	The MARS SPACE LTD spark plug and thruster cathode electrodes . . . . .	85
7.23	MSL-SP air test, typical breakdown voltage, Rogowski signal and current data . . . . .	86
7.24	MSL-SP vacuum test, $V_b \approx 9000$ . . . . .	87
7.25	MSL-SP vacuum test, $V_b \approx 7300$ . . . . .	87
7.26	MSL-SP vacuum test, $V_b \approx 4000$ . . . . .	88
7.27	TIC with SP4 vacuum test, $V_b \approx -10kV$ , $I_{max} \approx 23A$ . . . . .	89
7.28	TIC with SP5 vacuum test, multiple breakdowns . . . . .	90
7.29	TIC with SP5 vacuum test, minimum $V_i$ to have breakdown . . . . .	91
7.30	TIC with SP5 vacuum test, secondary breakdown with $V_i = 200V$ . . . . .	92
8.1	RLC series circuit schematic . . . . .	100
8.2	Case of double peak current . . . . .	103
8.3	RLC series modeling: step 2 and 3 . . . . .	104
8.4	RLC series modeling step 3 and $HV$ correction . . . . .	105
A.1	<b>MIC, SP1 with graphite breakdown tests (<math>p_w = 200ns</math>)</b> . . . . .	112
A.2	<b>MIC, SP1 with graphite breakdown tests (<math>p_w = 100ns</math>)</b> . . . . .	117
A.3	<b>MIC, SP1 breakdown tests (<math>p_w = 150ns</math>)</b> . . . . .	122
A.4	<b>TIC, MSL-SP breakdown tests in air</b> . . . . .	127
A.5	<b>TIC, MSL-SP breakdown tests in vacuum</b> . . . . .	129
A.6	<b>TIC, SP1 breakdown tests in air</b> . . . . .	131
A.7	<b>TIC, SP1 breakdown tests in vacuum</b> . . . . .	133
A.8	<b>TIC, SP4 breakdown tests in air</b> . . . . .	135
A.9	<b>TIC, SP4 breakdown tests in vacuum</b> . . . . .	137
A.10	<b>TIC, SP5 breakdown tests in air</b> . . . . .	138
A.11	<b>TIC, SP5 breakdown tests in vacuum</b> . . . . .	140
A.12	<b>RLC series modeling of spark plug breakdown for MIC, <math>HV = 1kV</math></b> . . . . .	143

---

A.13 RLC series modeling of spark plug breakdown for MIC, $HV = 2.5kV$ . . . . .	148
A.14 RLC series modeling of spark plug breakdown for MIC, $HV = 3.5kV$ . . . . .	151



# List of Tables

5.1	Absolute maximum ratings of the N-channel power MOSFET selected . . . . .	46
7.1	MOSFETs Ignition Circuit, MIC, breadboard earlier experiment	65
7.2	Summarizing table of manufactured spark plugs breakdown voltage . . . . .	91
8.1	SP1 MIC tests, average and standard deviation of $I_{max}$ and $dI/dt_{max}$ . . . . .	97
8.2	MSL-SP TIC tests, average and standard deviation of $V_B$ , $I_{max}$ and $dI/dt_{max}$ . . . . .	97
8.3	SP1 TIC tests, average and standard deviation of $V_B$ , $I_{max}$ and $dI/dt_{max}$ . . . . .	97
8.4	SP4 TIC tests, average and standard deviation of $V_B$ , $I_{max}$ and $dI/dt_{max}$ . . . . .	97
8.5	SP5 TIC tests, average and standard deviation of $V_B$ , $I_{max}$ and $dI/dt_{max}$ . . . . .	98
8.6	Comparison of breakdown voltage predictions made through the Paschen curve and Boxman et al. observation in VAST . .	108



## Part I

# Study of the Spark Plug Lifetime Problem



# Chapter 1

## PPT Spark Plug Lifetime

### 1.1 Introduction

In a Pulsed Plasma Thruster the ignition system is generally composed by a spark plug (1.1). It is mounted in the thruster's cathode into the discharge chamber. The spark plug is driven by an ignition, or trigger, circuit which gives a fast risetime voltage pulse and then allows a spark to form between the electrodes of plug. The result of the arc breakdown between the plug's electrodes, is the production of a plasma puff. This one initiates the discharge of the *main capacitor*, which provides the energy to produce the thrust, by forming an arc discharge between the thruster's *cathode* and *anode* electrodes. This arc is self-sustained by the ablation and ionization of the *solid propellant* bar until the energy storage capacitor has been totally discharged. The electromagnetic body forces, described by the Lorentz force and created by the closing circuit *discharging current*, accelerates the *plasma* layer with exhaust velocities that can reach  $50,000m/s$ . A Pulsed Plasma Thruster typically has an arc discharge pulse length on the order of  $10\text{-}\mu s$ , a spark plug trigger circuit pulse width on the order of  $1\text{-}\mu s$ , a lifetime of  $10^7$  pulses, yielding to a total impulse on the order of  $100,000Ns$ .

For its role, the spark plug is a critical component, which affects the operation of the thruster. The spark plug is the fundamental element, with its ignition circuit, that forms the *ignition system* of the PPT. For this reason, to understand the spark plug lifetime problem, an investigation on

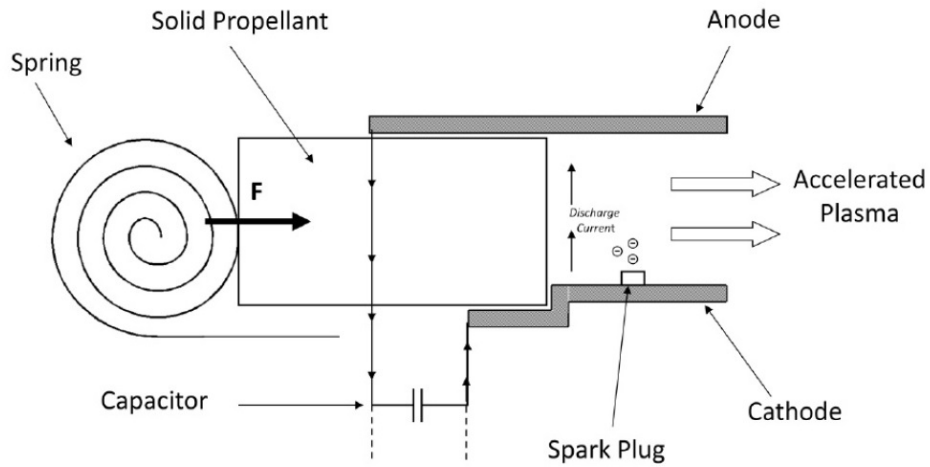


Figure 1.1: Solid propellant Pulsed Plasma Thruster configuration

the whole ignition subsystem of the PPT is essential.

As the spark plug is part of a spacecraft, it must satisfy some essential requirements. It has to be able to work reliably in the space environment, such as vacuum and radiation, and into the thruster environment as well. Considering its location into the thruster's cathode, for instance into the discharge chamber, its end-surface will operate at the same temperature of the main cathode and it will be contaminated by the propellant ablated products. These contaminating products, which deposit on the spark plug end-surface, and the repeated effect of heat and electricity change its conducting characteristics, eventually degrading the spark plug performance.

Differently from an automobile engine spark plug, which serves to ignite the fuel-air mixture, the PPT spark plug is used to initiate the main vacuum electric discharge of this thruster. Furthermore it has to operate during the entire lifetime of the spacecraft engine without any maintenance. Therefore, to work reliably during its lifetime, it should have abilities of anti-contamination and anti-erosion.

Parameters that affect the lifetime are discussed in the following sections. They are: spark plug structure, resistance between electrodes and breakdown voltage; surface deposition and erosion; electrical coupling between plug's and thruster's cathodes; last but not least, the ignition circuit characteristics.

For the many variables involved, it is clear that a total analysis of the problem would involve necessarily the testing of the spark plug mounted into the thruster and to produce a big amount of sparks for every change of the above mentioned parameters.

## 1.2 Selection of the Spark Plug Structure

Considering a coaxial spark plug, the possible geometries can be summarized as following:

**Gap type:** This is the kind of spark plug commonly used in a internal combustion engine. Typically such spark plug has a central electrode, electrically isolated from a metal threaded shell by a porcelain insulator. The central electrode is connected by an insulated wire to the output terminal of an ignition coil. Generally the breakdown voltage of this spark plug is very high, especially considering the purpose to use it in vacuum environment. The MDT thruster research group has tested this geometry using a tungsten wire for the inner electrode. Their conclusion is that this geometry is not suitable for space application, in fact to generate the high voltage pulses required, the ignition circuit would be too heavy.

**Surface Discharge type:** The idea of this configuration, is to produce the spark on the end-surface of the spark plug. For instance the two electrode are separated by the means of an insulator, that can be for example alumina ceramic. In a vacuum environment the spark produced between the two electrodes will certainly pass over the insulator ring-surface.

Xue-Zhang and Han-Ji [19] observed that the still high breakdown voltage of a *surface discharge spark plug*, but lower than the *gap type* one, can be beyond lowered treating the insulator ring-surface with carbon powder using a pencil. This particular semiconductor material decreases the insulation resistance of the spark plug surface, so that the breakdown voltage. Of course by applying the material by means of a pencil, that layer easily burn off the surface. Because of the spark plug

ability to exclude contamination spark by spark, and because of the deposition process of the propellant products on its surface, to reach a good equilibrium between these two phenomena is not a trivial task.

**Semiconductor Type:** A strengthened spark plug geometry, commonly used for PPT applications, is the *semiconductor spark plug* type, where the semiconductor layer is applied on the insulator using the *cathodic arc deposition* technology. The key to establish an equilibrium between the above mentioned phenomena, is the choice of the semiconductor coating material and the layer thickness. This configuration allows to reach attractive breakdown voltage on the order of  $10^2 - 10^3$ -V. Moreover, if the spark plug quality of the finish is high, then the breakdown voltage is independent on the pressure around it. The requirements for the ignition circuit are suitable for space applications.

Some important parameters affect the spark plug performance rather than the PPT performances:

- Influence of the spark plug diameter on its performance:

During the MDT spark plug selection, it was found that a bigger exterior diameter, of the external electrode, could improve the fashion of the ablated solid propellant profile, due to the increased moving area of the main discharge arc. It was also found that a proportionally bigger diameter of the center electrode, could mitigate the erosion of the same, slowing the breakdown voltage growth during the spark plug lifetime. The conclusion of this study led to select a large spark plug, in order to optimize the fashion of the ablated propellant area, and to use a large diameter for the center electrode with the purpose to mitigate the erosion of the same, improving the spark plug lifetime.

- Structure of the semiconductor layer:

In [19] they tested two different configuration of the semiconductor layer: a fully coated insulator and a grooved-type spark plug. The tests on this two configurations, showed that a fully coated configuration has up to the double lifetime, because the other

type of spark plug has little ability to contrast the solid propellant material deposition.

- End-surface structure:

Tests showed that the best configuration in terms of lifetime, is a flat-end surface. Some tests using a concave-end surface plug, where the end insulator surface coated with semiconductor material is rearward in respect to the electrodes, showed that this plug configuration accumulate easily deposit, obtaining a shorter lifetime.

For the reasons showed in this section, the best PPT coaxial spark plug structure has a flat-end surface, with a fully coated insulator with semiconductor and with a large center electrode.

## 1.3 The Performance of Spark Plug

### 1.3.1 Characteristic parameters

The main parameters that characterize the performances of spark plug are the following:

1. Resistance;
2. Breakdown voltage  $V_B$ ;
3. Lifetime of spark plug.

The resistance of a spark plug includes two parts: the resistance  $R_e$  between the electrodes, and the resistance  $R_s$  of the semiconductor layer. Because of the semiconductor negative temperature effect, such as the  $R_s$  decreases as the temperature increases,  $R_s$  depends on the temperature and obviously on the material. The relation between  $R_s$  and the temperature  $T$  is the following:

$$R_s(T) = R_{s0} \cdot e^{-b(T-T_0)}$$

where  $R_{s0}$  is the resistance of the semiconductor material when the temperature is equal to  $T_0$  and  $b$  is a temperature coefficient of the semiconductor material.

$R_e$  is dependent on the quality of the finish and on the assembly accuracy, which is characterized by the following formula:

$$A = R_{a0} - R_a$$

where,  $R_a$  is the resistance at normal temperature and in atmosphere, whilst  $R_{a0}$  is the plug resistance at normal temperature and in vacuum condition. The purpose is to minimize  $A$  in order to maximize the assembly accuracy. The spark plug lifetime is defined as the numbers of PPT main discharges that can be fired continuously by firing the plug.

### 1.3.2 Performance Requirements

In a Pulsed Plasma Thruster the performance parameters of the ignition circuit, and consequently of the spark plug, can be listed as follows.

#### 1. Breakdown Voltage $V_B$

The selection of the maximum spark plug breakdown voltage,  $V_B$ , follows from the particular ignition circuit used. The typical electric configuration of this one, see figure 1.2, uses a step-up transformer with a winding ratio of  $1 : n$ , in order to multiply by  $n$  the input voltage  $V_1$ . The closing switch,  $SW$ , showed in the schematics, is a device that can realize very fast operation in order to release the energy, which is stored into the capacitor  $C_1$  at voltage  $V_1$ , in the shortest time interval as possible. In the section 5.1 (p.36), the main categories of high voltage pulse generators will be discussed, in order to find out the most suitable configurations to realize and test.

The breakdown voltage of the spark plug has a maximum,  $V_{B,max}$ , and a minimum value,  $V_{B,min}$ . The minimum is defined by the smallest amount of energy necessary to initiate reliably the thruster discharge between the main electrodes. Therefore this value depends on the thruster electrode configuration and dimensions. In general, the same

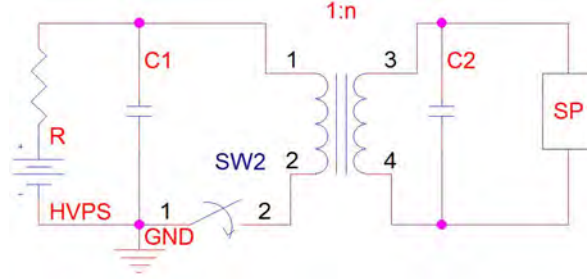


Figure 1.2: Typical transformer circuit configuration of a PPT ignition circuit

amount of energy can be delivered by the spark plug with smaller pulse width, but with higher current. In particular, the pulse energy  $\epsilon_{pulse}$  is defined as:

$$\epsilon_{pulse} = \int_0^T v(t)i(t)dt \quad (1.1)$$

Where,  $i(t)$  is the current pulse,  $v(t)$  is the voltage pulse and  $T$  the pulse period. These considerations, concerning the ignition circuit design, will be discussed in section 5.1. The minimum breakdown voltage should be defined in vacuum condition and at normal temperature. Finally, the maximum breakdown voltage can be estimated starting from the ignition circuit maximum output voltage. Considering a safety margin from that value,  $V_{B,max}$  can be fixed.

## 2. Semiconductor Resistance $R_s$

In the next section 1.4, the relationship between the carbonaceous deposit amount on the plug surface and the semiconductor resistance will be highlighted. The semiconductor resistance, a surface resistance, is measured by using a constant low DC current, on the order of  $100\text{-}\mu\text{A}$ , with a resistance measuring circuit. The current should be low because it can heat significantly the thin semiconductor layer, with a thickness on the order of  $100\text{ }\mu\text{m}$ .

## 3. Spark Plug Resistance $R_{a0}$

The breakdown voltage is related to the resistance value of the plug at the normal temperature and in vacuum condition  $R_{a0}$ . In particular, the higher the plug resistance, the higher the breakdown voltage. To increase the ability of the plug surface to exclude contamination,  $R_{a0}$  should be taken as high as possible.

#### 4. Lifetime

Depending on the PPT thruster mission requirement, the spark plug lifetime requirement is defined. A typical value is between  $10^6$  and  $10^7$  discharges. Of course it should be as high as possible because, as already mentioned, the spark plug is, in general, one of the most critical component in a PPT.

### 1.4 Coupling Element

Aston and Pless 3 found an important link between the connection of the spark plug and the thruster cathodes and the spark plug lifetime, using a coupling element (see Fig.1.3). In particular they studied the behavior of two coupling elements: resistor and inductor. They started their work noticing that the plug suffered severe erosion when it was slot into the thruster cathode, thus with thruster and plug cathodes directly connected together. By that observation, they tested the spark plug behavior with the above mentioned coupling elements. The spark plug was insulated from the thruster cathode by a little vacuum gap, less than 1-*mm*.

#### 1.4.1 Coupling Resistance

Due to the solid propellant depolymerization products, a certain amount of carbonaceous deposits accumulate on the plug surface. This is unavoidable, but for a reliable spark plug operation the deposit should not be too much or too low. In particular, with too low deposit the ignition firing leads to excessive plug wear. Conversely, too much deposit behave like a low impedance in parallel with the semiconductor ring, eventually it can be sufficiently thick and conducting to short the spark plug semiconductor element and thus leading to misfire.

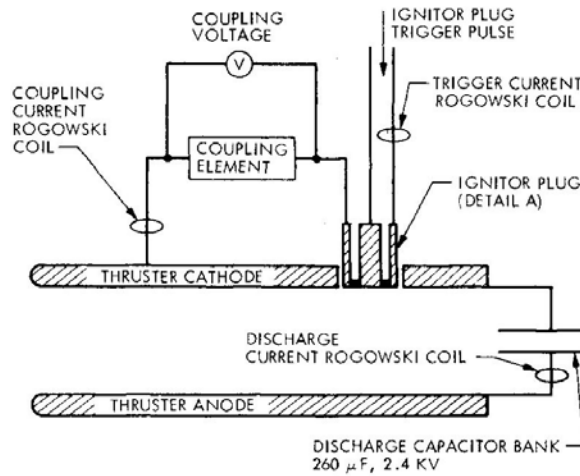


Figure 1.3: 1 – *mlb* pulsed plasma thruster discharge chamber component locations [3]

The plug deposition amount is affected by the value of the coupling resistor used to electrically couple the cathodes (Fig.1.3). The parameter that is most representative of the deposit amount on the plug face, is the semiconductor resistance  $R_s$ . Fig.1.4 shows that a smaller value of the coupling resistance has a negative effect on the plug operation. In the test showed, the plug misfiring became to happen when the semiconductor resistance reached about  $1.5 \Omega$ . The plug deposit increases with the number of thruster pulses. At the same time, a weak erosion of the plug anode is observed.

A lower value of the coupling resistance gives a larger value of the coupling current during the pulse operation. It is possible to measure this value using a Rogowski coil as indicated in Fig.1.3. The largest current value is obtained using a shorting wire to connect the cathodes. For these reasons, the hypothesis is that larger currents, and thus larger arc attachments to the plug surface, is the mechanism by which the ablated propellant products deposit on the plug surface. It is remarkable the fact that the coupling peak current on the resistor isn't proportional to its value. To reduce the peak current of one order, the resistance could be four order bigger (Fig.1.5).

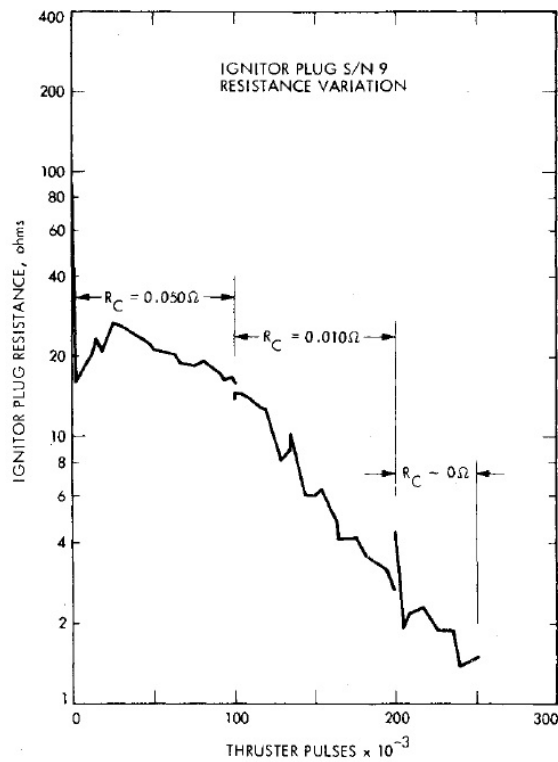


Figure 1.4: Semiconductor spark plug resistance variation varying the coupling resistor value [3]

### 1.4.2 Coupling Inductor

In order to limit the coupling current, an inductance elements can be also used. The test made by Aston and Pless, represent an example (Fig.1.5). The charging time of the inductor has a damping effect on the current. A spark plug lifetime test would show that the semiconductor resistance,  $R_s$ , would keep almost a constant value when using an inductor coupling. On the contrary a resistive coupling would reduce dramatically the resistance to reach a lower resistance value with respect of that one of the brand-new plug. Finally, the coupling inductance value and peak current have a hyperbolic relationship that can be experimentally evaluated. This means that, above a certain inductance value, the reduction of the coupling peak current is negligible.

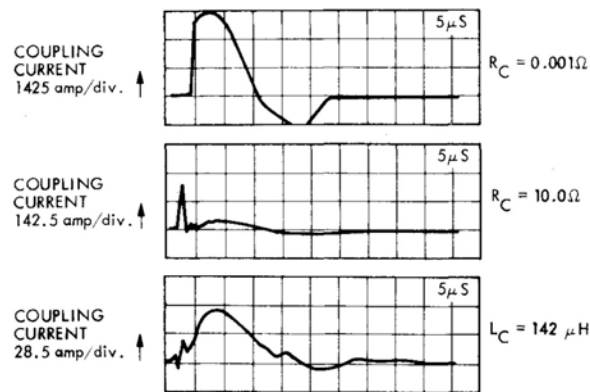


Figure 1.5: Coupling current comparison [3]

### 1.4.3 Conclusions

The inductive coupling of the spark plug and thruster electrodes, has a beneficial effect on the spark plug lifetime. The parameter to highlight that is the plug semiconductor resistance,  $R_s$ , which remain around a constant value. In particular, the inductance limits the coupling current peak and, at the same time as an effect, it significantly limits the carbonaceous deposit on the plug face.

## 1.5 Ignition Circuit

In section 5.1, the available and most important circuitry solution to produce high voltage pulses will be discussed. The aim of studying the possible solutions, has been to understand the functioning of a classical transformer-based circuit and to investigate on possible new solutions.

For what concerns the spark plug lifetime, the ignition circuit strongly affects it, and together with the spark plug characteristics, it defines the ignition system goodness. Especially, a lower voltage and higher current trigger pulse, thus keeping constant the energy, contributes to the reduction of plug deposition.

The important conclusion exposed above has been verified experimentally by comparing different trigger circuit to fire the spark plug and producing the main thruster discharge [3]. Adopting a trigger circuit composed by a 1.5 : 1 step-down 400V output pulse transformer, instead of a 3:1 step-up with 1800V output pulse transformer, the trigger circuit current increased significantly with a corresponding reduction of carbonaceous deposit. If the energy provided to the spark plug is constant, by increasing the switching speed and reducing the pulse length, the current must increase. In the case of the transformer-based circuit the pulse width depends on the transformer itself and on the closing switching device. An example is given by Fig.1.6.

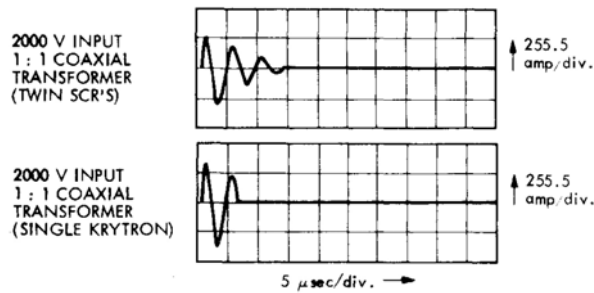


Figure 1.6: Effect of different closing switch device on the trigger current pulse [3]

For these reasons, a trigger circuit that provides a pulse length on the same order of the main thruster discharge, is to avoid. To minimize the contribution of the trigger current, concerning the plug surface deposit problem,

corresponds to minimize its pulse length.

## 1.6 Current Interactions

It has been observed that the coupling current, both with the coupling resistor or inductor, reaches very large values. Too large to be sustained by the ignition circuit energy capacitor. For this reason, it follows that the energy must come from the thruster energy storage capacitors. This means that, immediately after the plug ignition, the plasma puff created, or micro-plasma, creates a low impedance path between the cathodes. In fact the voltage drop across the coupling element is next to the energy storage capacitor voltage of the thruster. At a later stage, when the main discharge between the thruster electrodes occurs, the coupling voltage falls to zero. The explanation is that the plasma suddenly creates a shorting path between the plug and thruster cathodes.

The phenomena described shortly above, means that, if the trigger circuit pulse lasts further the thruster discharge starting, a current path will connect the plug anode with the thruster cathode. To limit this phenomenon, a short-pulse-length trigger circuit and an inductance coupling are the solutions to opt for.

## 1.7 Spark Plug Erosion

The erosion mechanisms that can be observed on the spark plug surface are, in order of importance: the *embrittlement*; the erosion due to the normal *plasma sputter erosion* processes; the amount of erosion by plug *vaporization* caused by the trigger circuit pulse. The former and most important erosion mechanism, is directly related to the amount of deposit located on the plug surface. This fact can be easily proven removing the deposit on the plug surface and observing that the embrittlement occurs mainly where the deposit layer is thicker. Most of deposit occurs on the cathode ring surface.

Finally, it has to be observed that a certain amount of deposit can prevent most of the damage caused by the trigger circuit current. In fact, if the semiconductor spark plug is tested alone in vacuum, higher erosion on the

anode would be observed and large amounts of cathode and semiconductor material would vaporize and be removed.

## 1.8 Spark Plug Lifetime

Once the spark plug structure and the ignition system have been selected, it is necessary to test the lifetime. Firstly the spark plugs selection process should happen. In fact, to manufacture a perfect coaxial semiconductor spark plug is challenging. Once they have been produced, it should be checked that they meet the requirements defined in section 1.2. Finally, through accumulative or/and accelerated lifetime tests, they can be qualified.

## Chapter 2

# Vacuum Arc Physics

## Background

The electric arc is defined as “*discharge of electricity between two electrodes in a gas or vapor that has a voltage drop at the cathode of the order of the minimum ionizing or exciting potential of the gas or vapor*”. In general, the arc is self-sustained and supports large current, on the order of  $kA$ , by the electron emission mechanism from the negative electrode.

Into the vacuum environment, the vacuum arc is defined instead as “*high current, low voltage electrical discharge between two electrodes situated in vacuum environment. Vacuum itself cannot support a high current discharge at low voltage*”. Hence, a medium is required to perform the vacuum arc. This medium is a highly ionized plasma produced by electrode material vaporization, and caused by the interaction between the plasma itself and the electrode. By this observation, the proper description would be “metal vapor arc in vacuum”, while it is commonly called *vacuum arc*.

The production of plasma comes from the *cathode spots*. They are highly luminous and tiny region on the cathode, which represent the most studied aspect of vacuum arc. They are responsible to provide the conducting medium in form of metal vapor and they provide the electron flow. Thanks to their small dimensions, even a small arc current can create extremely high local temperature and electric field that provide the condition for plasma and electron production. The metal vapor produced by the cathode is almost

fully ionized and it contains different ionized species.

The ions kinetic energy is around  $80 - 150eV$  even with  $20V$  voltage. The plasma flow velocity is on the order of  $10km/s$  with direction outward the cathode spots. The ion current plasma is only 10% of the arc current, while the rest is given by the electron flow.

The cathode plasma jets originated from the cathode spots, expand in all the directions. As a consequence a fraction of plasma reaches the anode electrode (Fig.2.1). It follows an electron flowing from the cathode to the anode, faster than the ion current, which has same charge density and direction. Plasma flow and current flux are subjected to magnetic fields that is either self-produced by the arc current or imposed externally. If the ion and electron flux heats the anode sufficiently, the anode can become a source of plasma by vaporization or anode spot formation.

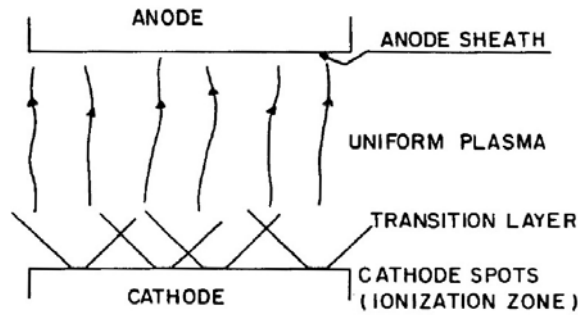


Figure 2.1: General structure of a Multi-Cathode Spot vacuum arc [5]

The properties of vacuum arc are used in several technological applications. While the vacuum is a good insulator, the metal vapor plasma and the metal arc electrodes are good conductors. Conduction can be initiated essentially in two ways: by *switch opening* and *switch closing* techniques. The former is more challenging to realize. The main issue is that, when high current is established between two electrodes in vacuum, when they are separated that current generates an arc and consequently a conducting plasma. This arc therefore continues the current flowing. To stop the arc, the current must reach momentarily zero.

The thermal time constant of cathode spots is extremely short, on the order of  $ns$ , while, because of the plasma velocity, the time required for the

plasma to reach a cool surface, where it condenses, is on the order of  $\mu s$ .

The vacuum arc production of large amount of electrode material, is a fact used in a series of technological application. In particular in metallurgical processes like the vacuum arc melting or vacuum arc degassing. But the most important application in the case of the PPT spark plug, is the coating, mentioned in section 1.2. It is obtained starting from the vacuum arc and using the metal vapor plasma flux produced, which condenses on the target cool surface to coat it.

Vacuum arc physics is a complicated field to study experimentally. The phenomena are complex e dynamically correlated and several are the unknown behavior still to understand. Anyway it was right and proper to develop a basic knowledge of vacuum arc science, at least to develop a global idea on what might happen on a spark plug surface for pulsed plasma thruster. The main reference of this chapter is [5] (Boxman et al., 1995).

## 2.1 Plasmas and Arc Discharges

An *electrical discharge* is the passage of current through a medium or an insulator. The *breakdown* happens when the insulator changes state to become conductor. This happens when sufficient high voltage or an electrical field is applied. A fraction of atoms of the medium is ionized and forms a plasma, of which the electrical current is established primarily by free electron movements and, secondly, by ions movement. The vacuum arc is self-sustained by the processes involved in the passage of electrical current and maintains the insulator in conducting state.

The processes involved in plasma and electric discharges, are the collision processes, the collective behavior, the conduction of electrical current, the magnetic effects and the electrode effects.

The motion of electrons is limited by collisions with ions and atoms. Some of them may ionize the atoms, the fundamental fact that maintain fraction of plasma ionized contrasting the losses. The collective behavior leads to concentration of charged particles, which, with their motion, cause electrical and magnetic fields. These fields influence the characteristic of plasma, such as concentration and motion. The plasma results to be neu-

tral as a consequence of the collective behavior. In particular, unbalanced positive and negative charges create an electric field, which put back the plasma in the neutrality condition. In particular, the magnetic fields confine the flow of electric current in perpendicular direction, making it responsible of the plasma macroscopic motion. Some neutral metal atoms are emitted by the electrodes sputtering or evaporation. The cathode spots supplies the rest of discharge providing electron current, which is approximately the 90% of the circuit current.

## 2.2 Arc Ignition

The metal vapor discharge can develop into an arc only if the external circuit resistance is sufficiently low. A variety of methods are adopted to initiate an arc: breakdown-to-arc transition; laser ignition; hollow cathode arc; arc ignition from low voltage sources. The latter considers low voltage the 50V to 200V range and it is capable to maintain several amperes of current needed to hold the arc. Ignition from low voltage can be achieved in several ways, one of which is the triggered arc. Each one of these methods is a mechanism to develop a stable cathode spot. Spark plug in a PPT is an example of triggered arc ignition.

As already described in section 1.2, the spark plug insulator can be coated with a semiconductor in order to increase the lifetime and, in particular, to reduce its breakdown voltage 2.2. Several references report the use of coating material on the spark plug insulator both in experimental work and in flight qualified PPT, such as LES series and MDT-2A [7, 2, 12, 5, 19, 6, 1, 3, 10, 18]. However in most cases the authors don't specify the material used, in the other cases they give some indications. Moreover, varying the coating, the PPT spark plug performances change widely, for example the breakdown voltage: between 200V and 300V in [18]; approximately 300V in [3]; between 100V and 500V in [6]; between 1000V and 2600V in [19]; between 1kV and 10kV in [13]. In addition also the erosion mechanism (section 1.7) varies with the coating material and deposition process parameters.

In [5], the Titanium hydride coating is suggested for the triggered arc ignition system shown in Fig.2.3. The main advantage to use this material is

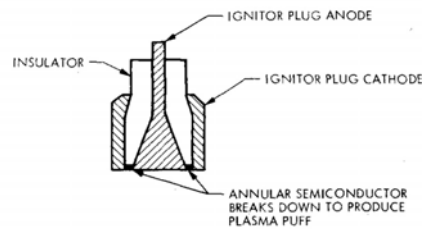


Figure 2.2: 1-mlb ignitor plug semiconductor [3]

that it releases gas that allows triggering at lower power. When the tube is newly, the breakdown voltage initially required is about  $1kV$ , but the breakdown voltage stabilizes at  $100V-500V$  after subsequent use. In [10], a similar device with Alumina as insulator and coated with a Mn/Ti alloy, has been tested in vacuum. This inorganic ceramic coating decreases the Alumina resistivity and, at the same time, the combination of this two elements allows a good penetration of the coating. This fact increases the insulator lifetime and protect it from the abrasion mechanism.

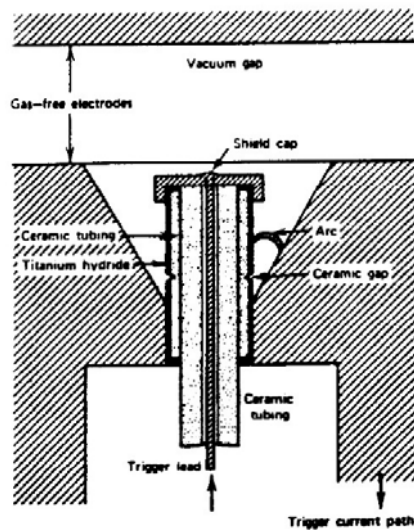


Figure 2.3: Hydride type trigger for ignition of vacuum arcs in a three terminal device [5]

Finally, a brief note on the *Paschen's Law* is necessary. This equation was formulated by Friedrich Paschen who discovered it empirically in 1889. This equation gives the breakdown voltage of two electrodes in a gas as a func-

tion of pressure,  $p$ , and gap length,  $d$ . Fig.2.4 shows typical Paschen curves assuming a uniform electric field (obtained with parallel metal plates), showing gas breakdown voltage versus the pressure and gap length product,  $p \cdot d$ . For example in air, with atmospheric pressure and  $1\text{cm}$  gap, the breakdown occurs at about  $30\text{kV}$ . Since the breakdown is a function of the product  $p \cdot d$ , the same value can be obtained with double the gap and half the pressure, or the contrary. The interesting fact is that, given a gas, there is a minimum breakdown voltage possible, above which it increases with the product  $p \cdot d$ , and below of which it increases with the reduction of the product  $p \cdot d$ .

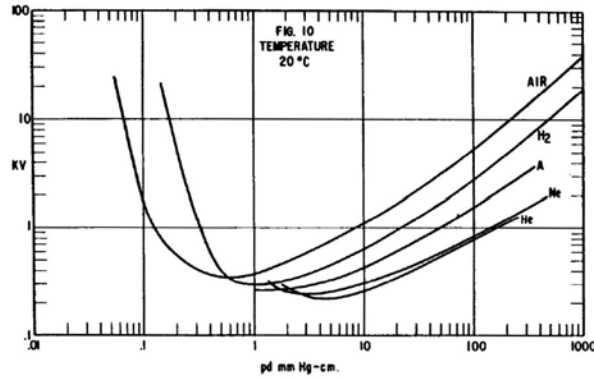


Figure 2.4: Typical Paschen curves, log-log plot, showing gas breakdown voltage versus the product of pressure and gap length,  $p \cdot d$  [5]

### 2.3 Cathode Spots

The cathode spot is a phenomenon not fully understood both in terms of experimental and theoretical characterization. It takes place in very limited surface area and it is of many forms. The most common consists on small, luminous spots that move over the cathode surface. Their displacements are chaotic and towards cold surface areas. As a result, neither their direction nor their motion is sufficiently understood. The cathode spot has many functions: it provides discharge medium into the electrodes gap and it provides current by emission of electrons. It forms a dense plasma in front of the surface and it contains four phases: solid, liquid, vapor and plasma.

From the cathode spot, a plasma jet goes away from it as a consequence

of the electrode local explosion. Several plasma jets, in the PPT cathode electrode, form the plasma bulk that is accelerated to give thrust. The origin process of cathode spots is shown in Fig.2.5. In general, the electrode are not smooth, instead their surface is rough. At these sharp geometric point, the field emission occurs and promotes the ion bombardment. The interested area is heated by the ion bombardment and thermionic emission starts. The increased presence of electrons promotes more ion bombardment and a thermal runaway heats the surface, until the local cathode surface explodes, leaving a crater.

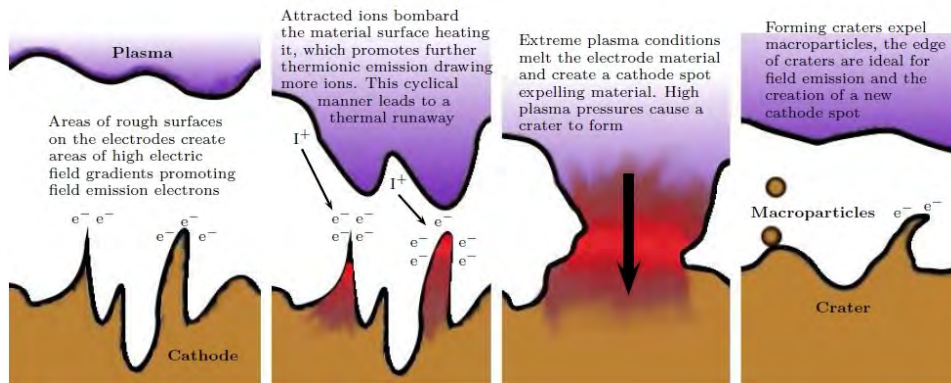


Figure 2.5: Evolution of the cathode spot process and macro particle formation as a result of plasma pressure on the liquid cathode material [14]



## Part II

# Test Design



# Chapter 3

## Foreword

The spark plug lifetime has been detected as one of the most critical parts to design in a pulsed plasma thruster total lifetime. In chapter 1, the main issues concerning the spark plug design and ignition circuit design have been exposed. In particular the parameters involved in the optimization of the spark plug lifetime are the following:

- Spark Plug structure;
- Ignition circuit characteristics: pulse length, breakdown current and voltage;
- Pulsed Plasma Thruster characteristics: coupling element between thruster's and spark plug's cathode electrodes.

The aim of the thesis project was to investigate on the spark plug lifetime. Obviously it was impossible to study all the numerous aspects of the problem, especially because a test facility had to be created and started. The test design therefore has been to be as simple as possible.

It was noticed that one of the main parameters involving the spark plug lifetime was the trigger pulse-length. Through a literature review on the existing high voltage pulse generator technologies (see section 4), a MOSFET based high voltage switch circuit, has been selected as a good candidate to test the spark plug breakdown. In particular it gives the possibility to change the pulse length parameter, for instance since a very narrow window on about  $100ns$ .



## Chapter 4

# Spark Plug Design

The MDT-2A spark plug design [1] is coaxial, with semiconductor coated insulator and with interior electrode of large diameter. With this design the spark plug lifetime was respecting the thruster requirement of the spacecraft, which was about  $10^7$  pulses.

In agreement with the supervisors, it was decided to do not investigate on the spark plug insulator coating. The decision was well motivated by the following reasons:

- there wasn't any clear information on certified coating materials and thickness;
- the coating would have took a long time, a couple of month in total, to be prepared and realized. In particular to have access to the nanofabrication facilities of the *Nano Research Group* through an induction;
- the coating introduces a variable on the breakdown mechanism that could complicate further the breakdown process understanding;
- the coating for the MARS SPACE LTD PPT thruster projects, are currently in phase of studying and approval. Moreover it wouldn't be possible to have precise information on the material composition and layer thickness.

For all the reasons described above, the spark plug insulator coating has been excluded from the design. The consequence of introducing this

parameter would have complicated the spark plug manufacturing, reliability and beyond extended the manufacture schedule. Finally, because of the poor details available, it was decided that the time-budget was too low to consider possible the investigation of this spark plug structural characteristic.

A possible spark plug parameter to investigate was the geometry. In particular the size of the interior electrode and the dimension of the insulator ring. For what concerns the material, several are those known to work reliably as electrodes even in the specific case of the PPT spark plug. But the most common used materials are Tungsten, Copper and Tungsten/Copper alloys. As insulator the choice can be between the Shapal<sup>TM1</sup>, Teflon<sup>®2</sup> and Macor<sup>®3</sup>.

The spark plug design proposed was the coaxial type shown in appendix B. In order to minimize the costs, some suitable materials, already available at the TDHVL mechanical workshop, were considered. In particular, a Tungsten (purity 99.95%) rod of 1.5mm diameter, was selected for the inner electrode. As insulator some Macor pipes were also available. There were two size pipes, of 1.55mm and 0.85mm interior diameter respectively, with 0.6mm and 0.25mm thickness respectively. Starting from these available material, two size of spark plugs have been designed, the big-SP and the small-SP. For both a stainless steel external electrode has been manufactured, drilling 5mm rods to slot in the insulator pipe and the interior electrode.

To roughly forecast the spark plug breakdown voltage in air, the Paschen curves for the air can be used (Fig.4.1). The separation between the coaxial electrodes is 0.6mm for the big-SP, and 0.25mm for the small one. Since the atmospheric pressure, at 20°C, is  $p = 760\text{torr}$ , the resulting  $p \cdot d$  values are respectively 45.6mmHgcm and 19mmHgcm, leading to the respective predicted breakdown voltages of 3.0kV and 1.5kV. If this values will occur during the in air tests, the spark plug breakdown will probably occur in air rather than on the Macor insulator surface.

---

<sup>1</sup>Aluminum nitride ceramics

<sup>2</sup>Polytetrafluoroethylene (PTFE)

<sup>3</sup>Macor is the trademark for a machinable glass-ceramic developed and sold by Corning Inc

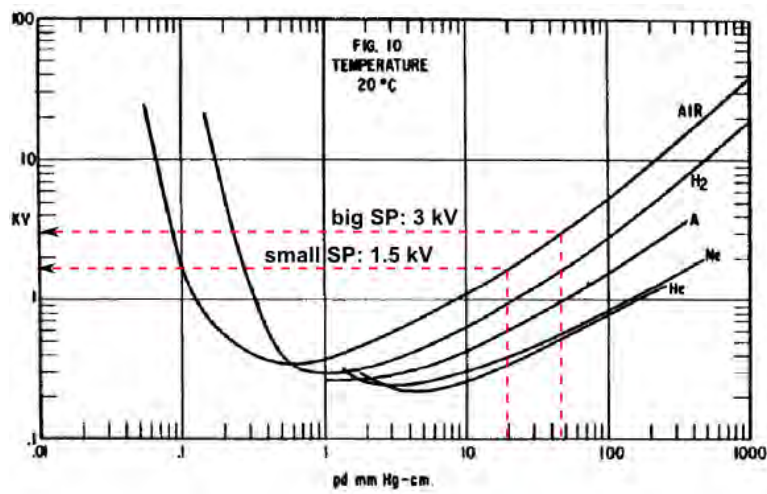


Figure 4.1: Paschen curve to forecast the air breakdown voltage of two types of the spark plugs manufactured



## Chapter 5

# Ignition Circuit Design

The power delivery of one watt, is defined as one joule of energy delivered in one second. If a certain amount of energy is delivered to the load in a short time, the resulting power is large. In a pulsed power application, even if the average power may not be large, the peak power may reach huge values. An example in nature is represented by the lightnings, which develop megajoules of energy in microseconds, while examples in technology are radar, particle accelerators and lasers. The purpose of using a pulsed power system, is to realize a power compression. The use of pulsed power is justified by two main reasons: to deliver the high power required is impracticable continuously or to use pulsed power lead to an efficiency advantage.

The vacuum arc plays three different roles in pulsed power systems:

1. it is used as switch, such as a mechanism to control the delivery of a high power pulse to the load;
2. it occurs in case of a catastrophic failure of the electrical insulation of a high power device;
3. the vacuum arc is used as the energy conversion mechanism to convert power into, for example, x-rays, or, in the case of a semiconductor spark plug, in metal vapor, or plasma.

The use of vacuum arc is practically as a switch or as a load. The case of interest, such as to manufacture the ignition system to generate a plasma puff by means of a spark plug, is to use it as a load. In this particular case,

the load that the spark represents, will probably be time-varying and with non-linear properties. For these reasons, in order to optimize the energy transfer to it, a careful design of the pulsed power system has to be done.

The temporal power compression is achieved by accumulating, in a certain amount of time, the energy required in a storage device. In order to maximize the pulsed power, this energy should be realized in a relatively short amount of time. The simplest form of a pulsed power system, which is all long used in the pulsed plasma thruster ignition system, uses an energy storage capacitor as the energy storage element (Fig5.1).

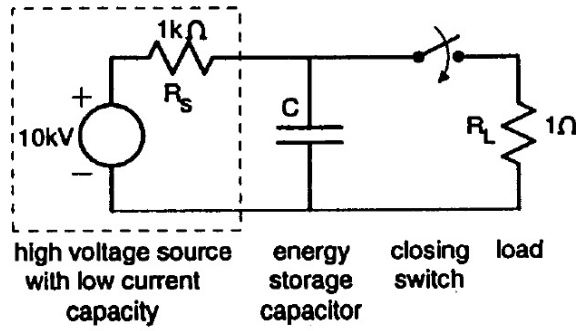


Figure 5.1: High peak power delivering to a resistive load,  $R_L$ , with a capacitive energy storage system. The current limited high voltage source charges the capacitor over a relatively long time interval. Activating the closing switch device, the energy is quickly delivered to the load [5]

The electrical energy accumulated by the capacitor is given by the following equation:

$$E = \frac{1}{2} \frac{C}{V^2} = \frac{1}{2} \frac{Q^2}{C} \quad (5.1)$$

Where  $Q$  is the quantity of charge stored,  $V$  is the voltage difference between the capacitor plates and  $C$  is the capacitance. The power delivered, as a function of time, by the source to charge the capacitor, is given by:

$$P_c(t) = \frac{V^2}{R_S} e^{-\frac{2t}{R_S C}} \quad (5.2)$$

Where  $R_S$  is the high voltage source limiting current resistor. Theoretically, half of the energy produced by the source, is dissipated in the source

resistance. The peak power delivered, when  $t = 0$ , depends on the open circuit voltage and on the source resistance value. The duration of the power delivery, depends instead on the charging time constant  $\tau_c = R_S C$ .

The stored energy is delivered to the load, which as already mentioned can be a vacuum arc itself, by the closing switch that connects the capacitor to the load. The closing switch can be also a vacuum arc but, in the case of a trigger circuit for pulsed plasma thruster, it is made by a particular device, for example a power MOSFET. The possible device to use and the ignition circuit possible solutions, will be discussed in the next section 5.1. In the case of a load resistance, also the power delivered to the load obtained by closing the switch, has the exponential form:

$$P_d(t) = \frac{V^2}{R_L} e^{-\frac{2t}{R_L C}} \quad (5.3)$$

In this case, the power decay is determined by the discharging constant  $\tau_d = R_L C$ . The power gain,  $P_{gain}$ , is defined as the *ratio of peak power delivery to the load over peak power delivered by the source*. The Temporal compression,  $T_{comp}$ , is defined instead as the *ratio of charging time constant to discharging time constant*. As a result these two parameters, are equivalent:

$$P_{gain} = T_{comp} = \frac{R_S}{R_L} \quad (5.4)$$

There are three main critical requirements concerning the capacitive energy storage system:

1. the closing switch must remain opened when the high voltage is applied across it, and for a time preferably much greater than the charging time constant  $\tau_c$ ;
2. the switching transition, from opened to fully closed, must occur preferably in a time much shorter than the discharging time constant  $\tau_d$ ;
3. the closing switch must reliably conduct the large current discharge.

## 5.1 Investigation of High Voltage Pulse Generators

The most commonly used techniques of high voltage pulse generation are: Marx cells and spark gaps, non-linear capacitor, static induction thyristor, modular high voltage, combination of energy storage components and transformer, IGBT and MOSFET series and parallel. These techniques have a long list of application, such as industrial, medicine and biotechnology. Some examples in biotechnology are electro-chemotherapy and water and food treatment. Industrial application of high voltage pulse generator are treatment of metal and polymer, laser technology and insulation testing.

In general, a high voltage pulse generator is composed by two modules: the High Voltage Power Supply, HVPS, which charges in a relatively long time an energy storage capacitor with a current-controlled output; and a power modulator that deliver the energy to the load in a short amount of time, obtaining a high power electrical pulse. The fast discharge of the energy storage capacitor is accomplished by a Pulse Forming Network, PFN. It consists normally of switching devices, resistors, inductors and capacitors. The switches can be one of the several available devices, which can accomplish fast operation and are characterized by many maximum rating parameters, such as power dissipation, continued and pulsed current, breakdown voltage and operating temperature. They are also characterize by dynamic parameters like delay times, rise and fall times and switching speed. The most used and common switches are: ignitron, thyatron, tetrode, spark gaps and semiconductors. The lifetime ratings are on the order of  $10^6$  for the spark gaps,  $10^8$  for thyatrons and  $10^{12}$  for semiconductor devices. Anyway if these devices don't operate in nominal conditions, such as arcing or non-optimal condition in general, their lifetime is drastically reduced.

The electric power, from a low utility level, is transformed into pulsed high intensity magnetic fields by the pulse modulation. The simplest circuit exposed in the previous section (Fig.5.1) has an exponential decay pulse. In the following sections two different types of pulse generators will be described. The first one is the high voltage pulse generator using energy storage device components and a transformer. The second is a high voltage pulse generators that uses a series or parallel MOSFETs configuration.

### 5.1.1 MOSFET Circuit

High voltage pulse generator using power MOSFETs can be divided into two categories: parallel and series solutions. In general it can provide an high voltage controllable square pulse with amplitudes proportional to the device's breakdown voltage and pulse width on the order of hundred nanoseconds.

#### Parallel-MOSFETs

A parallel-MOSFET pulse generator circuit diagram is shown in Fig.5.2, in the case of three parallel devices. As shown in the schematics, a resistor between the source terminals is not needed. In fact the MOSFETs have a positive temperature coefficient. This means that, if one of them starts to take more current, it heats up and, thus for that feature its on-state resistance increases reducing the amount of current passing through the drain-source terminals. The motivation to use the parallel-MOSFET configuration, is to decrease the equivalent on-state resistance of the switch. In particular, by switching two or three MOSFETs in parallel and assuming that they are identical (more precisely with the same on-resistance), it can be reduced to a half or a third. In Fig.5.2 the load is a *cuvette* made of resistor and capacitor in parallel. Here the load represents some kind of food, as this circuit can be used for the bacterial transformation application.

The circuit is composed by a low voltage MOSFET Driver Circuit, MDC, and by the power modulator to generate the high voltage pulse. The MDC is powered by 15VDC source and takes in input a microcontroller input signal. The output square pulse generated by the MDC, is the input of the MOSFET gate. The current-limiting resistor of 4Ω protects the device by damping the signal oscillation during the switch-on time. This resistor has a low value because added to the gate resistance of the MOSFET, it increases the switching time by increasing the charging time of the source capacitance  $C_{gs}$ . The anti-parallel diode to the gate resistor, serves to turn off the MOSFET faster by allowing the current to bypass the resistor. A good diode for this purpose has a short recovery time. The two zener diodes in back-to-back configuration (Fig.5.3<sup>1</sup>), serves to protect the gate source

---

<sup>1</sup>[http://www.electronics-tutorials.ws/diode/diode\\_7.html](http://www.electronics-tutorials.ws/diode/diode_7.html)

terminal of the MOSFET, thus to prevent from damaging the gate oxide. It is one of the most common cause of failure in power MOSFETs.

The HVPS charges, with the power MOSFET switch opened, the energy storage capacitor, here  $8\mu F$ , through the high voltage current-limiting resistor. When the capacitor is charged, a positive pulse of the MDC switch on the power MOSFETs, allowing the capacitor to discharge through the switch and load. Here, the pulse seen by the cuvette is negative. The bigger is the capacitance, the higher is the pulse energy and the lower is the possible number of pulse per second. A large capacitance is better for a single and relatively long pulse, but worst in terms of repetition rate.

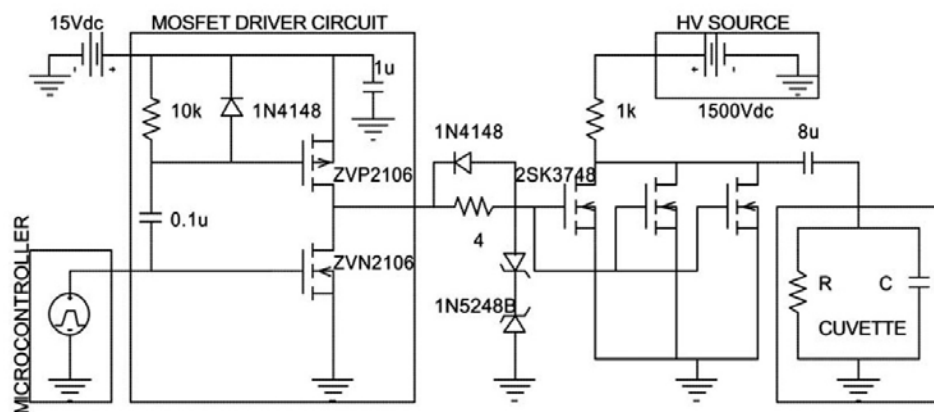


Figure 5.2: Parallel-MOSFET pulse generator circuit diagram [11]

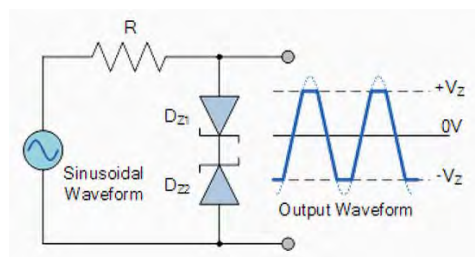


Figure 5.3: Zener diodes in back-to-back configuration

### Series-MOSFETs

The schematics of the series-MOSFET circuit shown in Fig.5.4 is similar to the previous. The difference is the power MOSFETs coupling. The aim of this configuration is to produce controllable square pulses with amplitude multiple of the single device breakdown voltage. Connecting for example two MOSFETs, with the configuration shown, they will be able to increase the high voltage applicable to the total switch. As in the parallel-MOSFET configuration, the same MDC and gate protection circuit can be used.

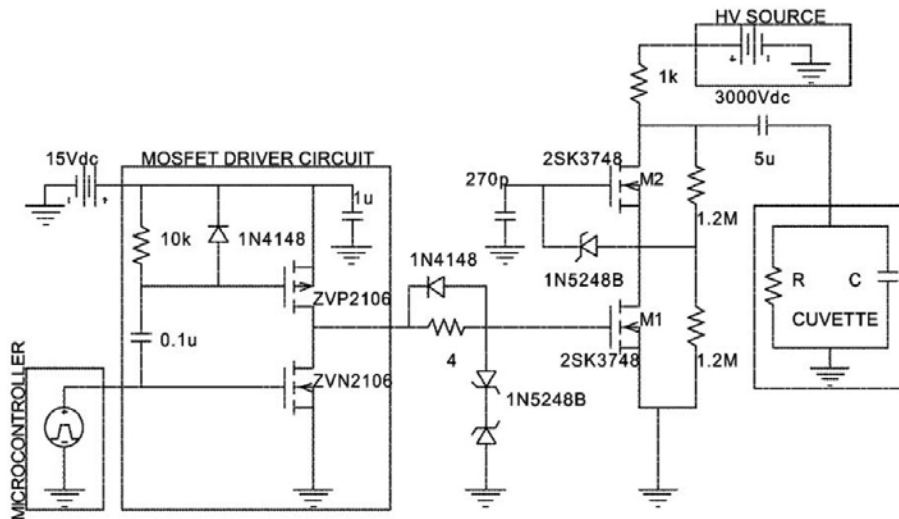


Figure 5.4: Series-MOSFET pulse generator circuit diagram [11]

The series operation of power MOS devices uses a gate-side technique, which make possible the synchronization of the gate signals, using their internal capacitance. As a result, a fast and balanced turn on of the switch is possible. The name of this technique, is *Capacitive Coupling of Gate Signals*. Most in general, Fig.5.5 shows the case of three MOSFETs in series.

The drain of each device is connected with the source of its neighbor. The most important aspects of this technique are the following:

1. The nearest MOSFET to the common ground, takes as input the triggering signal on the gate terminal. The other MOSFET gates have a capacitor linked to common ground;

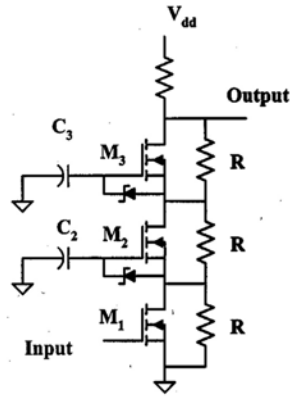


Figure 5.5: Methodology for reliable operation of stacked power MOSFETs [8]

2. A resistive divider, made by series resistors  $R$ , serves to stabilize the voltage rise at turn-off (because the pulse produced is negative);
3. A zener diode is adopted as simple protection circuit for the MOSFETs.

The switching behavior model, uses the following assumption: the drain current  $I_D$  is zero when MOSFET is in cutoff region of operation; the drain current is given by  $gm(V_{GS} - V_{th})$ , with  $gm$  the transconductance,  $V_{GS}$  the gate-source voltage and  $V_{th}$  the threshold voltage; the drain current in linear region is equal to  $V_{DS}/R_{DS,on}$ , with  $V_{DS}$  the drain-source voltage and  $R_{DS,on}$  the drain-source on-resistance. During the delay time, the time that occurs between the drive signal and the drain current flowing, the MOSFET is in cutoff region. It is in saturation region when the current is between 10% and 90% of the final value. Above the 90% the MOSFET is in linear region.

Given the power MOSFET parameter, it is possible to dimension the capacitor  $C_2$  and  $C_3$  using the following observations. Before the triggering signal, the drain-source voltages of the MOSFETs are DC and equal, such as  $V_{DS1} = V_{DS2} = V_{DS3}$ . The gate-source voltage of each device is instead 0V. When the trigger signal happens, and neglecting the drain-source capacitance, the effective capacitance between the gate and the source of each

MOSFET is given by:

$$C_{GS,eff} = C_{GS} + \frac{dV_d}{dV_g} \cdot G_{gd} \quad (5.5)$$

During the switch  $C_2$  and  $C_3$  are used to charge the  $C_{GS,eff}$  of, respectively,  $M_2$  and  $M_3$ . Assuming the the drain-source voltage are the same prior switching, the initial charge on  $C_2$  is:

$$Q = C_2 \cdot V_{DS} \quad (5.6)$$

After switching starts, the above described charge is given to  $C_{GS,eff}$  and  $C_2$ , that is:

$$Q = (C_2 + C_{GS,eff}) \cdot V_{GS} \quad (5.7)$$

Combining eq.5.6 and eq.5.7, the capacitance  $C_2$  can be calculated as follows:

$$C_2 = \frac{C_{GS,eff} \cdot V_{GS}}{V_{DS} - V_{GS}} \quad (5.8)$$

Similarly the next capacitance  $C_3$  can be calculate. Considering that it stores a charge of  $Q = 2 \cdot C_3 \cdot V_{DS}$ , its value is given by:

$$C_3 = \frac{C_{GS,eff} \cdot V_{GS}}{2 \cdot V_{DS} - V_{GS}} \approx \frac{1}{2} C_2 \quad (5.9)$$

Where the approximation is valid if  $V_{DS} \gg V_{GS}$ . Normally this is a valid assumption because, for power MOSFETs,  $20 - V < V_{GS} < 30 - V$  and  $500 - V < V_{DS} < 1500 - V$ . The procedure can be applied to an *m-series MOSFET circuit*, with  $m$  power MOSFETs. In particular  $C_n \approx 1/(n-1)C_2$ .

The gate capacitors can also be combined as shown in Fig.5.6. In this case, is  $C'_2$  to supply charge to the gates of  $M_2$  and  $M_3$ . In this case the result is given by  $C'_n \approx (m - n + 1) \cdot C_2$ .

### 5.1.2 PPT Ignition Circuit examples

In literature poor details have been found about the Discharge Initiator circuit, or Ignition Circuit of Pulsed Plasma Thrusters. Furthermore it wasn't possible to obtain circuitry design detail of the Pulsed Plasma Thruster



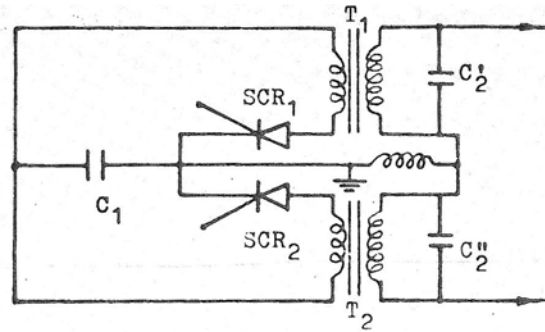


Figure 5.7: Ignition circuit schematic of MDT-2A [1]

used wasn't sufficiently sealed. Therefore, during the test, the trapped air leaked out slowly. At a certain point, the pressure inside the device was reduced to a critical value since the Paschen breakdown occurred. Because the minimum Paschen breakdown voltage is not less than 200V (independently from electrodes separation, pressure and gas composition), the transformer and capacitors were re-designed to give the same output voltage, but with a lower input voltage on the SCRs devices of 150V. The SCR failure didn't occur after this modification.

In [4] (1999) the Earth Orbiting 1<sup>2</sup> mission is described. The primary objective of the mission is to demonstrate new technologies in Earth imaging instruments. In addition to that, several complementary technologies have been selected for demonstration. One of them is a PPT for attitude control. Primary goals of the mission are to test a low mass PPT, with highly throttler system mass, high reliability and long life. In order to achieve these tasks, several improvements were required with respect of the LES-8/9 communication satellite PPT, which was taken as reference. These improvements were in the capacitor design, electronics, material and discharge initiation switching.

Fig.5.8 shows the schematics of the PPT grounding. The bottom-right components represent the ignition circuit (IGBT, Discharge Initial Transformer, 1 $\mu$ F energy storage capacitor, the command circuit and the spark plug). The selection of an high energy switching device for the triggering circuit has been a critical point. With respect of the LES-8/9 and the MDT-

<sup>2</sup><http://eo1.usgs.gov/>

2A closing switching device, even if the SCR has an important flight heritage and higher resistance to the space radiation, they have been replaced with the IGBT, because they had many latch up failures and they have bigger and heavier package with respect to IGBTs. The MOSFETs were ruled out because of their power and peak current limitations. The IGBT were selected for the following reasons: higher peak current capacity than the other devices; available in 1200V configuration; small size and mass; latch proof design. Anyway the IGBT integration were initially sensitive to the PPT discharges, producing spurious discharges without any trigger signal. This fact led to premature device failure. In order to validate the IGBT usage, several circuit modifications were adopted to provide additional filtering of the discharge circuit. For further protection a zener diode were installed on the device gate.

## 5.2 Ignition Circuit Design

After the electronics investigation, it was proposed the possibility to use a transformer-less ignition circuit to trigger the spark plug. The proposal was well accepted by the supervisors, mainly because of the following advantages:

- the output high voltage pulse generated is non-oscillating, like in the transformer case, but it is a square pulse with exponential decay;
- this kind of circuit gives the possibility to change the pulse length, such as the closing time of the switch.

A vacuum gap between copper electrodes may support an imposed average electric field up to  $10kV/mm$  while, at atmospheric pressure will usually breakdown when the applied electric field passes  $3kV/mm$ . Moreover, if the vacuum gap is bridged with an insulator, the breakdown voltage can perhaps be a third of these value [5]. In the manufactured spark plugs case, as their electrodes are bridged by a Macor pipe insulator (see section 6.1), the threshold should be about  $3.3kV/mm$  in vacuum and  $1kV/mm$  in air. Therefore, the breakdown voltage for the large and the tiny spark plug manufactured, can be estimated by these observation. For these reasons, the voltage output requirement for the Ignition Circuit, has been set to  $5kV$ .

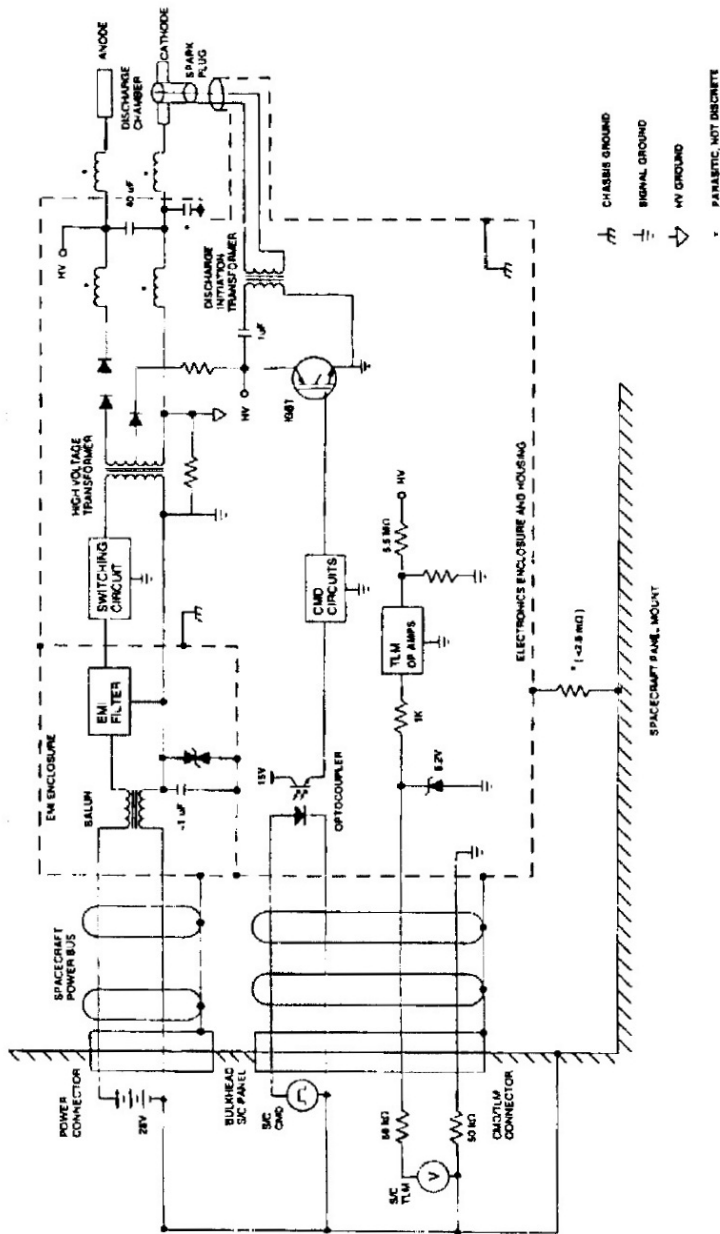


Figure 5.8: EO-1 PPT Ground schematics diagram [4]

### 5.2.1 MOSFETs Ignition Circuit

At the beginning, a single PCB including both the MOSFETs Ignition Circuit and the MOSFET Driver Circuit was designed (Fig.5.9). However it was decided to separate the two circuits, in order to use the MDC also to drive the Transformer Ignition Circuit. Moreover, it was more practicable to have the high voltage and the low voltage boards separated. Finally, the MIC was modified (Fig.5.10) to have larger PCB tracks to ensure the current transportation and to increase the tracks distance to avoid the breakdown to occur on the PCB. The components selected are indicated in the circuit schematic in appendix C. At the beginning the *STW9N150* power MOSFET was selected, but during the experiments, other two different devices were tested, both in the MIC and in the TIC circuits. A summarizing table of the power MOSFETs characteristics are shown in Table.5.1 (values from datasheets: [16], [17] and [9] respectively)

Table 5.1: Absolute maximum ratings of the N-channel power MOSFET selected

	STW9N150	IRFPG50	IPW60R045CP
$V_{DS}$	1500V	1000V	650V
$R_{DS(on)}$	2.5 $\Omega$	2 $\Omega$	0.045 $\Omega$
$I_{DM}^3$	32A	24A	230A
$E_{AS}$	720mJ	800mJ	1950mJ
$E_{AR}$	none	19mJ	3mJ
$P_D$	320W	190W	431W

Where  $V_{DS}$  is the breakdown drain-source voltage,  $R_{DS(on)}$  the drain-source on-state resistance,  $I_{DM}$  the pulsed drain current,  $E_{AS}$  the single pulse avalanche energy,  $E_{AR}$  the repetitive avalanche energy and  $P_D$  the maximum power dissipation.

<sup>3</sup>Pulse width limited by the maximum junction temperature

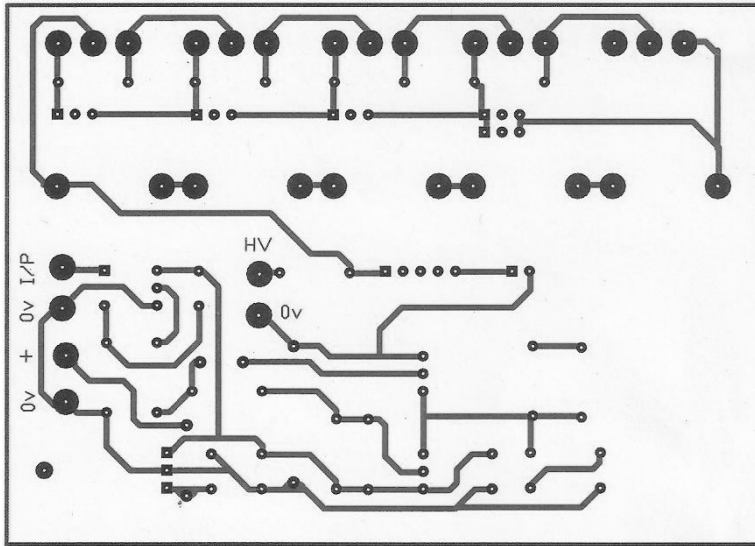


Figure 5.9: Former design of a single PCB including MOSFETs Ignition Circuit and MOSFET Driver Circuit

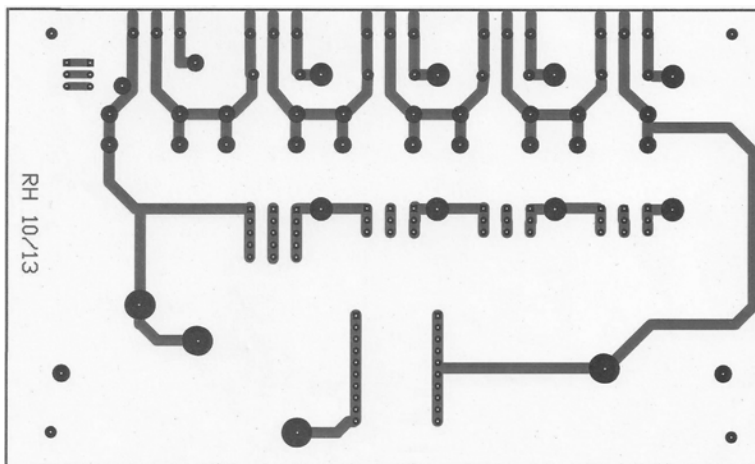


Figure 5.10: Separated MOSFETs Ignition Circuit adopted



## Part III

# Manufacturing, Testing and Modeling



## Chapter 6

# Test Devices Manufacturing

### 6.1 Spark Plugs

Five different spark plugs haven been manufactured. As already mentioned in section 4, they are two different size spark plugs:

- big-SP: SP1 (fig.6.1), SP2 (fig.6.2), SP3 (fig.6.3) and SP4 (fig.6.4).
- small-SP SP5 (fig.6.5).

For budget reasons, the following spark plugs have been manufactured in the TDHVL mechanical workshop without using CNC machines. For this reason the quality if the product is not the maximum, and it will give some consequences reported in the conclusions of this work 107.



Figure 6.1: Big size spark plug manufactured SP1



Figure 6.2: Big size spark plug manufactured SP2



Figure 6.3: Big size spark plug manufactured SP3

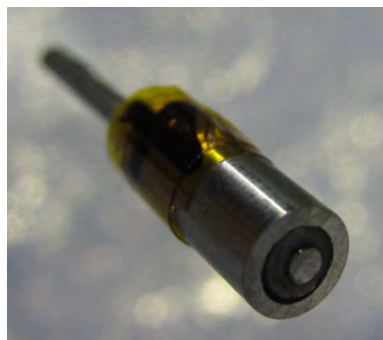


Figure 6.4: Big size spark plug manufactured SP4



Figure 6.5: Small size spark plug manufactured SP5

## 6.2 MOSFETs Ignition Circuit

The following figures show the PCB manufacturing detail. In particular an optocoupler (Fig.6.6) has been inserted in the circuit in order to insulate the pulse generator with MDC.

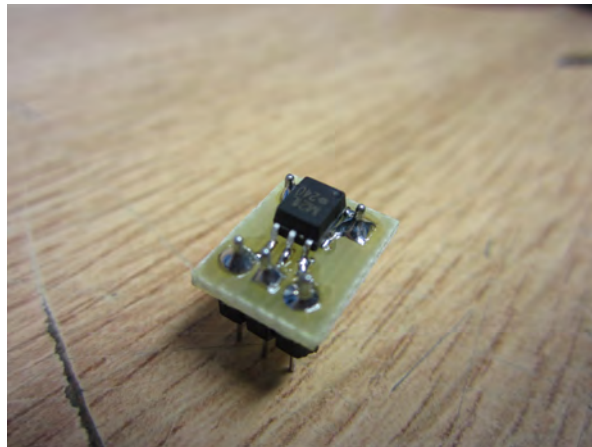


Figure 6.6: Optocoupler with PCB socket

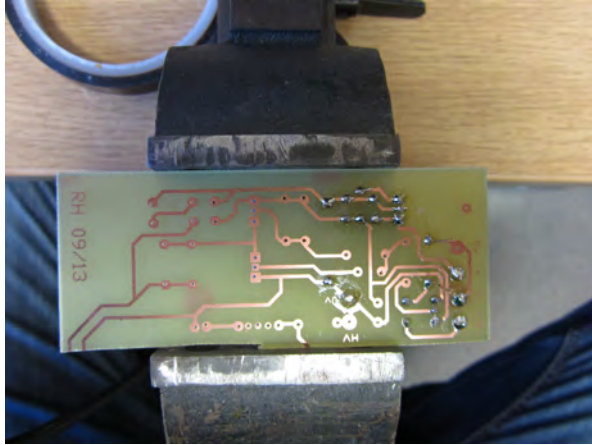


Figure 6.7: MOSFET Driver Circuit PCB track

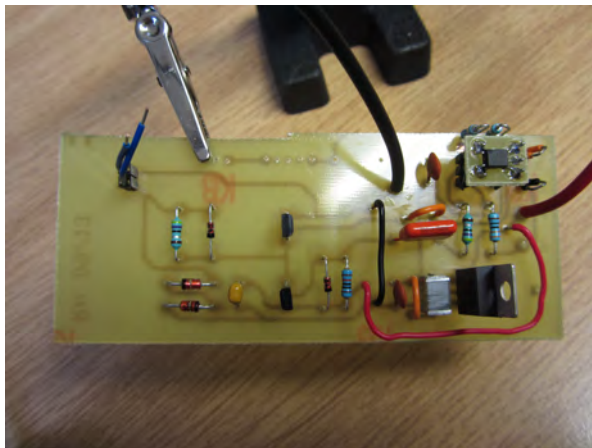


Figure 6.8: MOSFET Driver Circuit PCB completed with components

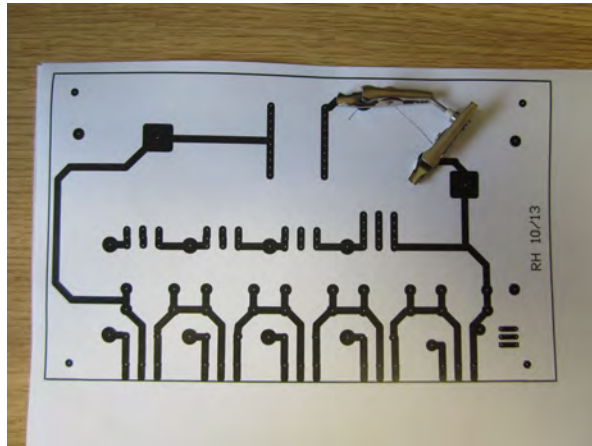


Figure 6.9: Sketch of spark plug crocodiles positioning on PCB

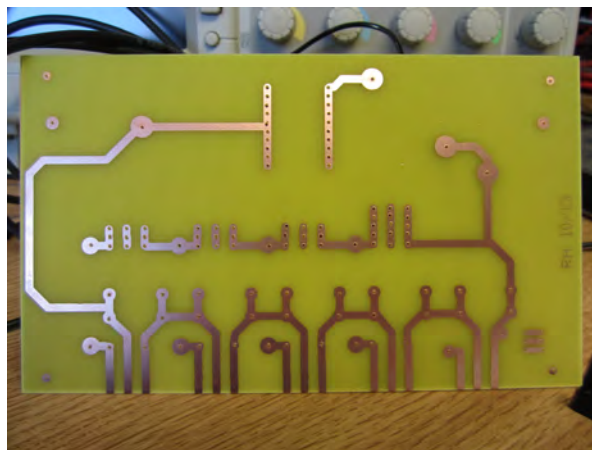


Figure 6.10: Power MOSFET high voltage PCB tracks

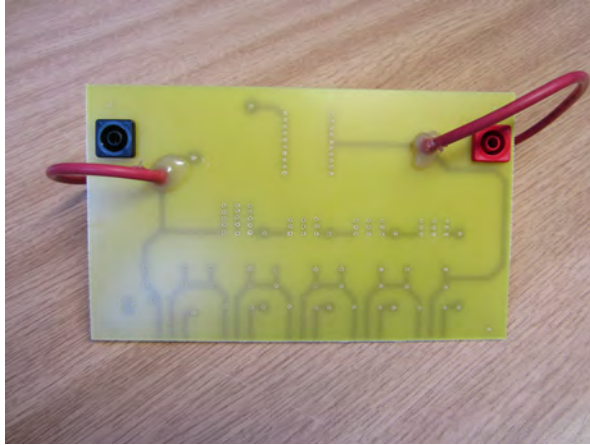


Figure 6.11: High voltage banana connectors

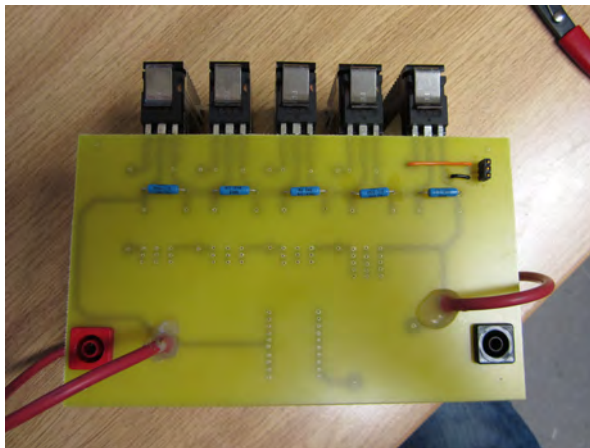


Figure 6.12: Power MOSFETs soldered and heatsinks mounted

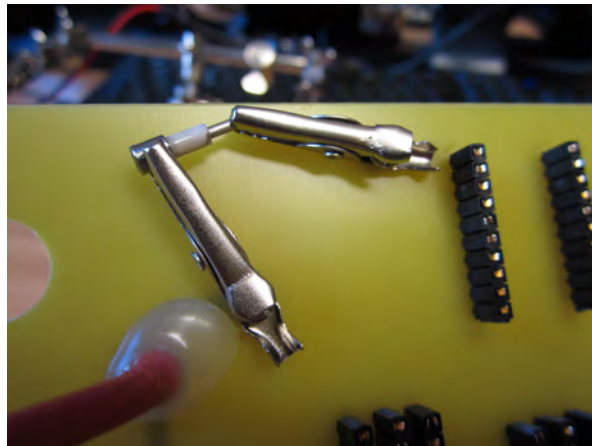


Figure 6.13: Crocodiles connectors to ensure the SP on the PCB

### 6.3 Coaxial Transformer

A coaxial pulse transformer has been manufactured starting from a ferrite core and plastic formwork provided gently by MARS SPACE LTD. The winding ration used is  $1 : n \approx 1 : 30$ . The additional material used are:

- double layer magnet wires SWG 24 (0.51mm, 0.8A) for the primary winding of 30 turns;
- double layer magnet wires SWG 30 (0.25mm, 0.22A) for the secondary winding of 900 turns;
- Kapton to isolate the winding layers;
- 1kVDC wire for primary winding external connection;
- 40kVDC wire for secondary winding external connection;
- fine sandpaper to remove the wire insulation to solder the wires tips;
- heat shrinking tubes to ensure mechanical reliability of the external connection.

The procedure used to realize the pulse transformer, followed these steps:

1. removal of a 5mm rubber coating insulation of the secondary winding wire;
2. pre-tin of it;
3. removal of 5mm insulation of the secondary winding magnet wire;
4. soldering of the two cables;
5. mechanical joint with a 3mm diameter heat-thermal shrinking tube;
6. secure the wire with masking tape;
7. winding of magnet wire insulating the layers with kapton and masking tape;
8. insertion of wire tips into the slats;

9. same procedure for the primary winding;
10. covering with a lot of masking tape and kapton.

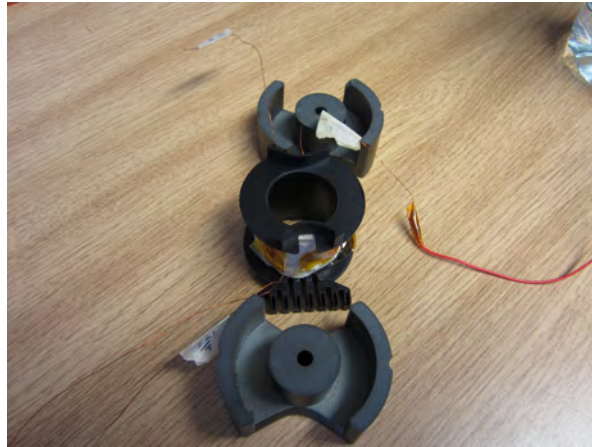


Figure 6.14: Coaxial transformer disassembled



Figure 6.15: Secondary winding wire SWG30



Figure 6.16: Primary winding wire SWG24



Figure 6.17: Primary winding mounted over the insulated secondary winding

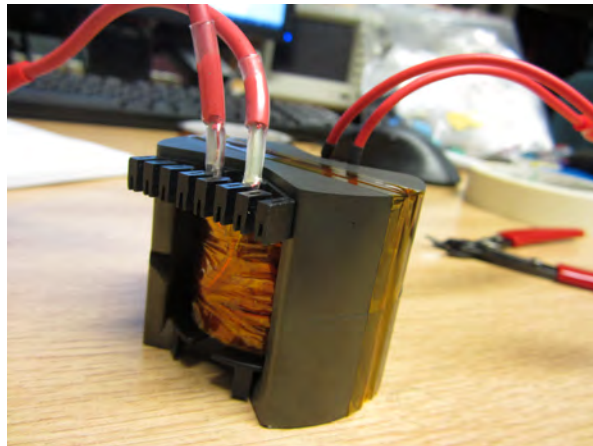


Figure 6.18: Pulse transformer completed with outer Kapton insulation



# Chapter 7

## Tests

### 7.1 Breadboard Preliminary Tests

A MOSFET Driver Circuit, MDC, breadboard has been designed and tested. Fig.7.1 shows the OrCAD schematic used for early circuit simulations. The input pulse named RD1, which will be provided by the *TGP110 10 MHz Pulse Generator*, has been modeled with an ideal pulse having both rise and fall times of  $25ns$ . Fig.7.2 shows the early MDC test.

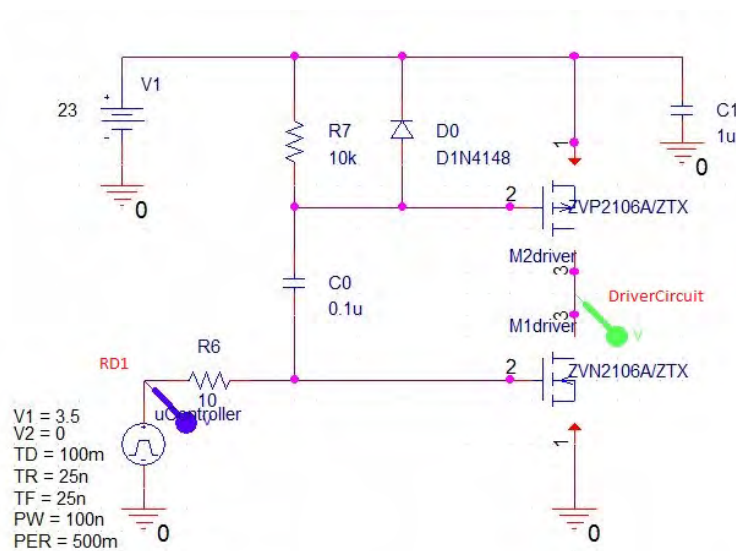


Figure 7.1: Mosfet Driver Circuit OrCAD schematic

A first breakdown test has been performed using the spark plug SP1 with

the MOSFET Ignition Circuit breadboard (Fig.7.3). The main experiment parameters used are: High Voltage Power Supplier set to  $HV = 1.2kV$ , energy storage capacitor  $C = 220nF$ , pulse period  $T = 4s$  and pulse width  $p_w = 200ns$ . With the capacitor and high voltage used, the energy stored was  $E = 1/2CV^2 \approx 160mJ$ . Because the  $HV$  was insufficient to have breakdown, the SP1 surface was coated with graphite using simply a pencil (Fig.7.5). At this early test, a video has been taken, and the following Table 7.1 shows the event succession. At the switch ON a tiny spark was produced. Several spark plug surface breakdown were recorded, Fig.7.4 shows two frames from the video. A part from the first spark caused by the HVPS switch on, the MIC pulse operation caused the following breakdowns starting from time 3 : 45. After the 7th spark, a first misfire occurred, then others as far as the 5 : 07 breakdown, after which 5 consecutive misfires happened. The cause of this behavior is the graphite coating outwear taking place spark after spark, of course due to the weak cohesion of it on the insulator surface.

The breadboard circuit has been tested with higher voltage. In particular it showed its limitation at about  $HV = 2kV$  when the breadboard tracks started to short in several points. Fig.7.6 shows the breadboard tracks, with the standard distance of 0.1" (2.54mm).  $HV = 2kV$  wasn't sufficient to breakdown the SP1 surface without using the graphite coating. After these preliminary tests, the breadboard was replaced with a PCB in order to reach reliably the high voltage required.

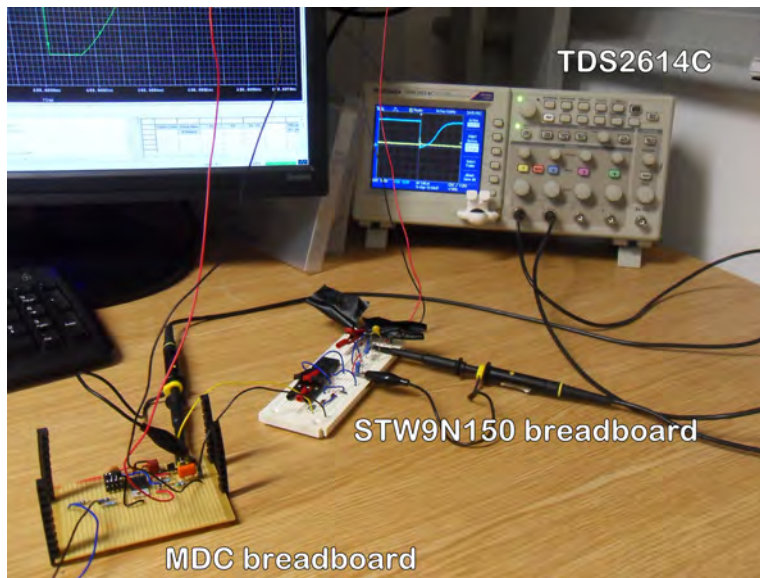


Figure 7.2: MDC breadboard test with one STW9N150 Power MOSFET

Table 7.1: MOSFETs Ignition Circuit, MIC, breadboard earlier experiment

Time	Spark#	Misfire# (cumulative)
3:31	switched ON	
3:45	1	
3:57	2	
4:00	3	
4:04	4	
4:08	5	
4:12	6	
4:16	7	1(1)
4:24	8	1(2)
4:32	9	1(3)
4:40	10	1(4)
4:48	11	
4:51	12	1(5)
4:59	13	1(6)
5:07	14	5(11)
5:32	15	

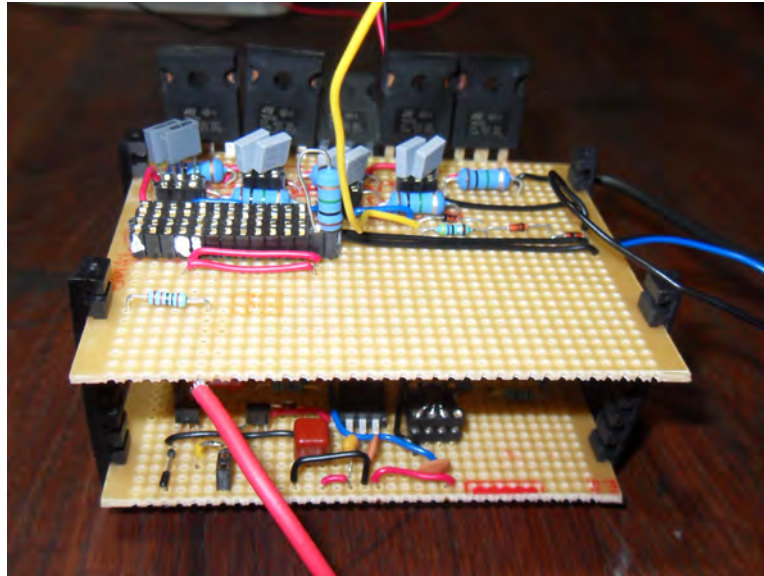
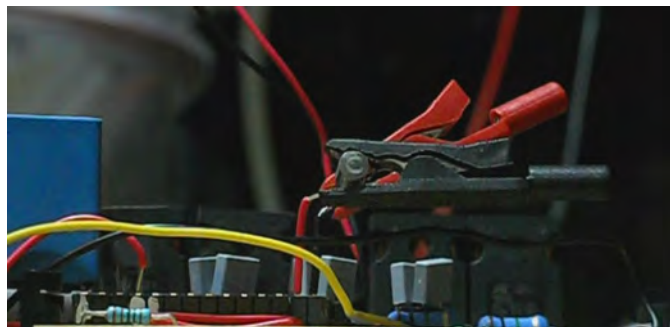


Figure 7.3: MOSFET Ignition Circuit breadboard



(a) Image frame from experiment video



(b) Spark on the SP1 surface

Figure 7.4: SP1 with graphite breadboard experiment



Figure 7.5: SP1 surface with graphite on the Macor insulator

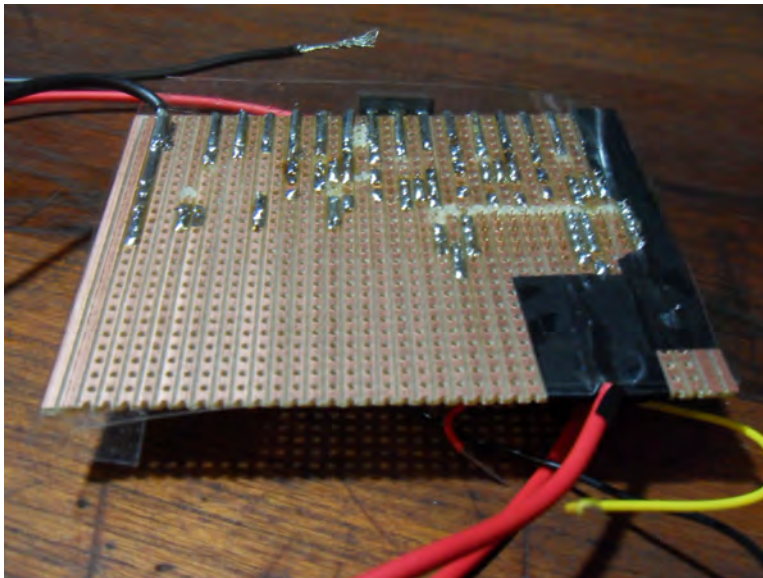


Figure 7.6: Power MOSFET breadboard copper tracks detail

## 7.2 MOSFETs Ignition Circuit - Air Tests

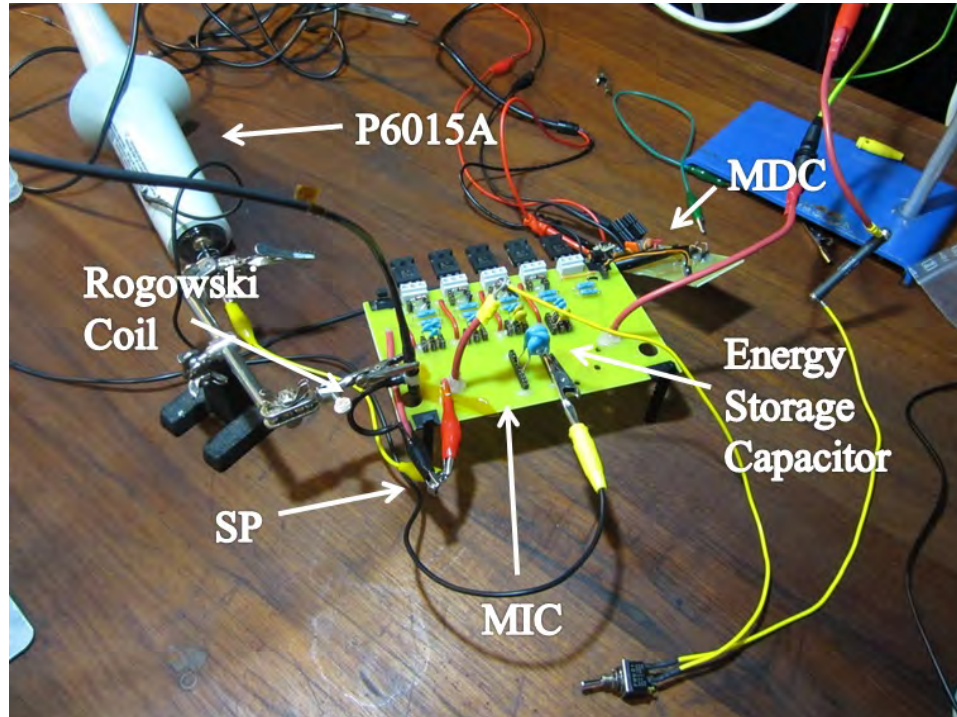


Figure 7.7: MIC Experiment setup for high voltage breakdown experiments at TDHVL

### 7.2.1 MIC Attempt 1

After the validation, with the preliminary breadboard tests, of the MOSFETs circuit, a Printed Circuit Board, PCB, has been designed and manufactured both for the MOSFET Driver Circuit and, most important, the Power MOSFET Circuit. The first test has been done to validate the MDC. Fig.7.8 shows the output signal of the circuit using an input signal of 4V, high-to-low pulse and with a 100ns pulse width. The test was made with  $V_1 = 23V$  DC current-limited source (see Fig.7.1). The equipment used for this test was: a *Tektronix TDS2614C* (100 MHz 2GS/s) oscilloscope; a *TGP110* 10 MHz Pulse Generator to provide the square pulse input of MDC; two 10x 200 MHz 300VDC *Tektronix* probes. The optocoupler output is irregular because of the load, but the current provided to the MOSFETs is sufficient

to give a beautiful MDC output (BLUE).

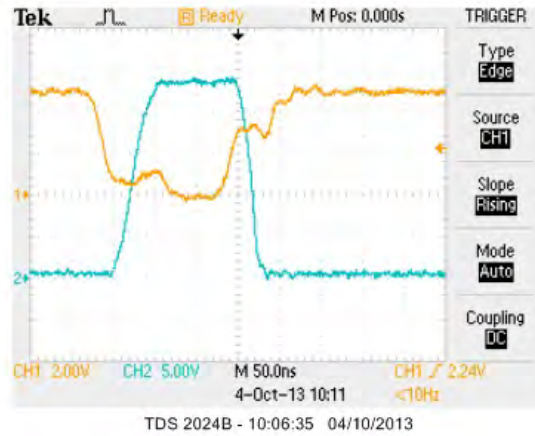


Figure 7.8: MDC output signal with:  $V_1 = 23V$ ,  $p_w = 100ns$  and  $V_{pulse} = 4V$ . BLUE:MDC output, ORANGE: optocoupler out

The MDC parameters above specified, are used in the following tests, unless otherwise specified. Using a high voltage resistor  $R_9 = 1.7k\Omega$  (10%), the MDC was used to the a single *STW9N150* Power MOSFET. Fig.7.9 shows the output signal of the circuit.



Figure 7.9: Single *STW9N150* Power MOSFET output signal with  $HV = 34V$ . BLUE: HV pulse, ORANGE: MDC output

The above test showed that MDC is working properly with one Power MOSFET, switched ON with the  $V_{GS}$  input signal. Therefore, a low voltage

test has been performed using the complete Power MOSFET PCB using 5-series devices. As expected (Fig.7.10), the HV pulse is not complete. The happened because the capacitor used wasn't correctly dimensioned, but a  $1kV$  set-up capacitor has been used.



Figure 7.10: 5-*STW9N150* Power MOSFETs output signal with  $HV = 34V$ . BLUE:HV pulse, ORANGE: Pulse Generator

After the low voltage validation of the circuit, the next tests where made at the TDHVL. The experiment setup is shown in Fig.7.7 and it includes: *DPO7254* real-time digital phosphor oscilloscope by Tektronix, 4-Channel,  $2.5GHz$ ; current-controlled HVPS up to  $5kVDC$  and  $5mA$ ; low voltage power supplier up to  $30VDC$ ; *TTi TGP 110 Pulse Generator*; the grounded cage used for the high voltage tests. This oscilloscope permits to collect data automatically each time an event occurs, when the signal is triggered. This instrument guarantees to collect every spark plug breakdown event during the tests, which is impossible to do manually above a frequency of about  $0.3Hz$  using the USB connection.

A former test where made with  $HV = 200V$  without using neither the energy storage capacitor  $C_{13}$  and the spark plug. The purpose of this test was to validate the PCB for the high voltage. At  $HV = 200V$ , it was noticed that drain-source signal of the five power MOSFET weren't perfectly shared. This happened because the  $C_2 - 5$  capacitors were dimensioned for  $HV = 1150V$ . Increasing the high voltage up to  $1kV$ , the perfect sharing

between the drain-source terminals during the switch operation occurred as designed. The period  $T = 2s$  was selected through the *FastFrame* setup of the oscilloscope (Fig.7.13).

Two high voltage probe were available:

**P6015A** High Voltage –  $20kV$  DC/ $40kV$  Peak ( $100ms$  Pulse Width), DC to  $75MHz$  Silicone Dielectric Optional 1000X Readout Coding Wide Compensation Range (7 to  $49pF$ )

**P5122** DC to  $200MHz$   $1000VRMS$  CAT II when DC-coupled, Floatable up to  $600 VRMS$  CAT II 100X

Because of the fast switching operation of the MOSFETs Circuit, which has fall time on the order of  $10ns$ , a comparison between the  $200MHz$  and the  $75MHz$  bandwidth probes was made. The results suggested that the  $75MHz$  probe was insufficient to record the MOSFETs Circuit output signal. Fig.7.14 shows the the P6015A probe, is unable to follow the  $1kV$  falling edge signal (the ringing effect can be attributed to the probe grounding cable length). For this reason, with the available probes, it hasn't been possible to measure accurately the breakdown voltage of the spark plugs and, in particular, above a pulse amplitude of  $1kV$  when using the  $200MHz$  probe needed. As a result, most of the voltage measured will be use to evaluate the general behaviors of the spark plug breakdown but without be useful for a numerical evaluation.

The Nyquist theorem says that the signal must be sampled at least twice as fast as its highest frequency component. Practically, because of the oscilloscope limitations of finite record length and measurement glitches, the above mentioned factor must be higher than two to completely reconstruct the signal. During experimentation the sample rate selected at least  $1GS/s$ , five times the hypothetical required bandwidth of  $200MHz$ .

In the following experiments the P5122 probe is used to measure  $V_{DS1}$ , because to observe the breakdown voltage directly on the SP electrodes resulted impossible with the probes available.

The MOSFETs Circuit has been certified to work (switch operation without spark plug load) with HV source up to  $5kV$  without incurring any issue.

A first test with the MOSFETs Ignition Circuit, MIC, with the the spark plug SP1 has been performed. Unfortunately, a conceptual design error prevent the breakdown happen. In particular the capacitor  $C_{13}$  doesn't charge, because the spark plug used is a open-circuit. If the spark plug was the semiconductor type, it had a even large resistance to permit the capacitor charging through it. Anyway the designer wouldn't use the SP to charge the capacitor! As a result, several issues appeared: a spark was produced at the HVPS switch on; when the HV level was increased with the circuitry on, sparks were produced; some sparks were produced only at the first trigger pulses at  $4 - 5kV$ ; after a few tests some power MOSFETs failed, it was noticed from their warming up. After that, the MOSFETs were analyzed to detect which one failed. Also a thermal camera, TESTO875, were used to monitor the power MOSFETs temperature.

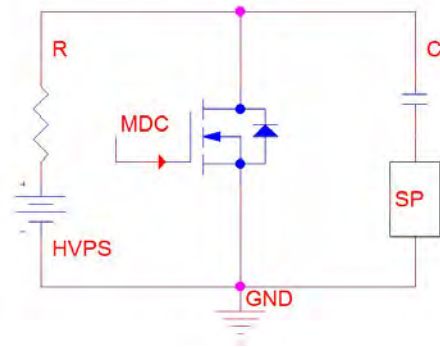
### 7.2.2 MIC Attempt 2

As in the MIC1 tests, in the following experiments the  $P5122$  probe is used to measure  $V_{DS1}$  and the power MOSFETs used are the STW9N150.

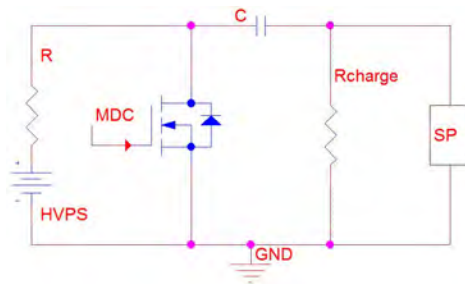
To solve the above mentioned problem, a second attempt were made on the design circuit. Fig.7.11a and 7.11b show the former and the latter MIC design. The MIC2 uses a parallel resistor,  $R_{charge}$ , to the SP, in order to charge the capacitor through it. MIC2 was tested at  $3kV$  recalculating the  $C2 - 5$  capacitors. In the preliminary switch test, without SP, there were verified: perfect drain-source voltage sharing between the 5 MOSFETs; perfect temperature sharing with a stable value of about  $35^{\circ}C$ . A test was made selecting: period  $T = 2s$ ,  $HV = 3kV$ ,  $C_2 = 150pF$  and  $p_w = 200ns$ . Fig.7.15 shows a later test made with  $p_w = 400ns$ . In both cases the spark produced were a few: 10/100 with the  $p_w = 200ns$  test and 6/100 with  $p_w = 400ns$ . Another test was made using the new SP2, instead of SP1. Only a few breakdown occurred (one of them: Fig.7.16), and after 5-6 of them the circuit stopped to work again. A possible cause of failure is the transient over-voltage of the drain-source terminals (observed in  $V_{DS1}$ ), eventually above the device breakdown voltage of  $1500V$ .

Next to this second failure of the STW9N150 Power MOSFETs, after

Figure 7.11: MOSFET Ignition Circuit schematics



(a) MIC attempt 1 schematic



(b) MIC attempt 2 schematic

further investigation, the avalanche rating was detected as a possible critical parameter to consider. In Power MOSFETs, with built-in avalanche capability, this feature serves to safeguard against unexpected voltage that over-stresses the device<sup>1</sup>. The STW9N150 is avalanche tested for a single pulse, with an avalanche energy  $E_{AS}$  of  $720mJ$  and an avalanche current  $I_{AR}$ , repetitive or not, of  $8A$ .

A new power MOSFET was selected, the IRFP50, which has  $E_{AS} = 800mJ$  and, in addition, it is repetitive avalanche tested with  $E_{AR} = 19mJ$ . To test these new devices both the zener diodes and the  $C2 - 5$  capacitor were changed. To make a conservative test, the energy storage capacitor  $C_{13}$  was selected to give a maximum energy of  $19mJ$ , the same as the MOSFET  $E_{AR}$  rating. In the meanwhile a Rogowski coil was available to measure the spark plug current during the breakdown. A test was performed and only one spark was produced before MOSFET failure. The current peak measured was about  $155A$  well over the maximum pulsed drain current  $I_{DM}^2$  of  $24A$ .

### 7.2.3 MIC Attempt 3

A last attempt on the MOSFET Driver Circuit design was made. The schematic showed in Fig.7.12 was realized modifying the PCB. The concept of this circuit is different from the typical transformer circuit, in which the spark plug breakdowns because of a trigger pulse that goes from  $0V$  to  $-HV$  to come back again to  $0V$ . Looking at the schematic, MIC3, when the switch made of 5 STW9N150 in series is opened, the spark plug electrode is floating. When the trigger pulse closes the switch, the spark plug electrode is ideally connected to the ground. At this point, the energy storage capacitor discharges through the 5 series MOSFETs  $R_{DSon}$ .

The tests confirm this behavior. Fig.7.17 shows one of the several sparks produced with:  $HV = 3500V$ , SP2,  $C_2 = 150pF$ ,  $p_w = 150ns$  and  $C_{13} = 0.33nF$  leading to a maximum energy  $E_{max} \approx 2mJ$ . The working key points of MIC3, and some observation are in the following:

<sup>1</sup>VISHAY SILICONIX - Application Note AN-1005

<sup>2</sup> $I_{DM}$ , Peak or Pulsed Drain Current, is the maximum drain current the device is allowed to carry for a pulse of  $10\mu$  or less.

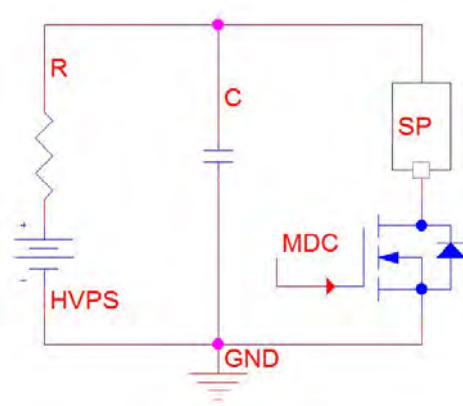


Figure 7.12: MIC attempt 3 schematic

1. Immediately after the switch closes, the SP electrodes have a potential drop equal to the  $HV$  provided;
2. If the SP  $V_b < HV$ , the surface breakdown happens;
3. the current measured on the spark plug rapidly rises to a maximum of about  $32A$  (see Table 8.1), which happens to be the maximum MOSFET rating  $I_{DM}$ . The  $I_{DM}$ , normally equal to the peak source current  $I_{SM}$ <sup>3</sup>, is fixed by the current limit to prevent die heating that otherwise could result in a burnout site<sup>4</sup>;
4. the MOSFETs switch should stay closed for the  $p_w$  provided, on the order of  $100ns$ , which is the time allowed to the spark electrode to be grounded;
5. holding the HVPS ON shouldn't affect the current measure, because it charges the energy storage capacitor through the high voltage resistor, with a time constant much higher than the discharging time (for example in a test where  $C = 33nF$  and  $R = 1.7k\Omega$ , the charging constant results  $\tau = 56.1\mu s$ , while the discharging time constant on the order of  $100ns$ );

<sup>3</sup>The peak source current  $I_{SM}$  is the maximum current pulse that the MOSFET body diode is guaranteed to carry

<sup>4</sup>ADVANCED POWER TECHNOLOGY, Application Note ATP-0403 Rev B, March 2, 2006

6. during the discharge, both the MOSFETs and the plasma resistance could vary in time.

Sometime, the SP electrode potential doesn't go to zero, but it should if all the energy stored into the capacitor is used. Cause of the  $75\text{MHz}$  probe, the measurement doesn't represent the reality. The probe issue was already discussed and showed in Fig.7.14. The RLC series semi-empirical model proposed (see chapter 8), shows that effectively the voltage measured is not correct; anyway sometimes, not all the energy is used during a single breakdown. Statistical values of MIC breakdown tests, are reported in section 8.2.1 and the most important data collected and processed are shown in appendix A, section A.1.



Figure 7.13: DPO7254 oscilloscope *FastFrame* setup window to set the pulse width of MDC

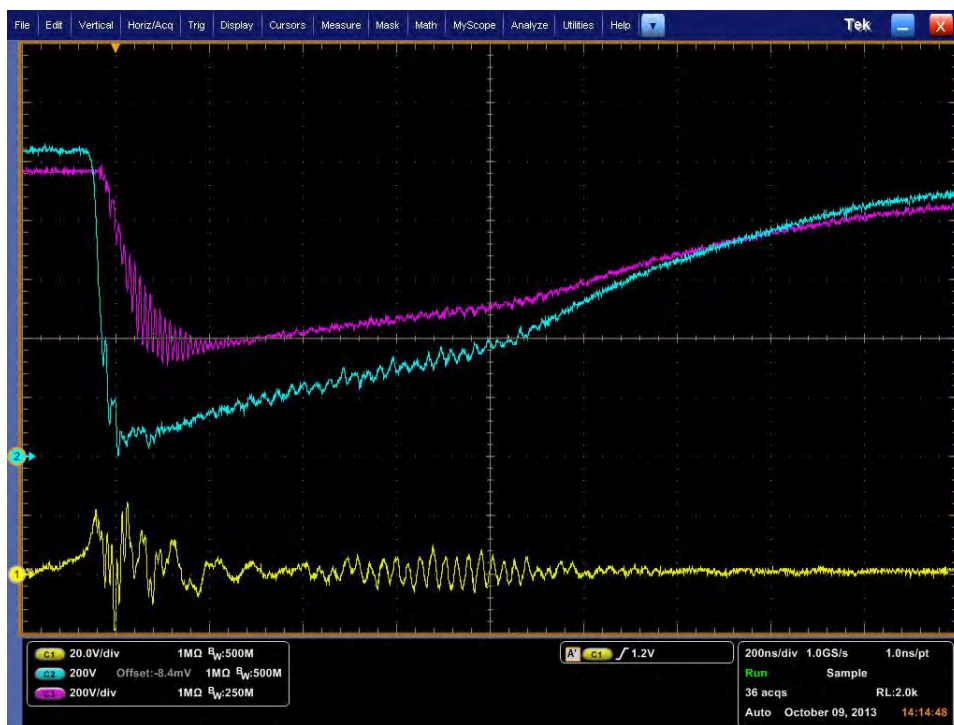


Figure 7.14: HV probes comparison on the MOSFETs Circuit output signal.  
CH1:  $V_{GS1}$ , CH2: P5122 probe, CH3: P6015A probe

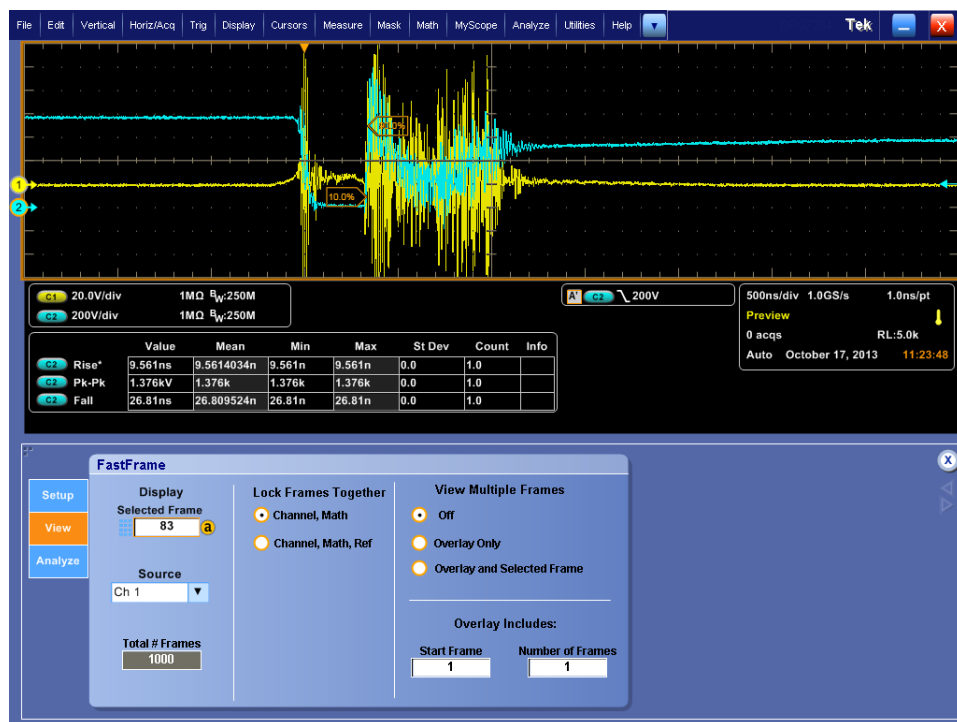


Figure 7.15: SP1 breakdown with period  $T = 2s$ ,  $HV = 3kV$ ,  $C_2 = 150pF$  and  $p_w = 200ns$

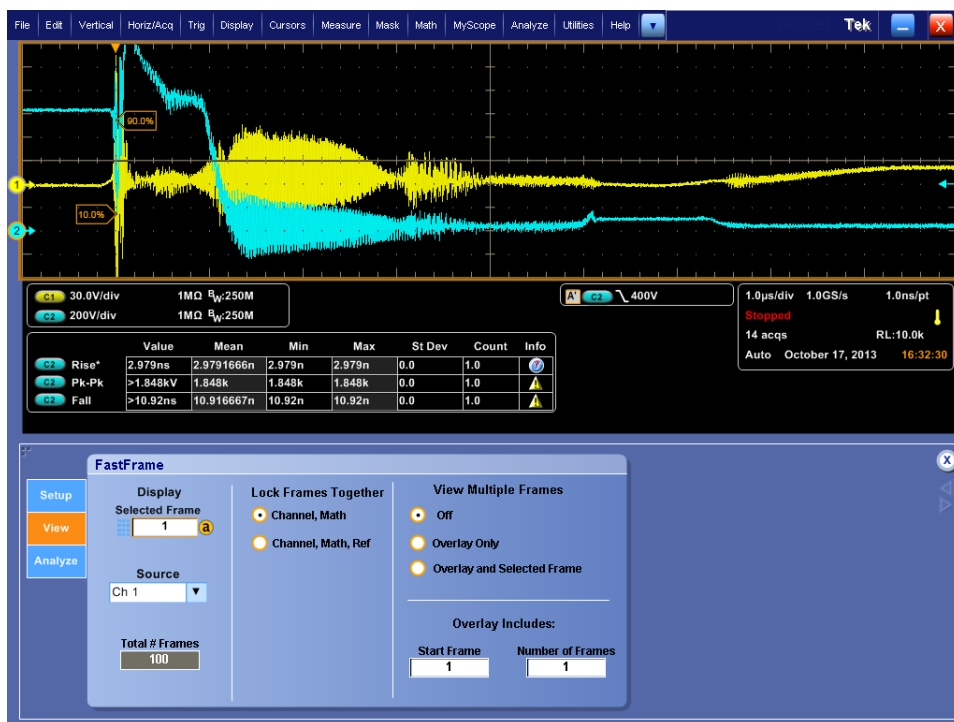


Figure 7.16: SP2 breakdown with period  $T = 2s$ ,  $HV = 3kV$ ,  $C_2 = 150pF$  and  $p_w = 200ns$

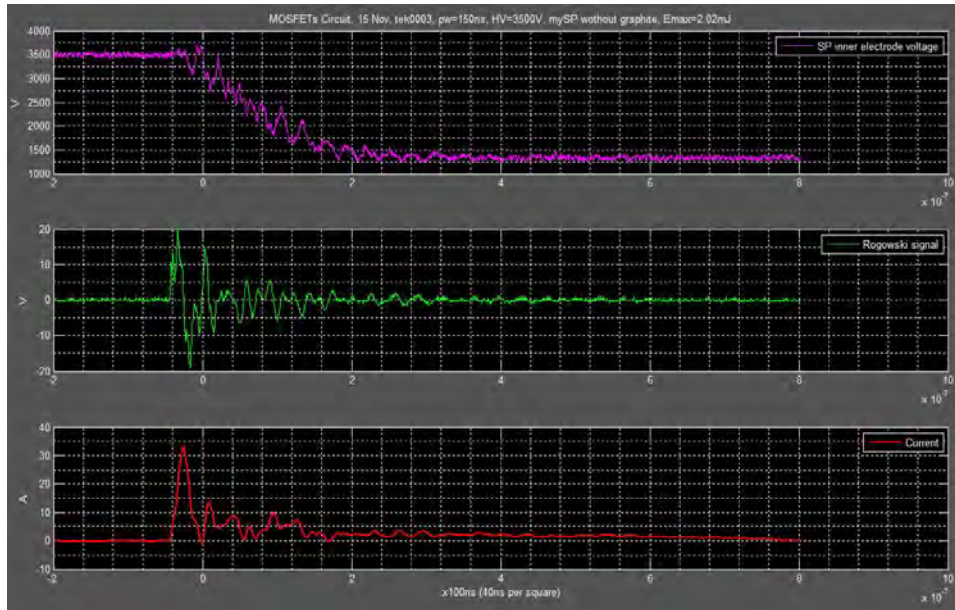


Figure 7.17: MIC3 test:  $HV = 3500V$ , SP2,  $C'_2 = 150pF$ ,  $p_w = 150ns$  and  $C_{13} = 0.33nF$  leading to a maximum energy  $E_{max} \approx 2mJ$

### 7.3 Transformer Ignition Circuit - Air and Vacuum Tests

A coaxial transformer of 1 : 30 winding ratio has been manufactured6.3. The power MOSFET used as switch device is the IPW60R045CP[9], which is driven by the MOSFET Drier Circuit. The TIC schematic is reported in Fig.7.18. At the beginning the *IRFPG50* power MOSFET was used but it resulted inadequate since it broke very soon after some tens spark plug breakdowns.

The MDC has been set to give an output  $p_w$  of  $1.2\mu s$ . With this value it is guaranteed that all the energy is transferred to the coaxial transformer, or better to the primary winding inductor (validated experimentally). The energy storage capacitor bank value is  $1.2\mu F$ , made with 8  $150nF$  ceramic capacitors in parallel. A transformer output lead is grounded to make possible the use of the high voltage probe. The SP has been connected in order to have a negative pulse on the central electrode. Tests have been performed on the following spark plugs: a spare Spark Plug gently offered MARS SPACE

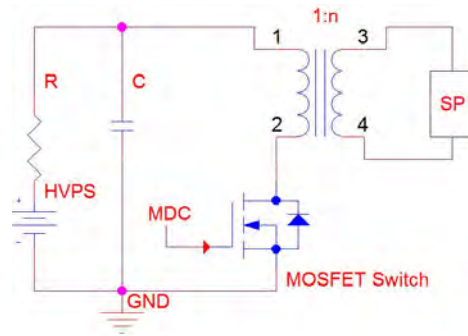


Figure 7.18: Transformer Ignition Circuit schematic

LTD coming from the Micro-PPT for NanoSats (NanoSat PPT) project<sup>5</sup>; SP1 large spark plug; SP4 tiny spark plug. Fig.7.20 and 7.21 shows the air and vacuum experiment setups. The vacuum experiments have been performed at the Tony Davis High Voltage Laboratory, using one of the vacuum chambers available (called *Delta v micro HV4 – 5*, Fig.7.19).

Once the experiment has been setup into the vacuum chamber, the following procedure followed to test the Transformer Ignition Circuit with the different spark plugs:

1. Test the system in air and save a set of breakdown events (voltage and current);
2. Create vacuum;
3. Perform the vacuum test and save a set of breakdown events;
4. Depressurization.

The connections between the TIC and the outside instrumentation, has been performed using some of the available connectors. The vacuum chamber connections used are:

- DB9 connector with the following ordering: (1,6)  $\Rightarrow$  ground, (2)  $\Rightarrow$  + MDC pulse, (3)  $\Rightarrow$  - MDC pulse, (8)  $\Rightarrow$  +28V, (5,9)  $\Rightarrow$  +300V;
- HVPS and low voltage power supplier grounded to the chamber structure;

<sup>5</sup><http://www.mars-space.co.uk/Pages/NanosatPPT.aspx>

- Rogowski coil located in the vacuum chamber and connected using BNC cable to the oscilloscope;
- *P6015A* high voltage probe outside the chamber. Grounded to the chamber body and signal crocodile clip connected with high voltage connection;

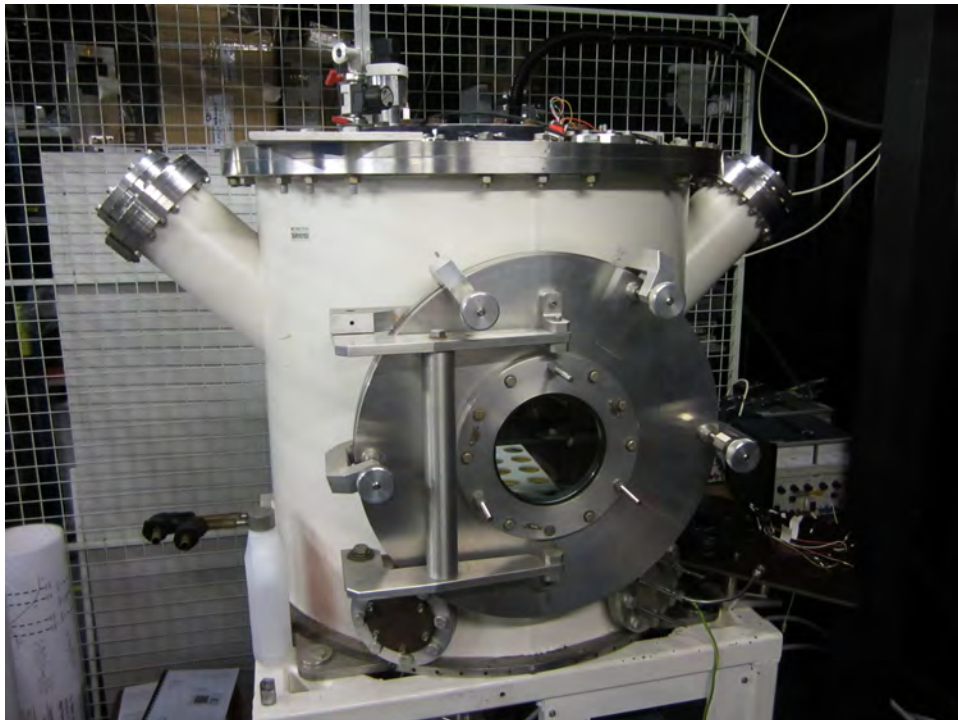


Figure 7.19: Vacuum chamber used for tests (location: *Delta v micro HV 4-5* at TDHVL)

Unfortunately two issues involve the measurements: the Rogowski coil used does not give reliable current measurement for low current (less than 5A); the *P6015A* high voltage probe can guarantee the breakdown voltage,  $V_B$ , measurement but not the after-breakdown high frequency oscillation.

### 7.3.1 MSL Spark Plug Test

The MARS SPACE LTD spark plug has a different design. In particular, the cathode electrodes of plug and thruster are the same. The plug is inserted

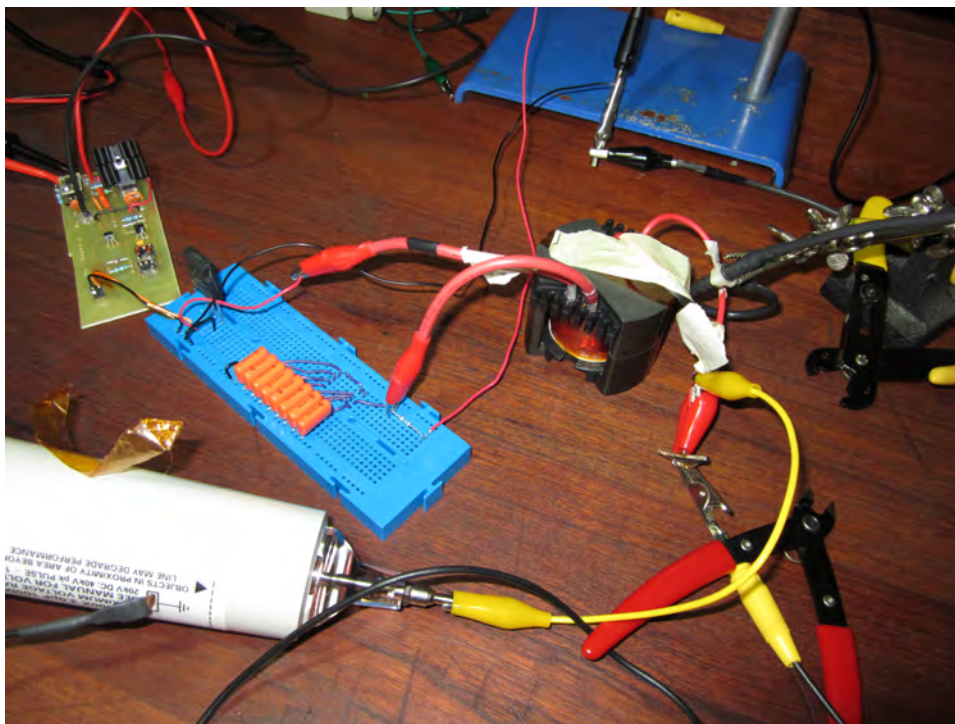


Figure 7.20: Transformer Ignition Circuit, air experiment setup. Energy storage capacitor bank of  $1.2\mu F$

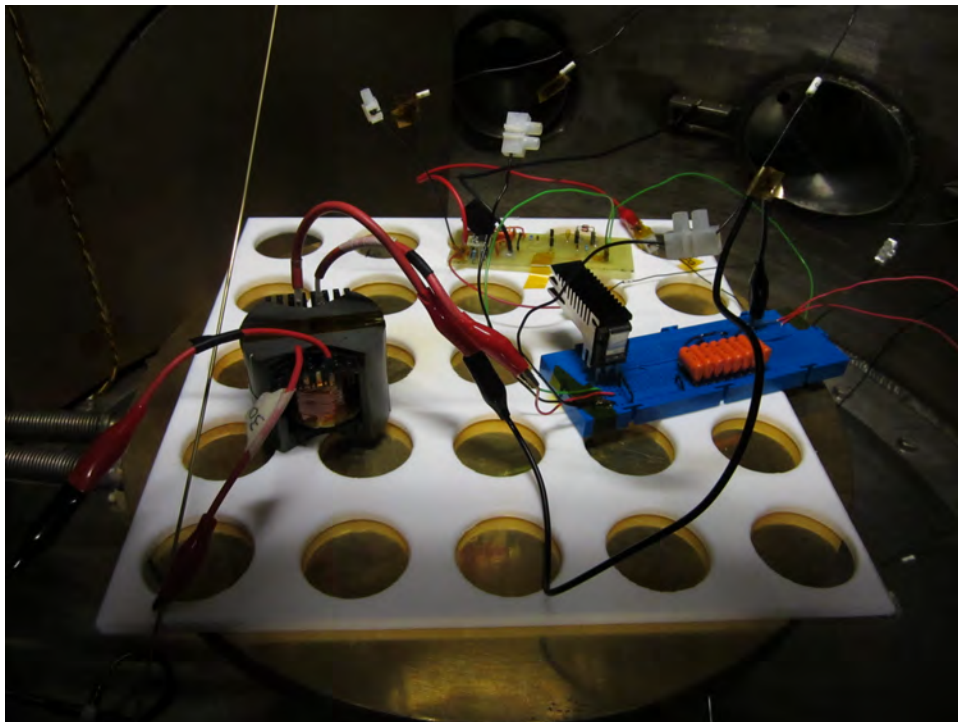


Figure 7.21: Transformer Ignition Circuit, vacuum experiment setup. Energy storage capacitor bank of  $1.2\mu F$

in the thruster cathode electrode and it is coupled with an insulator pipe coated with a particular semiconductor. Fig.7.22 shows the MSL spark plug unmounted. The thruster electrode has a particular geometry that won't be discussed. The materials for both the electrodes are a Copper/Tungsten alloy, while the pipe insulator is made of Teflon and its surface is coated with not specified semiconductor layer. The insulator that serves to separate cathode and anode, wasn't provided. Hence, it was used some Kapton tape to do that. It has to be noticed that this spark plug wasn't brand-new and the Teflon pipe end-surface wasn't flat. Moreover this spark plug geometry is different from those one produced for this project. In particular they have been design to have a flat end-surface, with both the spark plug electrodes and the pipe insulator aligned. Instead, the MSL spark plug provided, has the thruster cathode electrode, the spark plug anode electrode and the insulator end-surface on different levels.

Former tests were made with MSL Spark Plug, MSL-SP, in air. These tests led to a breakdown between  $1.5kV$  and  $1.8kV$ . Fig.7.23 shows a typical breakdown current and voltage profiles. In the middle of these one, also the Rogowski coil signal is reported. The current peaks registered are between  $5A$  and  $-6A$ .



Figure 7.22: The MARS SPACE LTD spark plug and thruster cathode electrodes

After the air tests, the vacuum tests took place. Unfortunately the breakdown voltage slowly decreased, spark after spark, as a result of the Kapton tape layer degradation. At a certain point the thruster and plug electrodes shorted, bringing to spark plug failure. More exactly the breakdown still

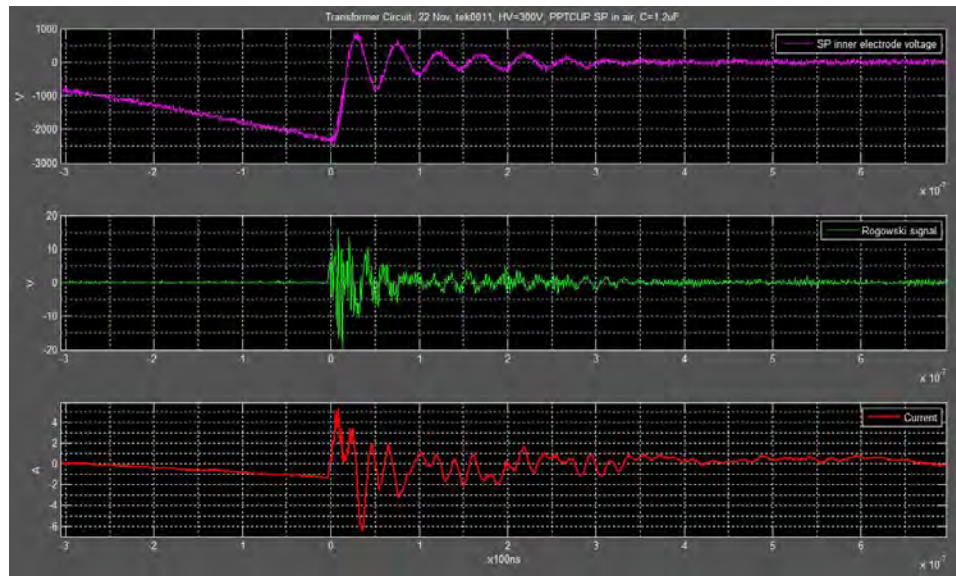


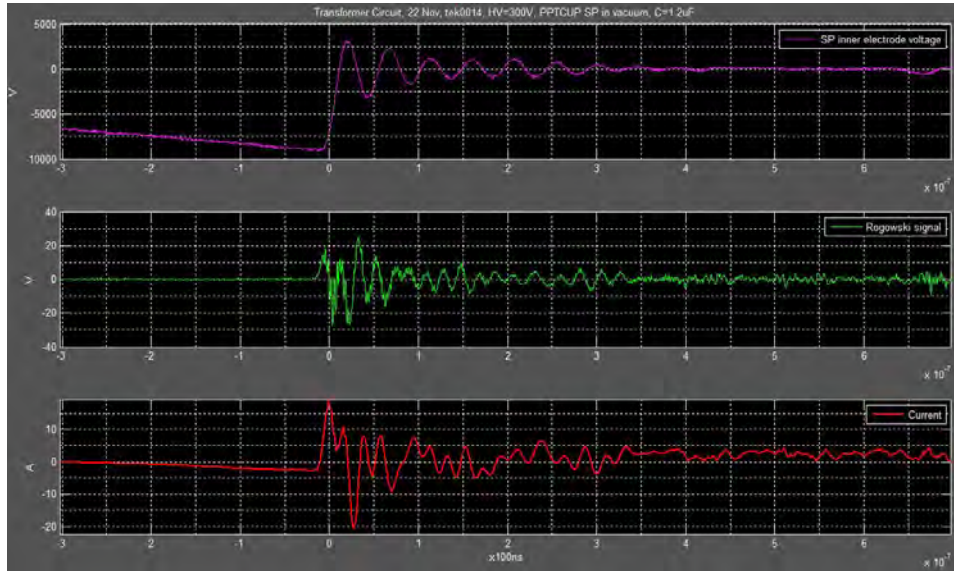
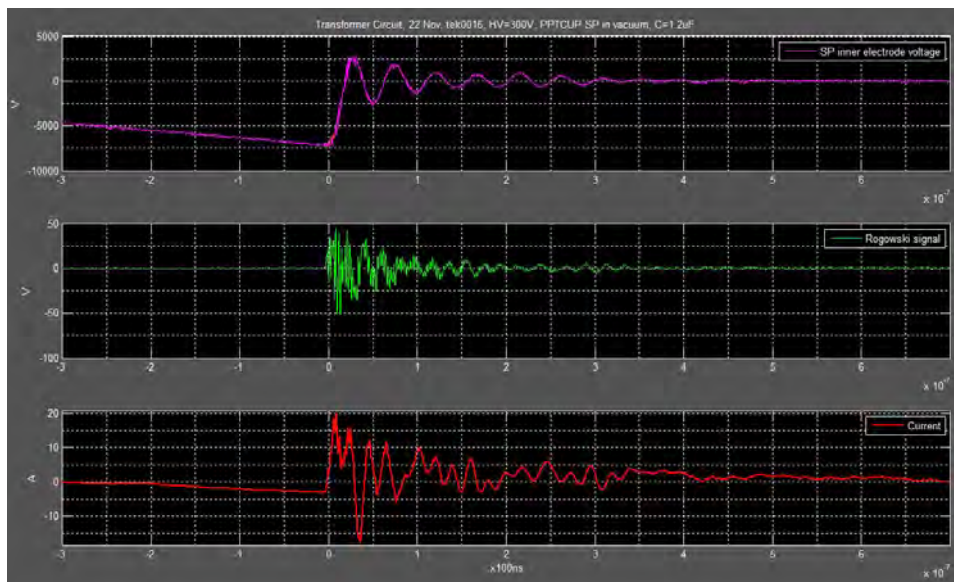
Figure 7.23: MSL-SP air test, typical breakdown voltage, Rogowski signal and current data

occurred, but at much lower voltage and with irregular and much longer signals. Some data before the Kapton failure are reported in Fig.7.24, 7.25 and 7.26. Respectively the breakdown voltage measured are:  $9kV$ ,  $7.3kV$  and  $4kV$ .

### 7.3.2 Manufactured Spark Plugs Tests

For the low manufacturing quality of the spark plugs, only three of them were able to generate repetitively the breakdown: the large insulator type SP1 and SP4, and the small insulator type SP5. The breakdown voltage firstly collected for these spark plug are summarized in Table 7.2, for the complete statistical overview see chapter 8, section 8.2.2. Unfortunately it isn't possible to compare the breakdown voltage between the MSL-SP, which uses a semiconductor coating on the insulator discharge surface, and the manufactured coaxial spark plugs. While the latter produced repetitively the breakdown, of course with shot to shot variations, the MSL-SP, because of the Kapton issue, decreased its breakdown voltage till premature failure.

While testing SP4, the breakdown in air test was 30% higher than that

Figure 7.24: MSL-SP vacuum test,  $V_b \approx 9000$ Figure 7.25: MSL-SP vacuum test,  $V_b \approx 7300$

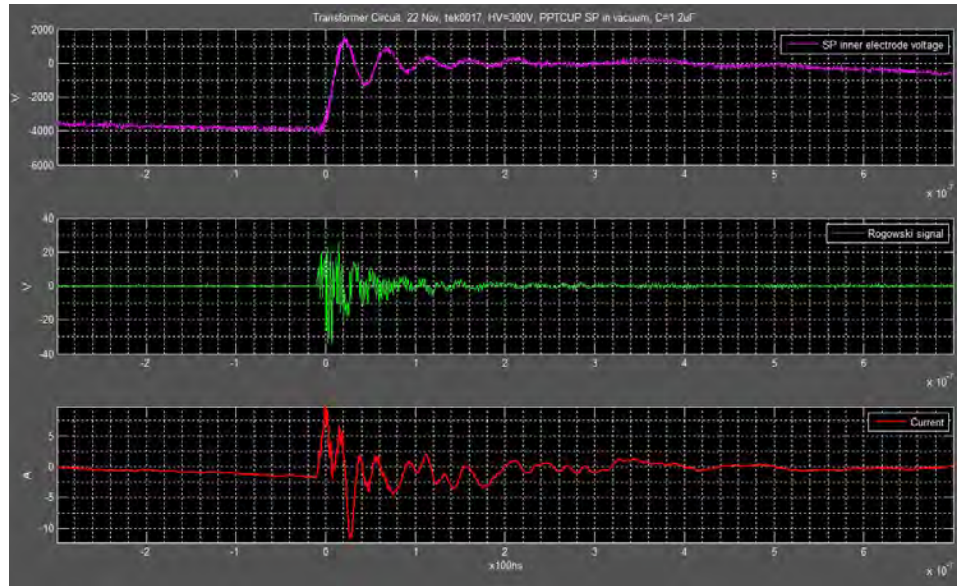


Figure 7.26: MSL-SP vacuum test,  $V_b \approx 4000$

one of SP1, which hypothetically should be identical. Obviously, also the vacuum breakdown was bad, such as with very high  $V_b$  and peak current (??). The cause was the lower quality of the spark plug breakdown surface, actually possible to check naked-eye. In fact there was non-regular space between the spark plug electrodes and the insulator alongside the ring circumference. For this reason the  $V_b$  happened to be almost 60% higher than with SP1. After the first breakdown the power MOSFET prematurely broke.

With the SP5 testing, a particular behavior was observed. Successively it will be noticed that also with the other spark plugs, SP1 and SP5, it occurs. Fig.7.28 shows that after the main breakdown, sometimes a succession of secondary sparks, at lower  $V_b$ , happens. In particular this phenomenon is more marked when the energy provided by means of the energy storage capacitor, is higher. In order to try to solve this inconvenient, the minimum voltage input,  $V_i$ , was found. By slightly increasing the input voltage, the minimum SP5  $V_i$  was found to be about 85V. Fig.7.29 shows that the breakdown occurred at about  $-4000V$ . After that voltage again goes down, because there's still energy into the secondary winding of the transformer.

Since, with  $V_i = 85V$ , the breakdown in vacuum didn't occur after ev-

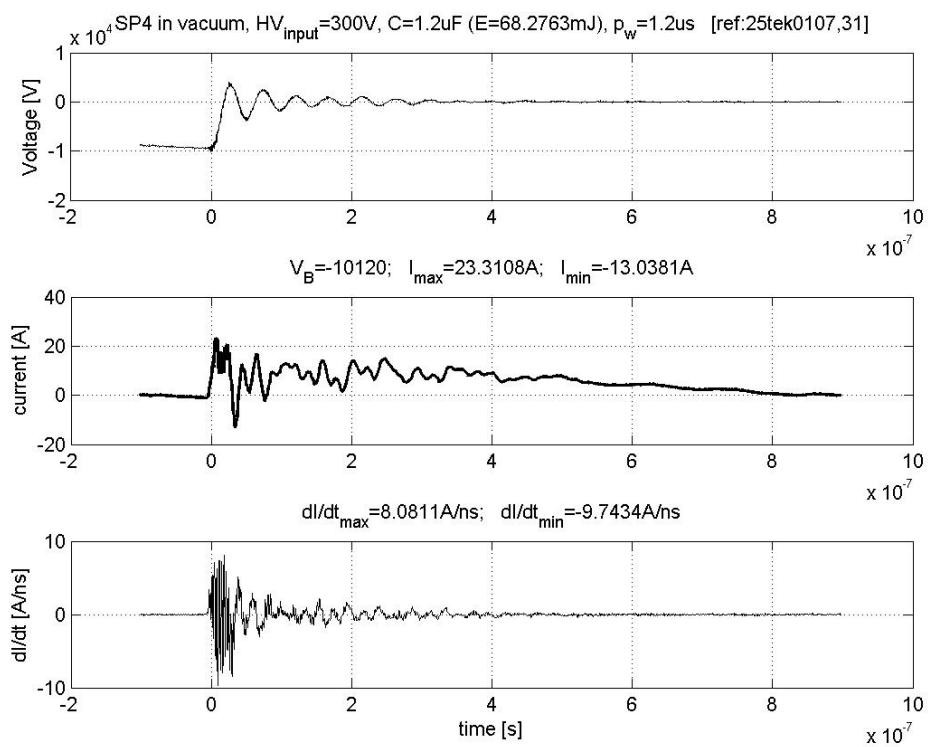


Figure 7.27: TIC with SP4 vacuum test,  $V_b \approx -10kV$ ,  $I_{max} \approx 23A$

ery trigger pulse , it was increased to  $V_i = 200V$  that seemed to ensure breakdown continuity. But of course, increasing the input voltage, also the energy increases, for instance with the voltage squared value. Therefore, sometimes secondary breakdown occurred (7.30). From these consideration, the conclusion about the TIC are:

- if the energy provided to the spark plug is too high, secondary spark can occur;
- not all the energy in the tests is consumed in a single spark. The reason can be that for the SP characteristics (size, geometry, materials, finishing), the maximum energy that it can deliver by means of a vacuum arc, is lower than that one provided.

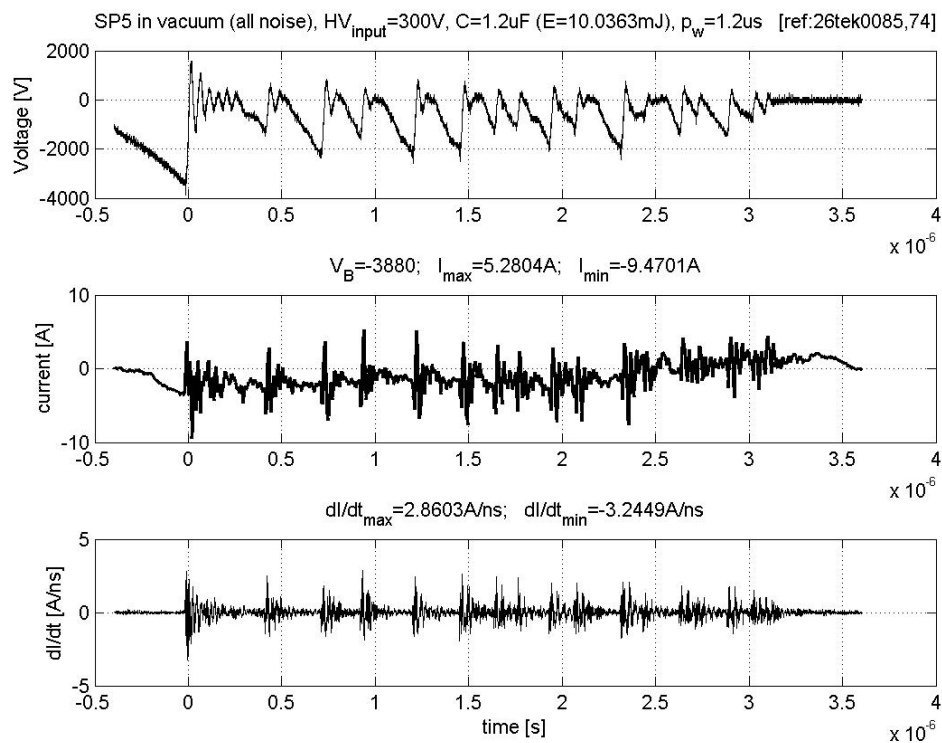


Figure 7.28: TIC with SP5 vacuum test, multiple breakdowns

<sup>6</sup>Only one measurement before MOSFET failure

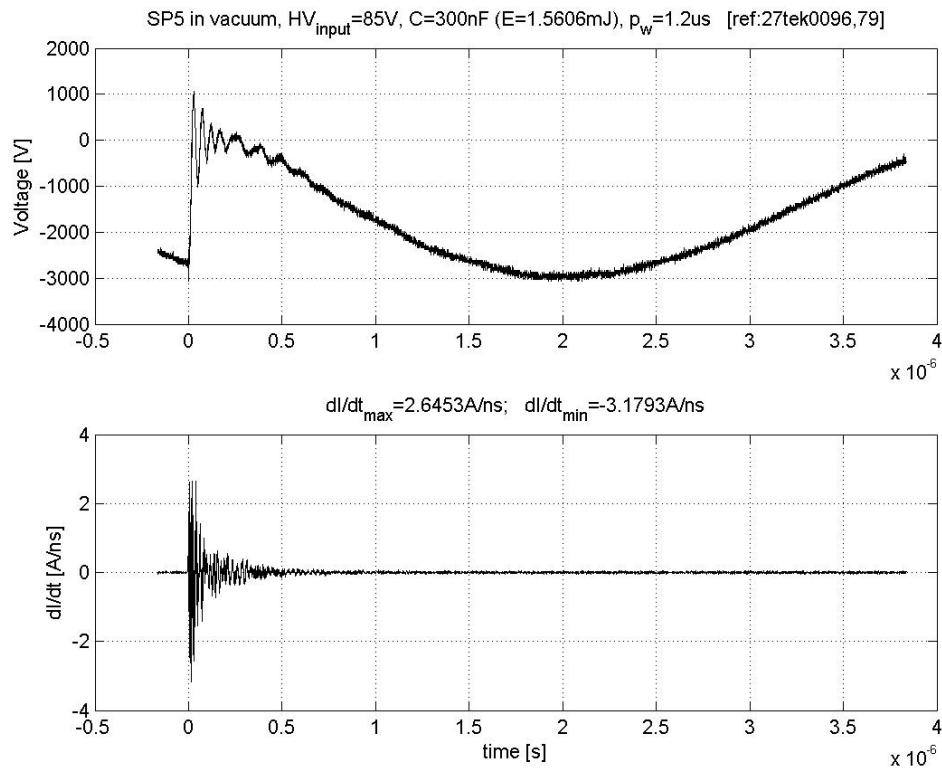
Figure 7.29: TIC with SP5 vacuum test, minimum  $V_i$  to have breakdown

Table 7.2: Summarizing table of manufactured spark plugs breakdown voltage

Spark Plug	Air test ( $kV$ )	Vacuum test ( $kV$ )
SP1	[2.6, 3.0]	[3.5, 5]
SP4	[3.2, 3.6]	7.6 <sup>6</sup>
SP5	[1.8, 2.2]	[3.8, 5.2]

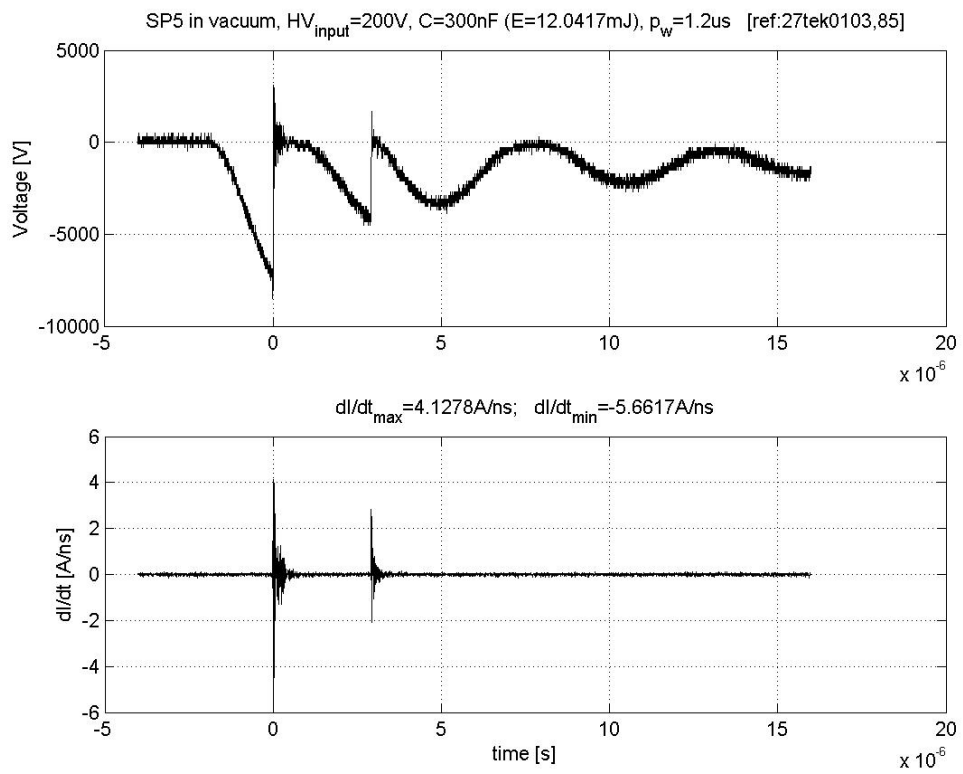


Figure 7.30: TIC with SP5 vacuum test, secondary breakdown with  $V_i = 200V$

Complete statistical values of the TIC breakdown experiments, are reported in section 8.2.1 and the most important data collected and processed are shown in appendix A, section A.1.



## Chapter 8

# Semi-empirical Breakdown Model

### 8.1 Foreword

A semi-empirical model for the MOSFET Ignition Circuit (attempt 3), has been realized. The current measurements made by the Rogowski coil, are considered valid above about 10A of peak current. Under this value the current measurements aren't enough accurate. This condition occurs in the transformer air tests. Before to consider a semi-empirical model of the spark plug breakdown, the data collected for both MIC and TIC have been evaluated statistically.

### 8.2 Statistical Data

#### 8.2.1 MOSFET Ignition Circuit statistics

The experiments that have been consider with a statistical value for the MOSFET Ignition Circuit (all in air), are shown in Tab.8.1 and summarized in the following:

- SP1 with graphite coating,  
 $HV = 1kV$ ,  $C = 4.4nF$ ,  $p_w = [100ns, 200ns, 400ns]$ ;
- SP1,  $HV = 2.5kV$ ,  $C = 0.5nF$  ( $E = 1.6mJ$ ),  $p_w = 150ns$ ;

- SP1,  $HV = 3.5kV$ ,  $C = 0.33nF$  ( $E = 2.02mJ$ ),  $p_w = 150ns$ .

### 8.2.2 Transformer Ignition Circuit statistics

The experiments that have been consider with a statistical value for the Transformer Ignition Circuit, are the following:

**MSL-SP statistic values**, the row of Tab. 8.2 refers to following test parameters: AIR,  $C = 1.2\mu F$ ,  $V_i = 300V$ .

**SP1 statistic values**, each row of Tab. 8.3 refers to following test parameters:

- row1: AIR,  $C = 1.2\mu F$ ,  $V_i = 300V$ ;
- row2: VACUUM,  $C = 1.2\mu F$ ,  $V_i = 120V$ ;
- row3: VACUUM,  $C = 1.2\mu F$ ,  $V_i = 140V$ ;
- row4: VACUUM,  $C = 1.2\mu F$ ,  $V_i = 160V$ ;
- row5: VACUUM,  $C = 1.2\mu F$ ,  $V_i = 300V$ .

**SP4 statistic values**, each row of Tab. 8.4 refers to following test parameters:

- row1: AIR,  $C = 1.2\mu F$ ,  $V_i = 300V$ .

**SP5 statistic values**, each row of Tab. 8.5 refers to following test parameters:

- row1: AIR,  $C = 150nF$ ,  $V_i = 300V$ ;
- row2: VACUUM,  $C = 300nF$ ,  $V_i = 200V$ ;
- row3: VACUUM,  $C = 1.2\mu F$ ,  $V_i = 300V$ .

Table 8.1: SP1 MIC tests, average and standard deviation of  $I_{max}$  and  $dI/dt_{max}$ 

$p_w =$	100ns	200ns	400ns	150ns	150ns
$HV =$	1kV	1kV	1kV	2.5kV	3.5kV
$\overline{I_{max}}$	22.7126	24.8772	26.2478	22.4684	30.8166
$\sigma_{I_{max}}$	4.0144	4.0939	1.6390	0.7796	4.4613
$\overline{dI/dt_{max}}$	0.9890	1.0757	0.8082	1.9178	3.3537
$\sigma_{dI/dt_{max}}$	0.2110	0.1046	0.1624	0.1504	0.5517

Table 8.2: MSL-SP TIC tests, average and standard deviation of  $V_B$ ,  $I_{max}$  and  $dI/dt_{max}$ 

$\overline{V_B}$	$\sigma_{V_B}$	$\overline{I_{max}}$	$\sigma_{I_{max}}$	$\overline{dI/dt_{max}}$	$\sigma_{dI/dt_{max}}$
-2800	313.4	6.1805	0.99187	0.93843	0.29362

Table 8.3: SP1 TIC tests, average and standard deviation of  $V_B$ ,  $I_{max}$  and  $dI/dt_{max}$ 

$\overline{V_B}$	$\sigma_{V_B}$	$\overline{I_{max}}$	$\sigma_{I_{max}}$	$\overline{dI/dt_{max}}$	$\sigma_{dI/dt_{max}}$
-2802.7	225.95	6.0972	0.66588	0.86174	0.19795
-5960	1002.2	12.253	2.0971	5.3632	0.98166
-6216	497.67	13.028	0.82119	5.7139	0.57683
-6212.9	1065	12.999	2.3351	5.4053	0.99093
-4104	684.35	8.1802	3.3854	3.3413	0.9986

Table 8.4: SP4 TIC tests, average and standard deviation of  $V_B$ ,  $I_{max}$  and  $dI/dt_{max}$ 

$\overline{V_B}$	$\sigma_{V_B}$	$\overline{I_{max}}$	$\sigma_{I_{max}}$	$\overline{dI/dt_{max}}$	$\sigma_{dI/dt_{max}}$
-3450.7	110.01	6.1979	0.50776	2.0521	0.43777

Table 8.5: SP5 TIC tests, average and standard deviation of  $V_B$ ,  $I_{max}$  and  $dI/dt_{max}$

$\overline{V_B}$	$\sigma_{V_B}$	$\overline{I_{max}}$	$\sigma_{I_{max}}$	$\overline{dI/dt_{max}}$	$\sigma_{dI/dt_{max}}$
-2029.7	120.47	2.8021	0.41068	1.0454	0.13689
-5336.8	1062.9	9.5648	1.9661	3.6706	0.74359
-6410.5	1234.8	11.858	2.5943	5.9075	1.0845

### 8.3 RLC Series Circuit Semi-empirical Model for MIC

A semi-empirical model for the MIC3 (using STW9N150 power MOSFETs) spark plug breakdown, has been created using MATLAB. The model is based on the resolution of a series RLC circuit, considering R, L and C constants. Each component has the following meaning:

- $R_{TOT}$ : total resistance. The resistance value includes the contribution of the MOSFET switch equivalent  $R_{DS_{ON}}$ , the spark plug breakdown resistance  $R_B$  and the MIC tracks resistance in series. The last value is considered to be approximately zero;
- $C_{TOT}$ : energy storage capacitor. The value of the total capacitance is fixed for each experiment, considering the energy storage capacitor the only contribution;
- $L_{TOT}$ : total inductance. The inductance value includes the contribution of the MIC inductance and the spark plug breakdown inductance.

Let apply the Kirchhoff's voltage law to the circuit shown in Fig.8.1<sup>1</sup>:

$$\begin{cases} V_R(t) + V_L(t) + V_C(t) & = const \\ Ri(t) + L\frac{di}{dt} + \frac{1}{C}\int_{t=\tau}^{-\infty} i(\tau)d\tau & = V_{cap} \end{cases} \quad (8.1)$$

Differentiating second of eq.8.1 and dividing by L, the ODE equation to integrate results:

$$\frac{d^2i}{dt^2} + \frac{R}{L}\frac{di}{dt} + \frac{1}{LC}i(t) = 0 \quad (8.2)$$

Normally expressed with the parameters  $\alpha$ , the *attenuation*, and  $\omega_0$ , the *angular resonance frequency*:

$$\frac{d^2i}{dt^2} + 2\alpha\frac{di}{dt} + \omega_0^2i(t) = 0 \quad (8.3)$$

The MATLAB script accomplishes the following steps:

---

<sup>1</sup>NOTE: the current in the model is called  $i(t)$ , while the current measured in the experiment is called  $I(t)$ .

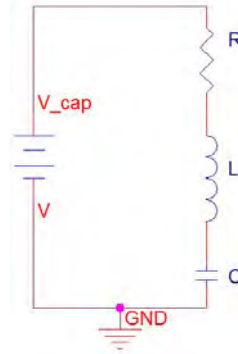


Figure 8.1: RLC series circuit schematic

1. load the data of a single experiment. In particular, it load the breakdown peak current,  $I_{max}$ , and the maximum current derivative  $dI/dt_{max}$ ;
2. solve the differential eq.(8.2), implemented as a system of 2 ODE:

$$\begin{cases} y'(1) = y(2) \\ y'(2) = -R/L \cdot y(2) - 1/LC \cdot y(1) \\ \quad + i.c. \\ y_0(1) \\ y_0(2) \end{cases} \quad (8.4)$$

Where  $y(1)$  is the current  $i(t)$ , and the initial condition are taken as  $y_0(1) = i(0) = 0A$  and  $y_0(2) = di/dt(0) = 2dI/dt_{max}$ . The solver used is the *ode23s*, good for stiff differential equations. As already mentioned the model uses constant values of R, L and C. Therefore, for the first resolution of the model the value of R and L are taken from the *critically damped* case. In this case the analytical solution of  $i(t)$  can be found imposing the initial conditions. Then, calculating the derivative and posing it equal to zero, it is possible to find the time which maximize  $i(t)$ :

$$t_{max} = 1/\alpha \quad (8.5)$$

Substituting this value in the current equation, the values of R and L,

in the critically damped case, can be found:

$$\begin{cases} L_c &= (e^2 i_{max}^2) / (C y_0 (2)^2) \\ R_c &= 2\sqrt{L_c / C} \end{cases} \quad (8.6)$$

Where  $e$  is the Euler's number and I put  $i_{max} = I_{max}$ . At this step, the time evolution of  $i(t)$  and  $di/dt(t)$  have been found;

3. starting from the critically damped solution, through an iterative cycle<sup>2</sup> the value of the inductance is increased or decreased in order to adjust the  $V_{cap}$  value. The final value requested is the high voltage,  $HV$ , at which the capacitor is charged at the beginning of the experiment;
4. a following iterative procedure adjusts the value of the resistance. Changing this value, the maximum current changes. In particular by decreasing  $R$ , the peak current increases. Hence, a final value of  $R$  is chosen iteratively asking the current peak to be equal to the experimental value, with a tolerance.
5. the final solution is plotted together with the experimental breakdown.

In addition to the script procedure, if the resulting current doesn't fit the experimental data, by trial and error a lower value of  $HV$  is chosen, until the right value is selected. This strategy is adopted when the breakdown doesn't consume all the energy stored into the capacitor. In fact, during the experimentation, it was noticed that sometimes the  $V_{cap}$  didn't go to zero after the breakdown. This information wasn't sure at early experiment, but later it was confirm by measuring  $V_{cap}$  with a multimeter and a DC high voltage probe.

A brief discussion of the model is necessary. Fig.8.1 is not the same as the circuit configuration. Let consider Fig.7.12 (page 75). The left branch can be excluded from the model because it doesn't affect the breakdown. In fact, the HVPS is limited in current, and the charge constant of the capacitor is very big in comparison with the breakdown discharge time. In particular,  $\tau_{charge} = R \cdot C$ , is on the order of  $k\Omega \cdot nF = o(\mu s)$ , while the discharge

<sup>2</sup>the ODE system, described by eq.(8.4), is solved for each iteration.

time is ten time faster  $\Omega \cdot nF = o(ns)$ . Moreover, it was checked during experimentation, that disconnecting the HVPS, the breakdown data doesn't change in terms of noise. For this reason, it has to be considered in the model only the second and third branches.

The second branch of Fig.7.12, contain the capacitor charged at  $HV$ . The right branch during the breakdown, can be considered as an RL circuit, where L and R are the sum of the spark plug, power MOSFET switch and circuit inductances and resistances. The equivalence of the RLC series circuit and the breakdown MIC approximation described above, follows from the equivalence, with opposite sign, of the current  $i(t)$  in the following two cases: capacitor, charged at  $HV$ , that discharges through R and L; capacitor charging, to  $HV$ , through R and L. Hence, when in an experiment the breakdown doesn't discharge completely the capacitor, the equivalent model is obtained selecting a lower  $HV$ .

An complete example of the above described procedure is shown in the Fig.8.3 and 8.4. In appendix A, a set of model examples is reported. For each of these examples, the damping factor,  $\zeta = R/2\sqrt{C/L}$ , is also reported. Among the data analyzed, is possible to notice a wide range of  $\zeta$ , from 0.4 to 1.47 depending on the different experiment parameters. It has to be noticed that the initial condition  $di/dt(0)$ , has been taken as  $2dI/dt_{max}$  rather than  $dI/dt_{max}$ . This fact has been noticed occasionally and can be attributed to following reason: the RLC series model, is a second order ODE model while the breakdown is of higher order. In fact a second order model can describe an oscillation either exponentially convergent or divergent, but not both cases at the same time. The model is clearly an approximation of the breakdown using the MIC circuit but fits quite well the experimental data. In some cases it is possible to distinguish more the one current peak, like that one reported in Fig.8.2. Possibly, the meaning is that a second breakdown occurs immediately after the first one, causing the double current peak. This can be attributed to the formation of another plasma jet located in another on the spark plug surface.

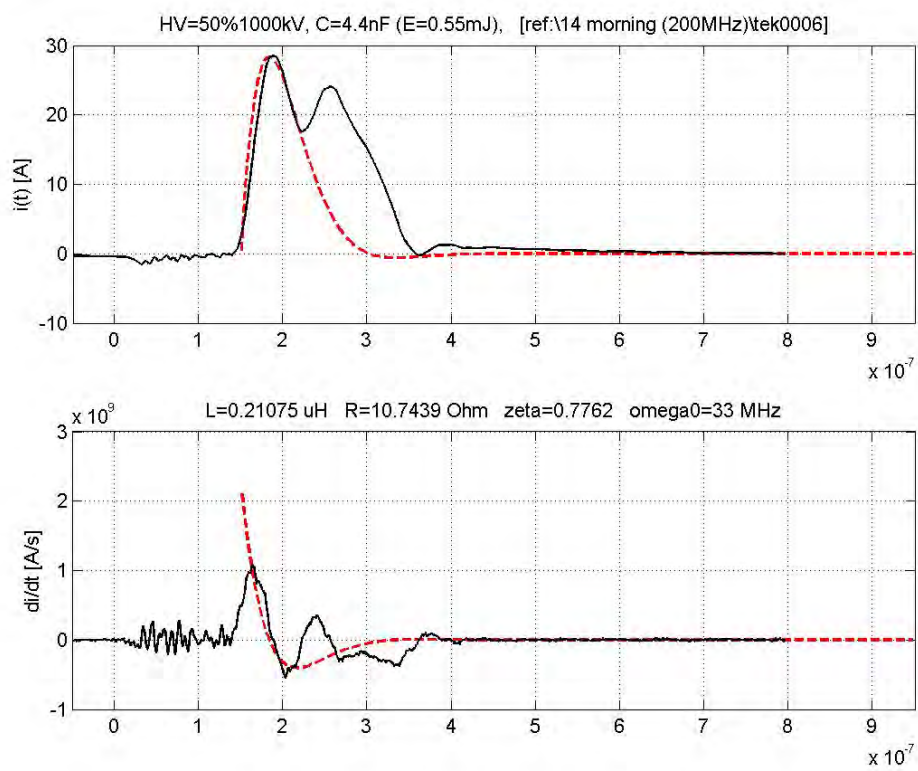


Figure 8.2: Case of double peak current

Figure 8.3: RLC series modeling: step 2 and 3

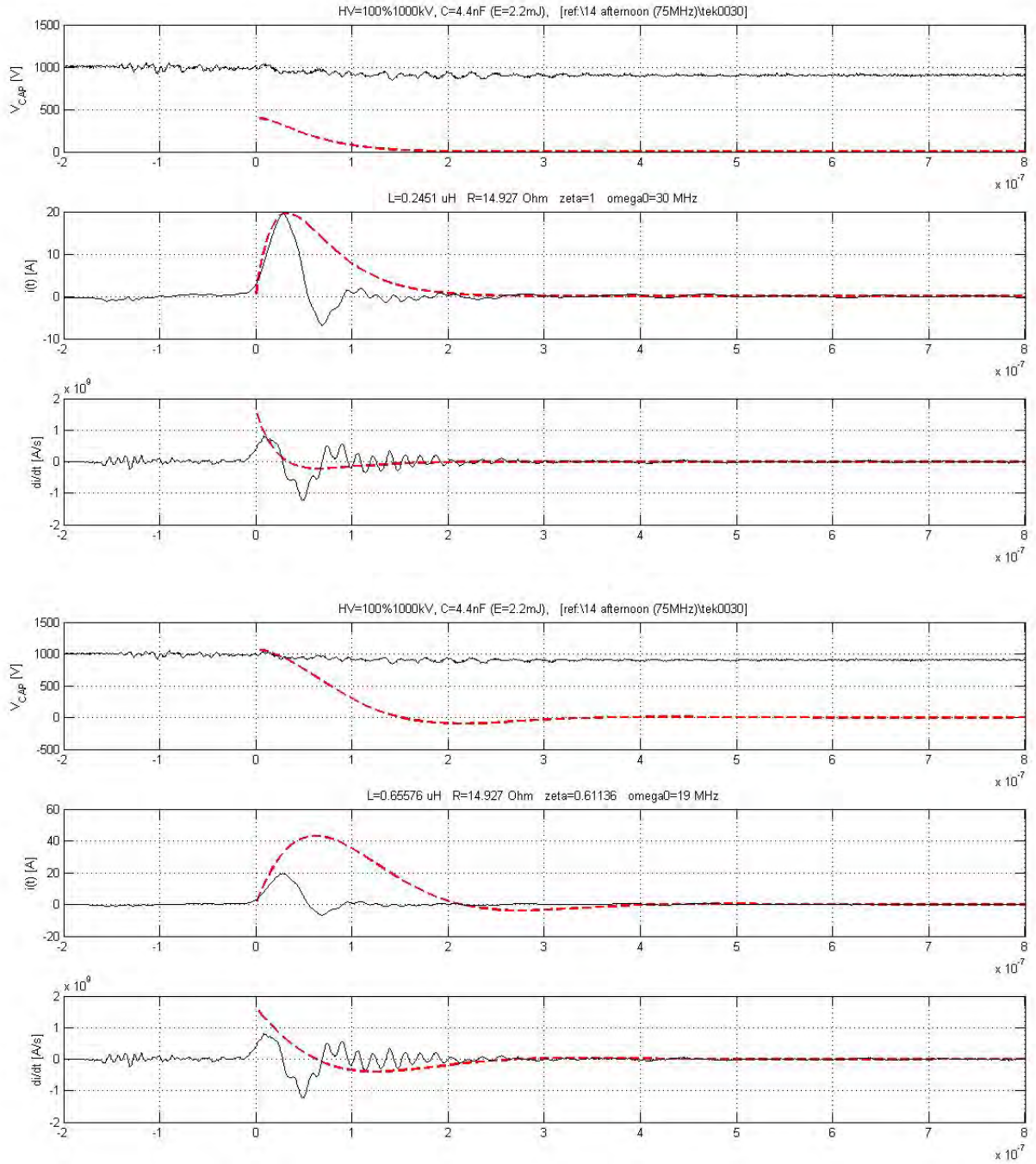
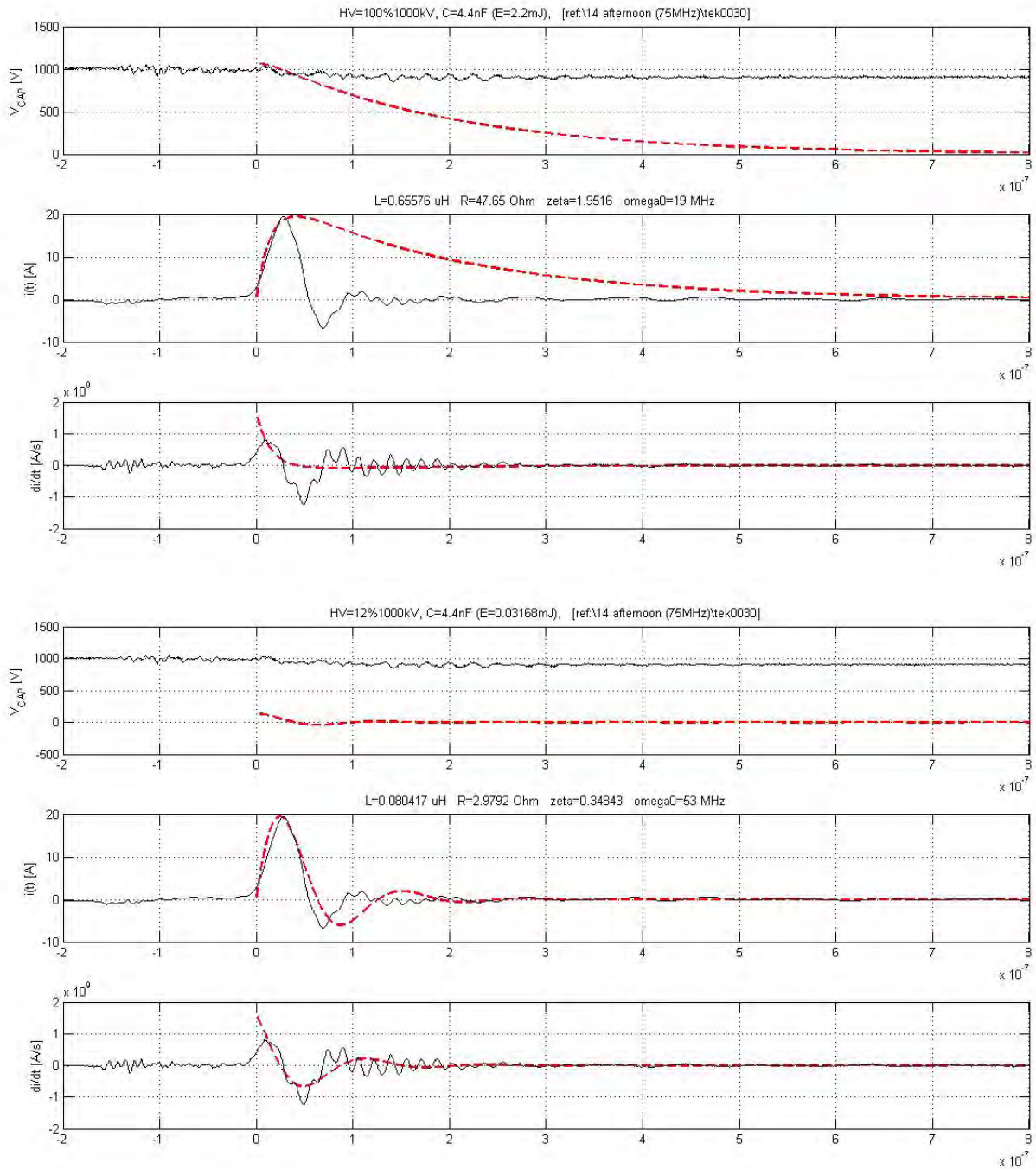


Figure 8.4: RLC series modeling step 3 and  $HV$  correction



# Summary and Conclusions

After the literature review made on the Pulsed Plasma Thruster spark plug lifetime problem, it was clear that the parameters involved-in were too many to investigate together in a six months period of research. In particular the thesis project has been started from zero, with the purpose to produce some test facility to look into some new aspect of the problem. Some conclusions have been made and summarized in the following.

Let compare the breakdown voltages of the spark plugs with the predictions made through the Paschen curve and with the Boxman et al.[5] observations made in section 5. Table 8.6 shows the comparison between the two predictions considering the insulator size of the big-SP and small-SP. The following nomenclature adopted (VAST: *Handbook of Vacuum Arc Science and Technology - Fundamentals and Application* [5]), means the breakdown voltage predictions, as it follows:

- VAST A: considering two electrodes in air;
- VAST A+I: considering two electrodes in air bridged by an insulator;
- VAST V: considering two electrodes in vacuum;
- VAST V+I: considering two electrodes in vacuum bridged by an insulator;

Making a comparison with the experimental results of the breakdown voltage (section 8.2.2), some conclusions can be made:

1. the average big-SP (SP1 and SP4) breakdown voltage in air tests, is similar to the Paschen value. For this reason, these spark plugs probably didn't use the insulator as means of breakdown, but the breakdown

Table 8.6: Comparison of breakdown voltage predictions made through the Paschen curve and Boxman et al. observation in VAST

$V_B$	Paschen (V)	VAST A (V)	VAST A+I (V)	VAST V (V)	VAST V+I (V)
big-SP	3,000	1,800	600	6,000	2,000
small-SP	1,500	750	250	2,000	825

occurred through air. If the breakdown, registered during the air tests, was less than  $1kV$ , it would occurred using the insulator;

2. the same considerations count for the small-SP;
3. the average SP1 breakdown voltage in vacuum tests, are similar to the VAST V values. This means that probably this spark plug didn't use properly the insulator surface to lower the breakdown voltage. Anyway SP4 registered higher  $V_b$ , that means SP1 has better manufacture quality;
4. the average small-SP, SP5, breakdown voltage in vacuum tests, are higher than the VAST V value. This means that is almost sure that the breakdown of this spark plug never occurred using the insulator.

The general conclusion on the spark plugs breakdown voltage, is that all the spark plug are not well manufactured, otherwise they didn't ensure sufficient continuity between electrodes and insulator. One spark plug showed better behavior in this sense, SP1. For this reason, it is to notice that over the 5 spark plugs produced, only one of them was decent.

During the literature review on the high voltage pulse generator, the MOSFETs circuit has been selected as a good candidate to produce a very short-pulse-length ignition and in particular with very fast rise time. Then, the direction of the MSc thesis project looked mostly toward the research of advantages/disadvantages obtainable using a classic transformer-based ignition circuit versus a MOSFET-based ignition circuit.

A reliable MOSFETs Ignition Circuit is MIC3, where the spark plug is forced to breakdown immediately after the MOSFETs switch closure. As a

result, the energy storage capacitor discharges through the discharge vacuum arc, formed on the spark plug surface, in series with the equivalent MOSFETs switch resistance ( $R_{MOSFET,Switch} = R_{DS(on)} \times 5$ ). Not only the spark plug impedance, but also the MOSFETs resistance changes in time, in particular with  $I_D$  and the junction temperature. Hence, the discharging profile is exponentially decaying and gives a current mostly positive and larger with respect of the Transformer Ignition Circuit (considering the same switch device).

Finally, in this MSc thesis project, for the reasons already specified, the spark plugs manufactured didn't use a semiconductor coated insulator. It follows a relatively high breakdown voltage, sometimes higher than that one estimated, because of the materials and manufacture low quality (in particular surface smoothness and mechanical matching of the spark plug electrodes and insulator). For future work the following suggestion go in the direction of further investigation on the MOSFETs Ignition Circuit application:

- test this circuit using semiconductor type spark plugs with low breakdown voltage, on the order of  $100V$ ;
- consider to test a parallel-MOSFETs Ignition Circuit in order to carry higher current. In fact, while in the series MOSFETs circuit the capacitor discharge through the SP and the five  $R_{DS(on)}$  in series, in this case a fraction of the current is taken by each MOSFETs.

The power MOSFET device provides fast operation ( $MHz$ ) with respect of the IGBT rather than the SCR devices, which have respectively a frequency domain on the order of  $10 - 100kHz$  and  $100Hz$ . On the other hand the power MOSFET have a lower power rating, hence lower peak voltage and current. These limitation can be overcome by utilizing different architectures, like the mentioned parallel or the experimented series MOSFET configuration, and maintaining the fast operation. Of course the peak power limitation exists but it has to be investigated the possible applications of such Ignition Circuit.

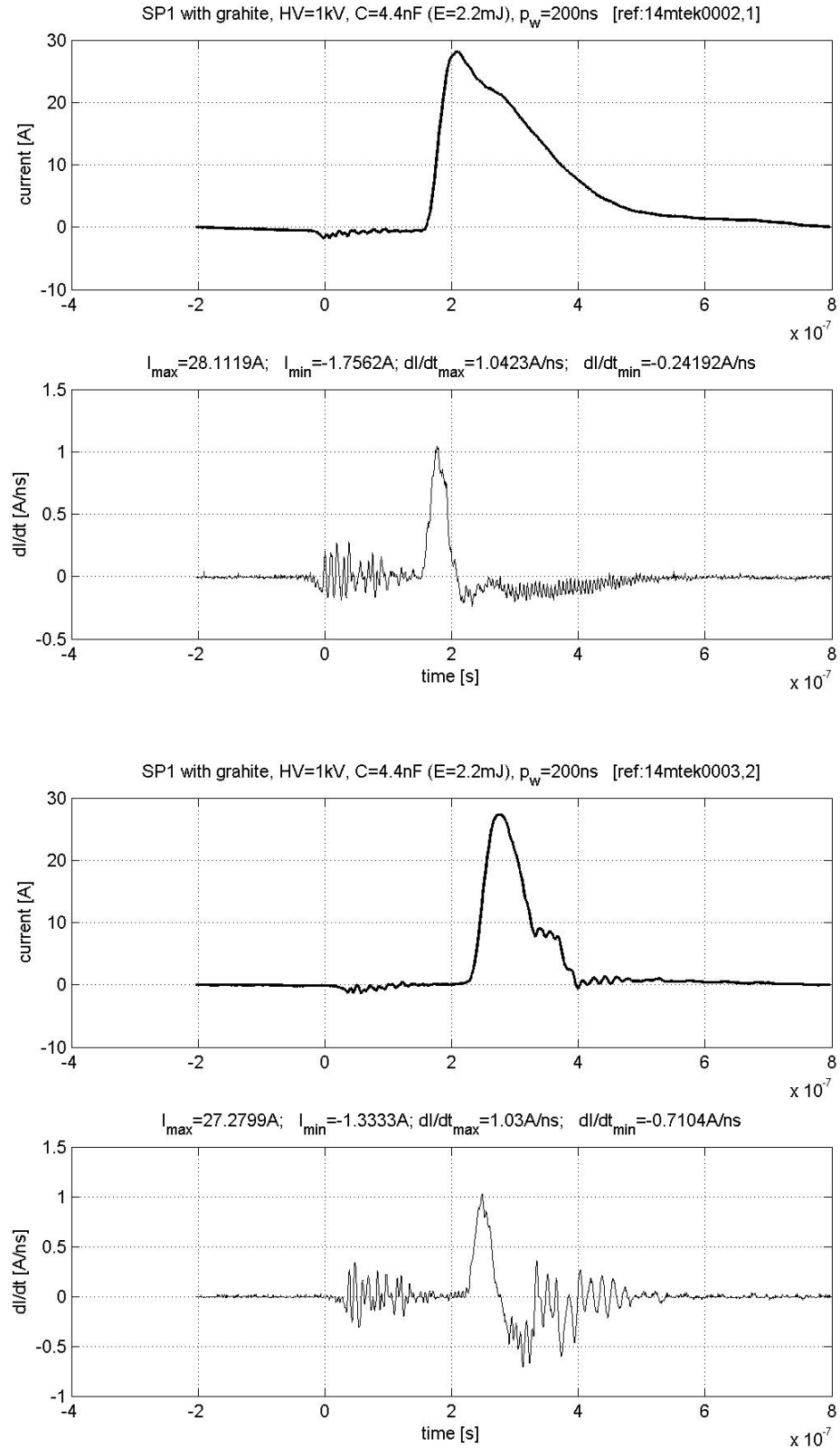
For what concerns the spark plug manufacturing an important fact has been notice observing the behavior of the TIC. In particular, the spark plug

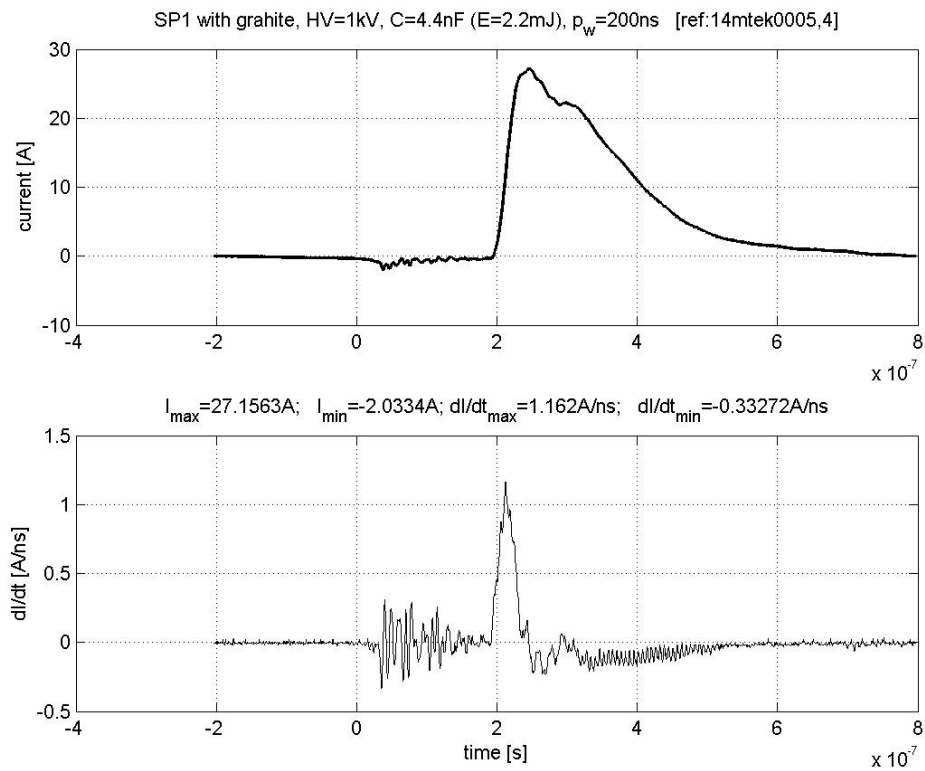
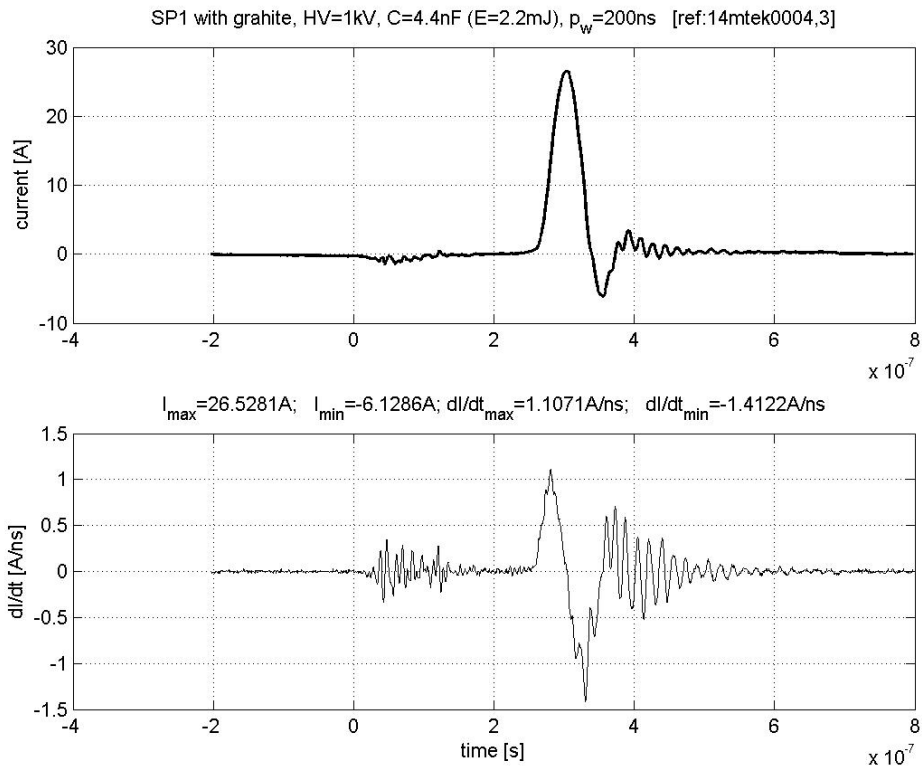
should be designed to provide the right amount of energy for the PPT ignition. This means that, in the particular analyzed case of coaxial and flat end-surface spark plug, the property of the breakdown surface must guarantee to sustain the vacuum arc for a sufficient time. Of course, the circuit must be designed to assure a low impedance in order to provide the highest peak current possible.

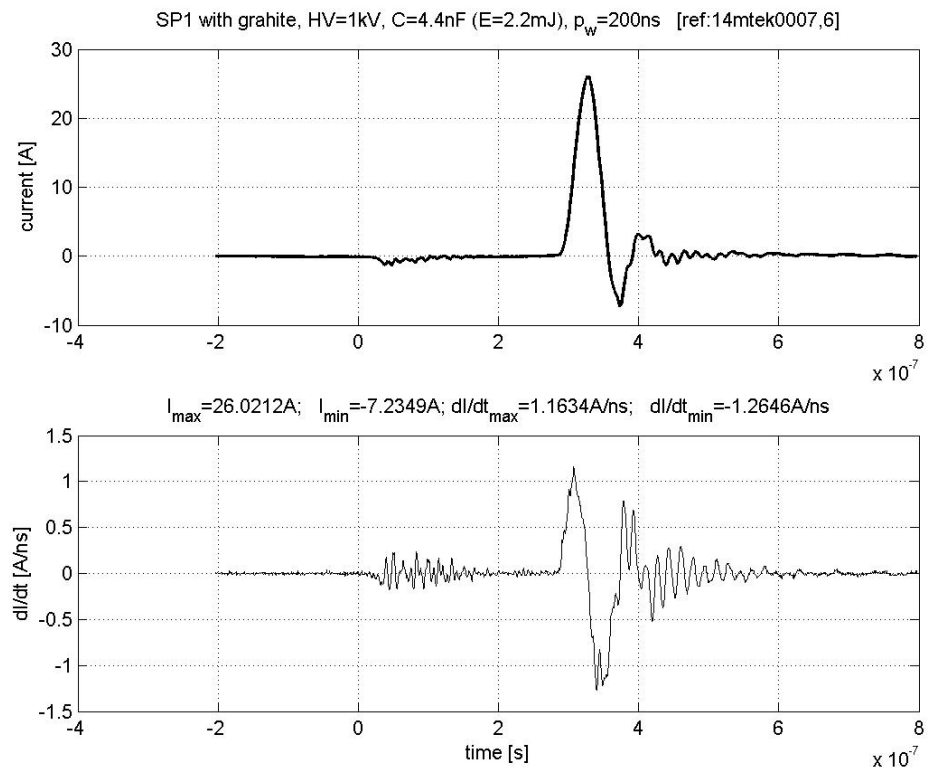
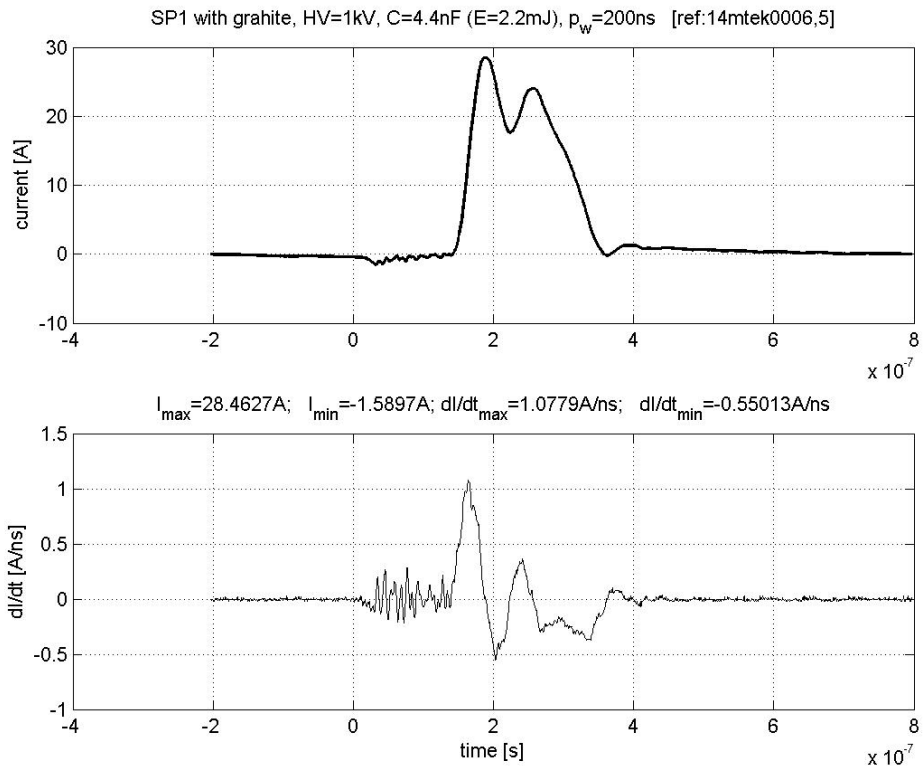
## Appendix A

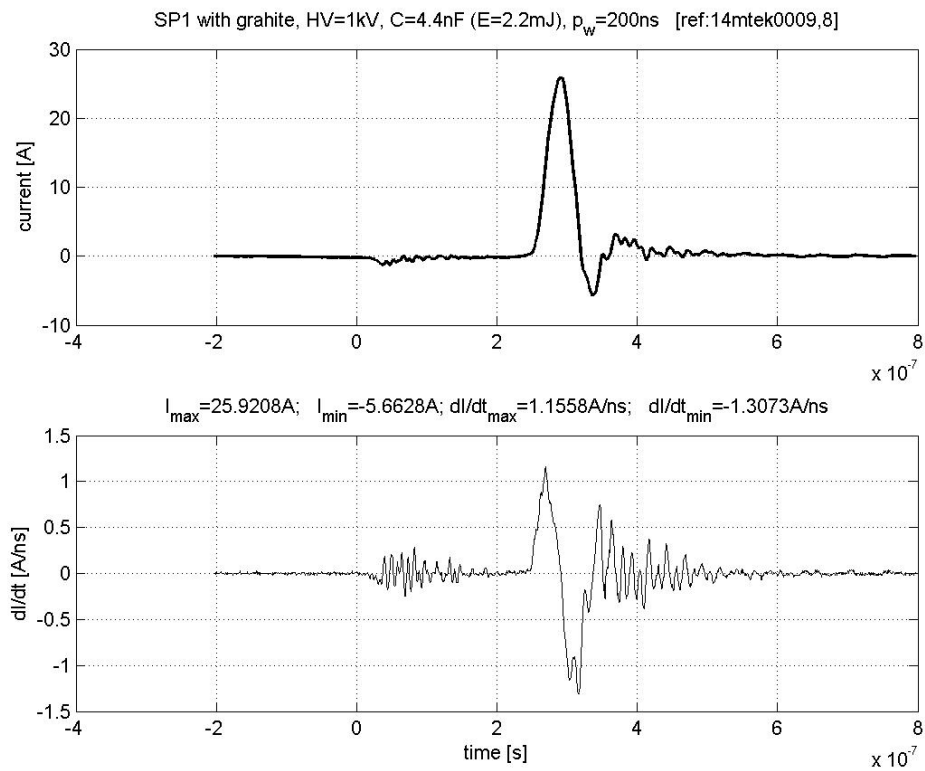
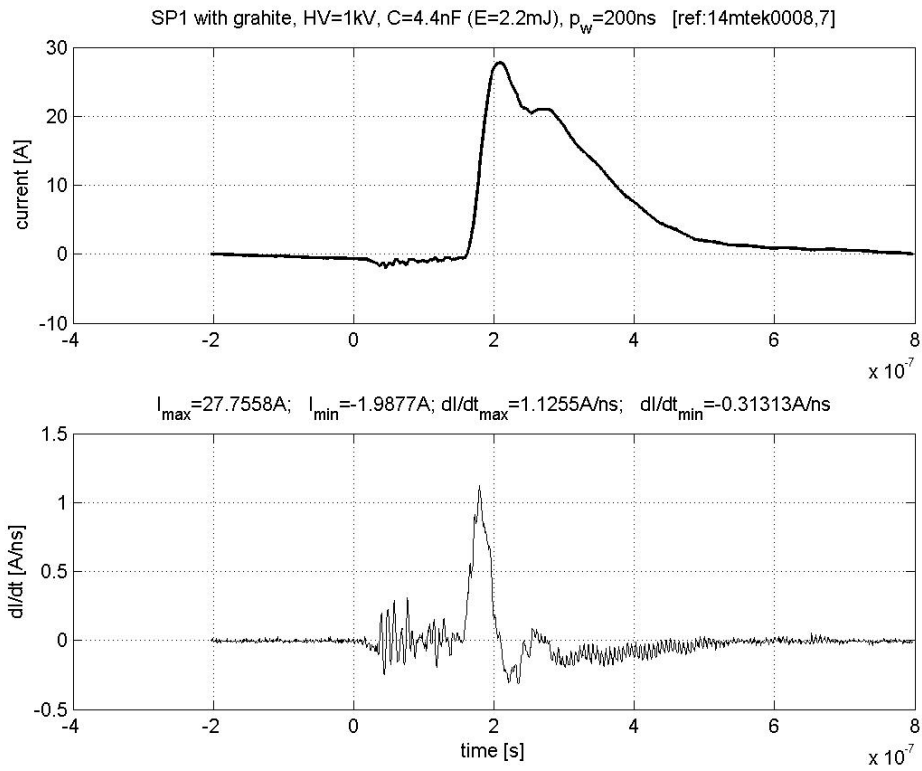
# Experimental Data and RLC Series Model

### A.1 Experimental Data

Figure A.1: MIC, SP1 with graphite breakdown tests ( $p_w = 200ns$ )







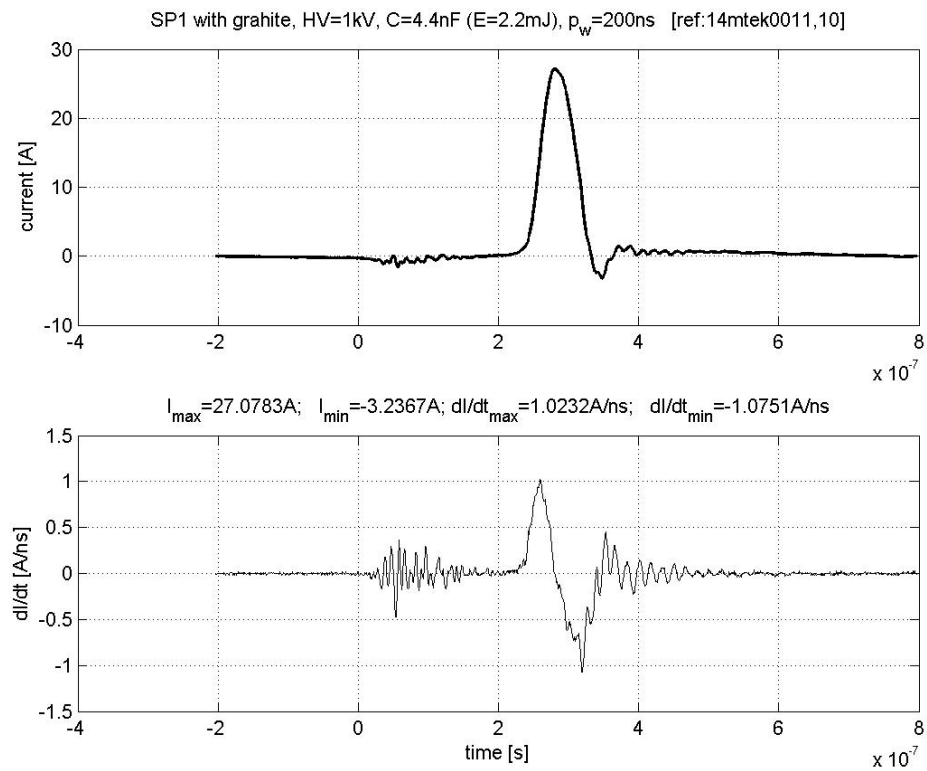
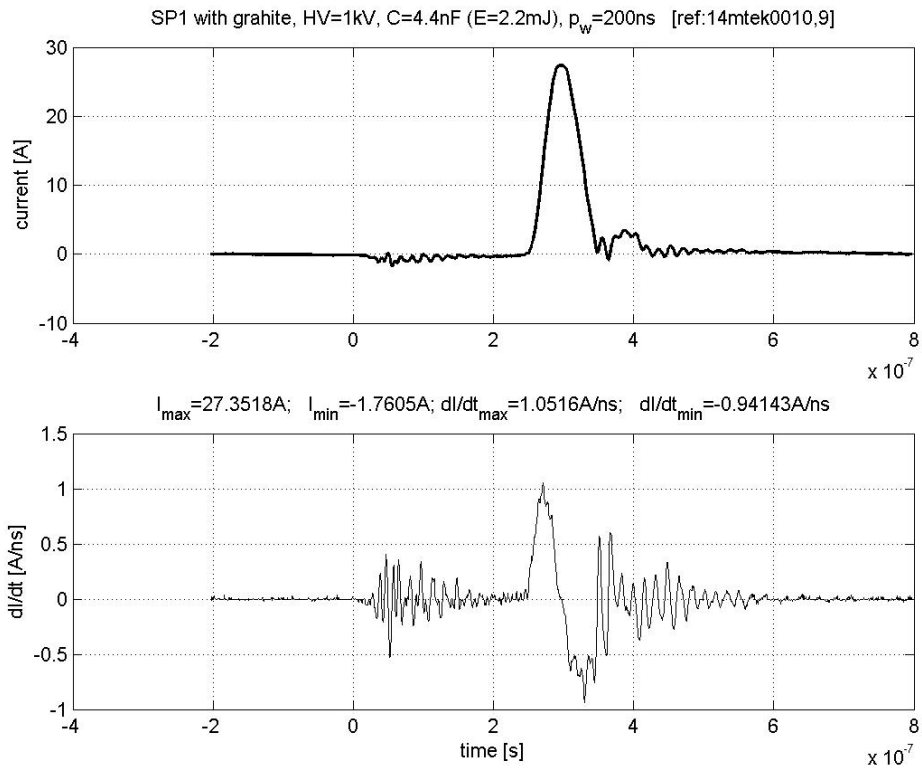
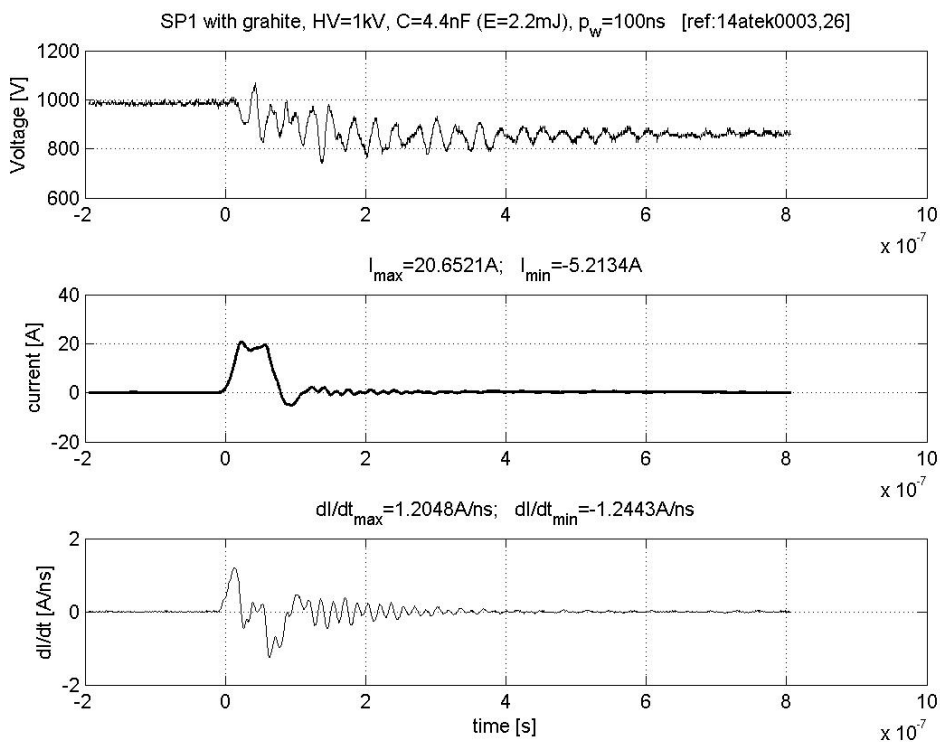
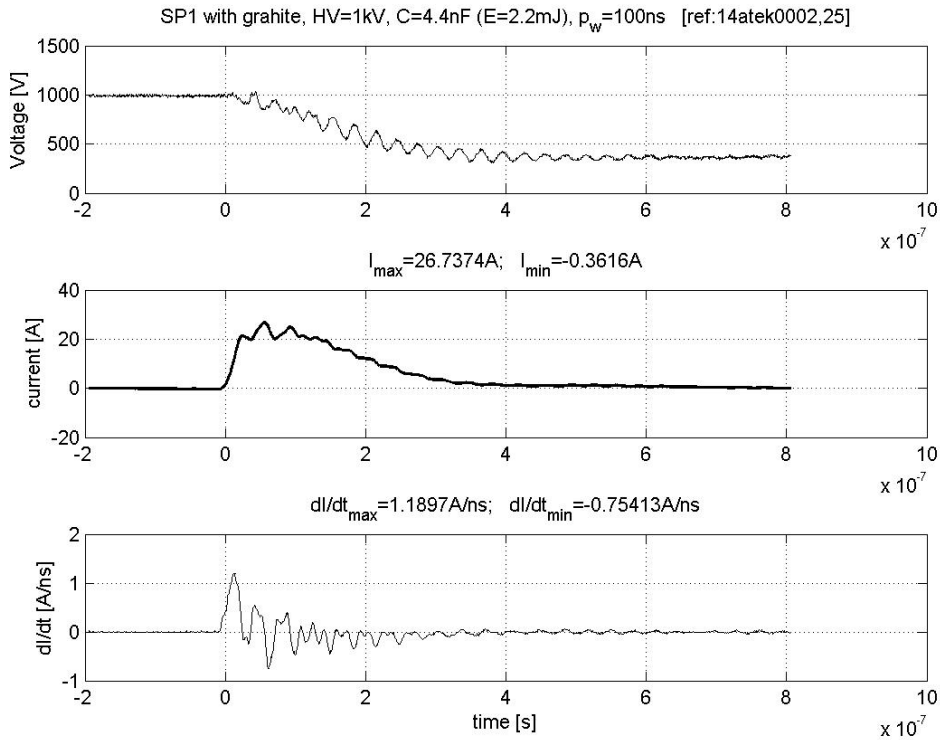
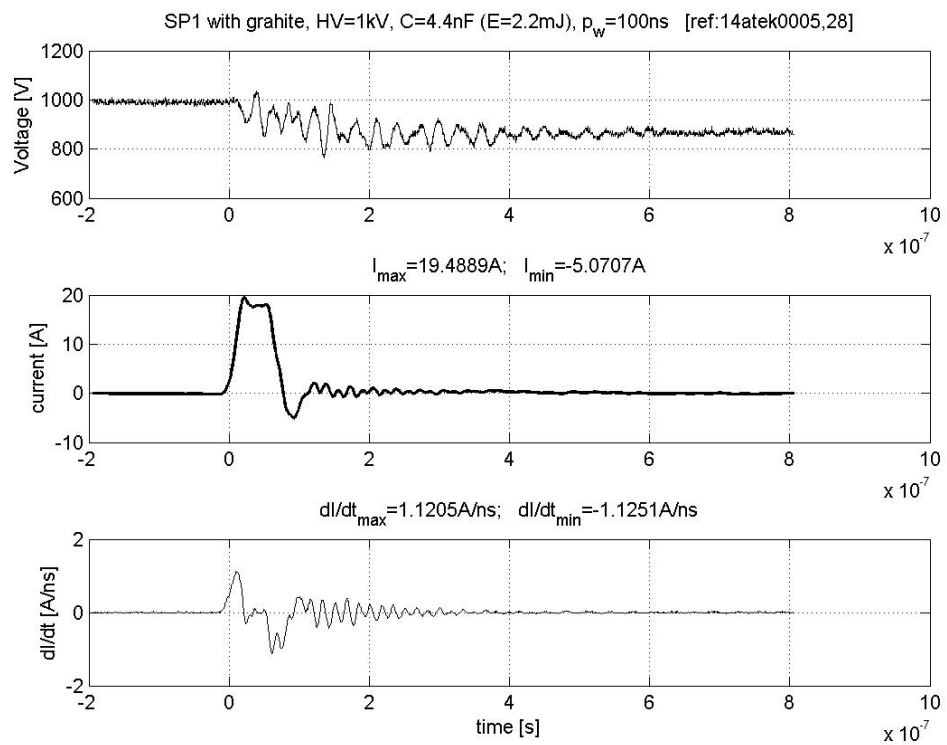
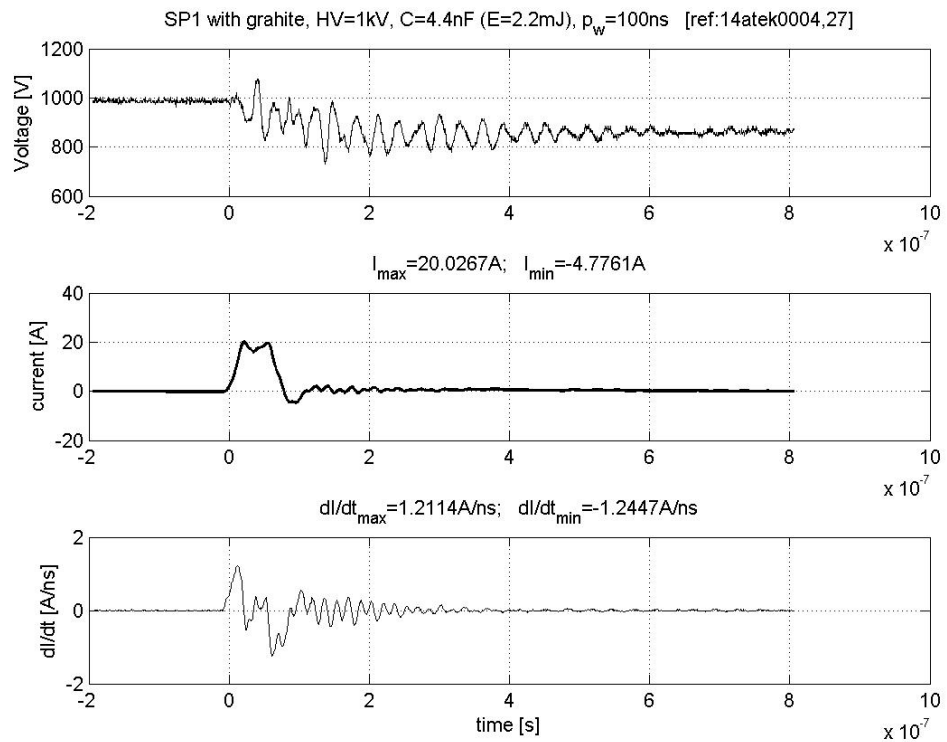
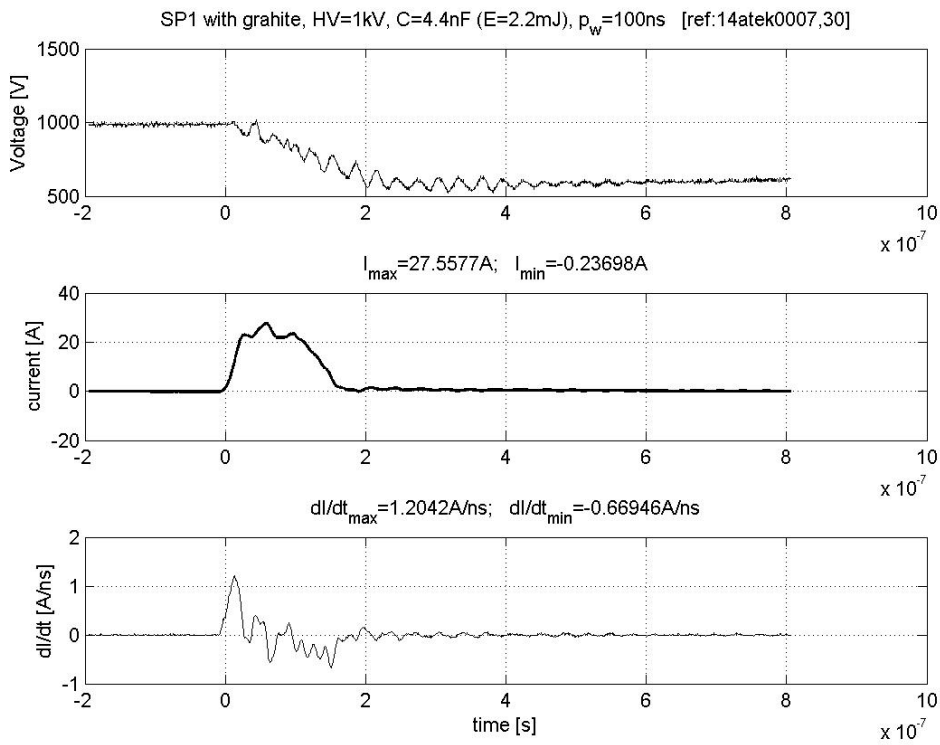
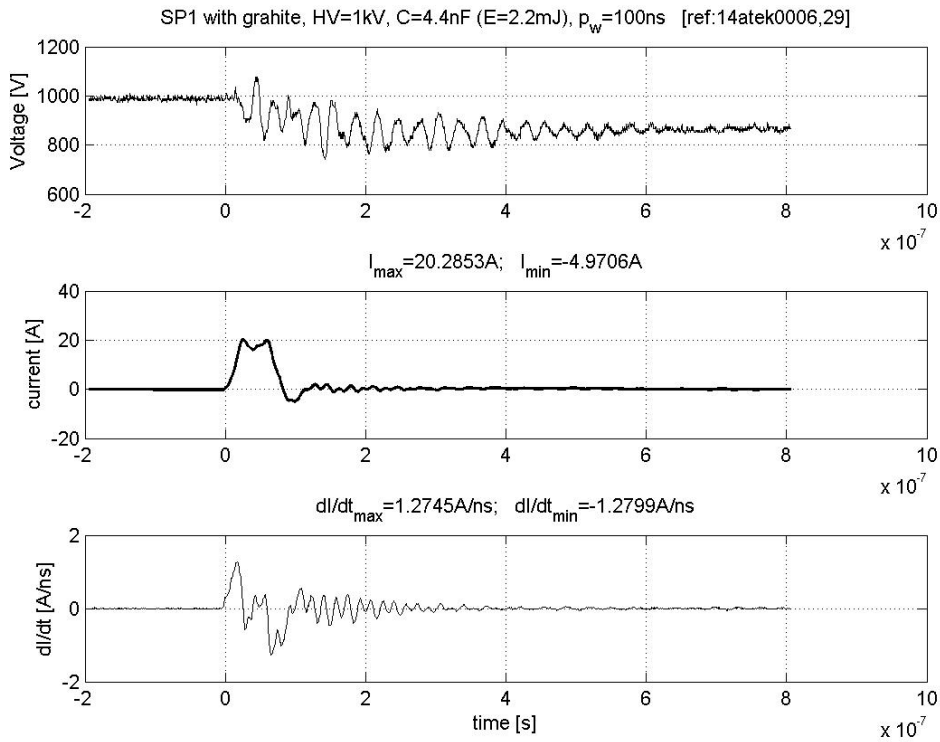
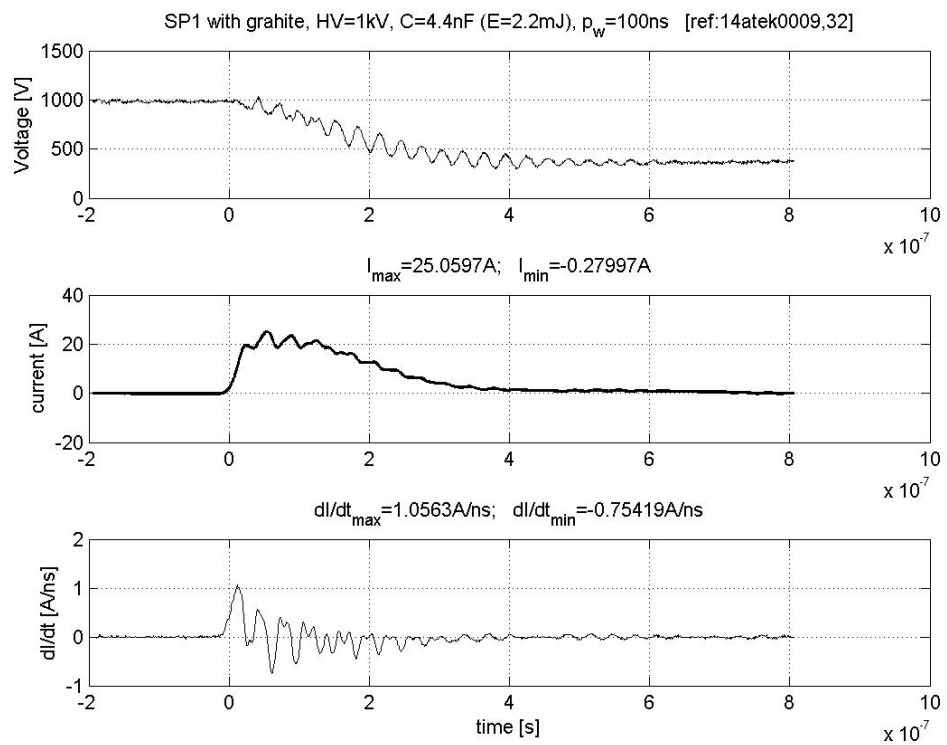
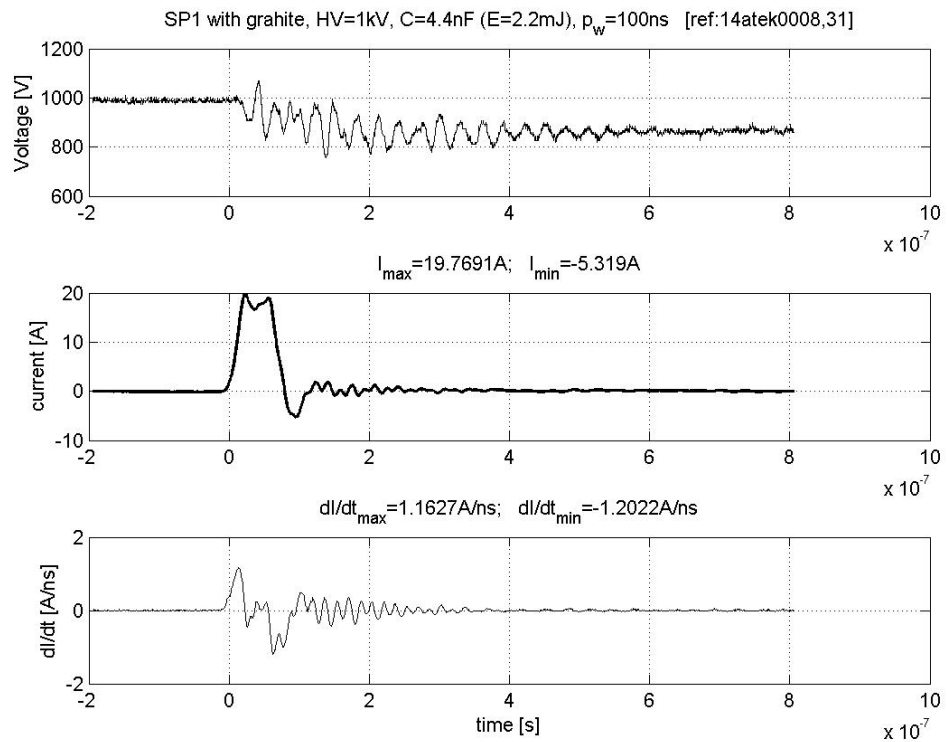


Figure A.2: MIC, SP1 with graphite breakdown tests ( $p_w = 100ns$ )









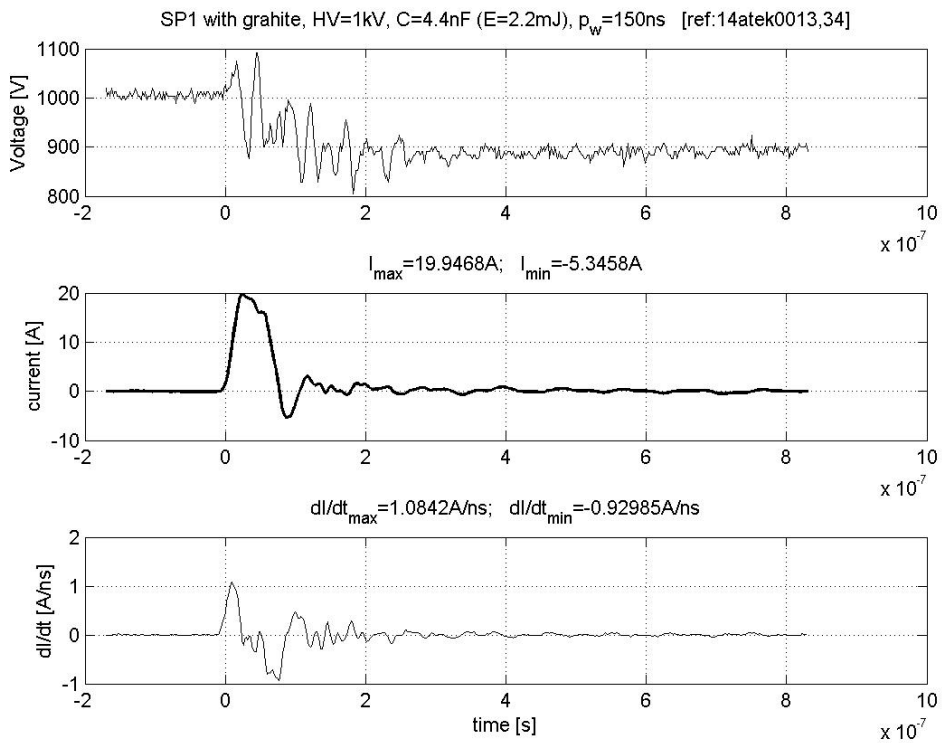
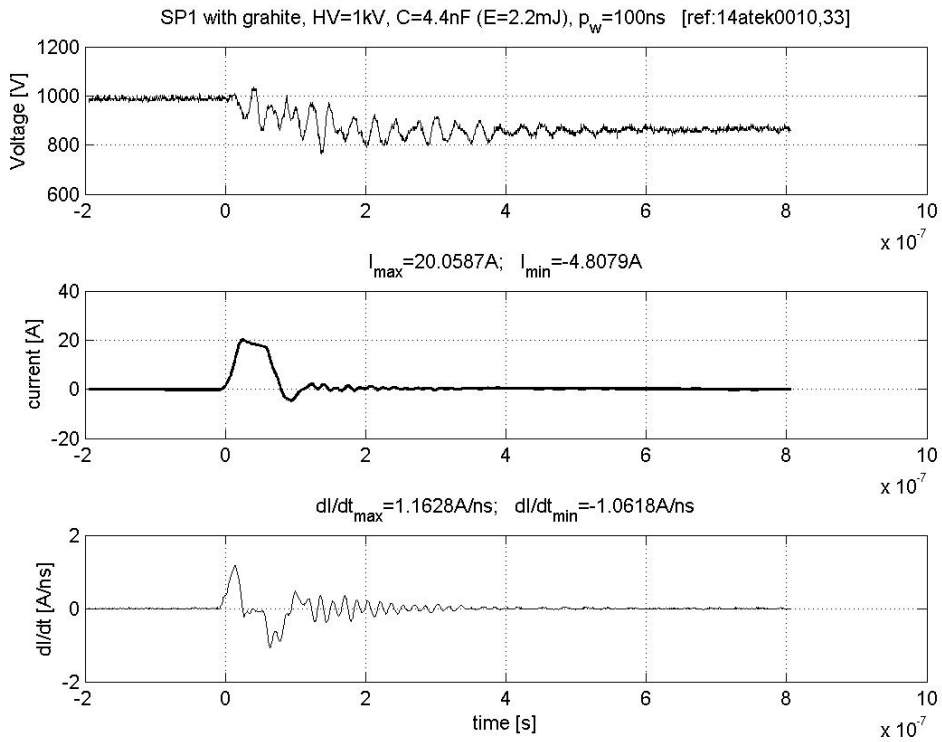
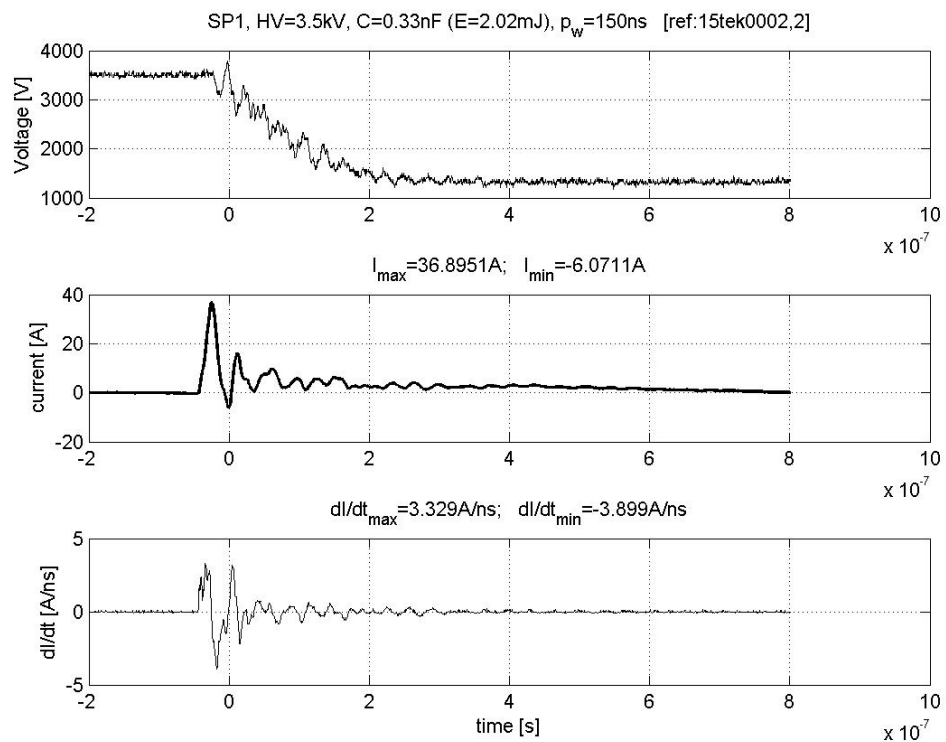
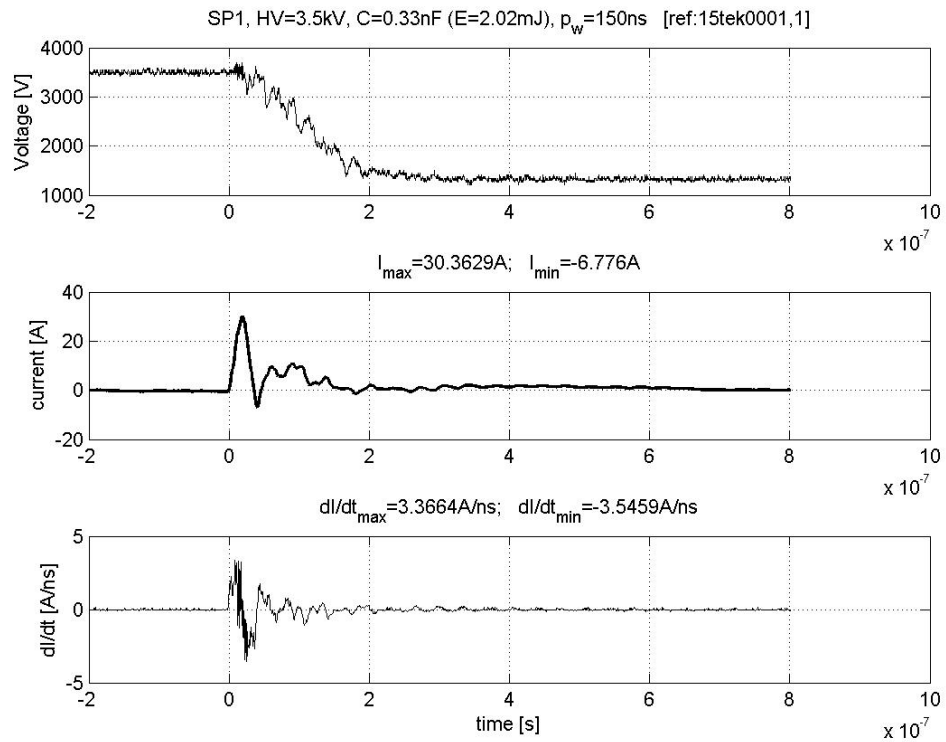
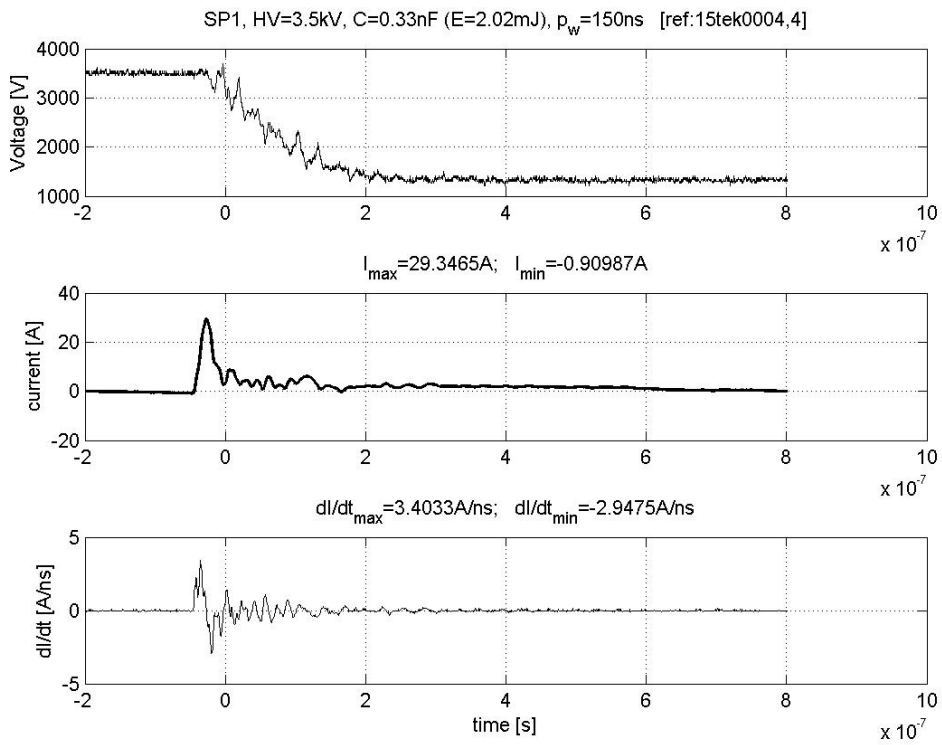
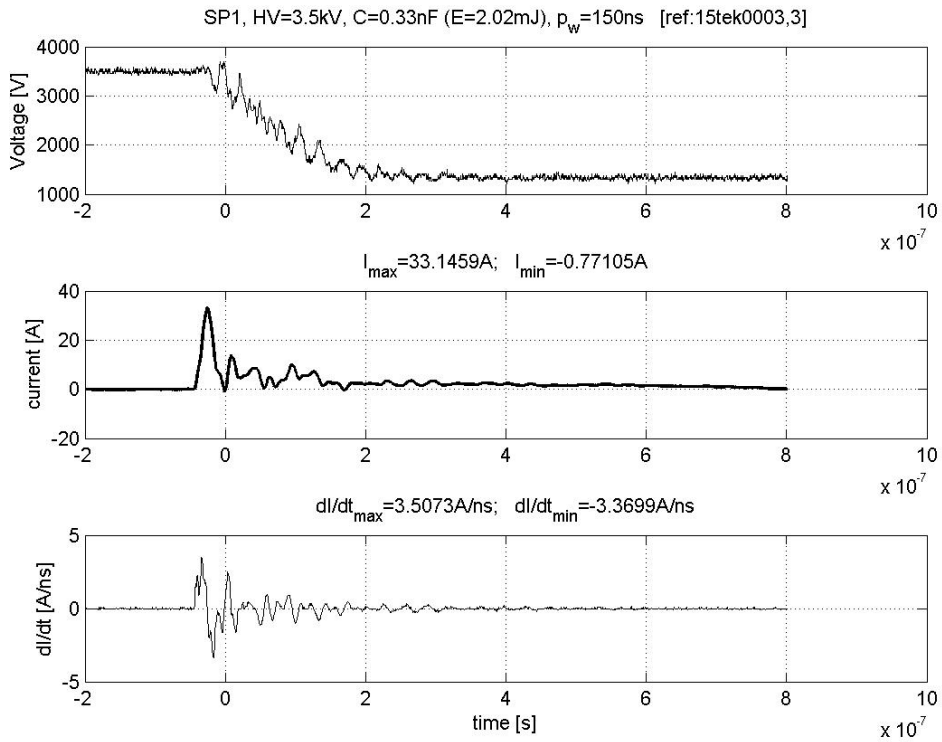
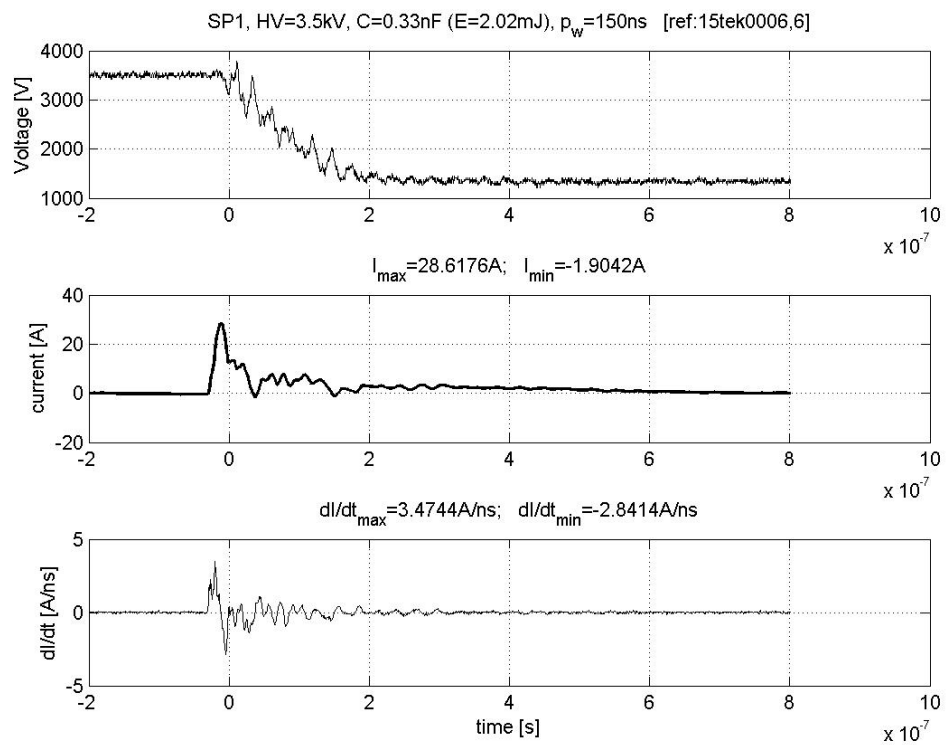
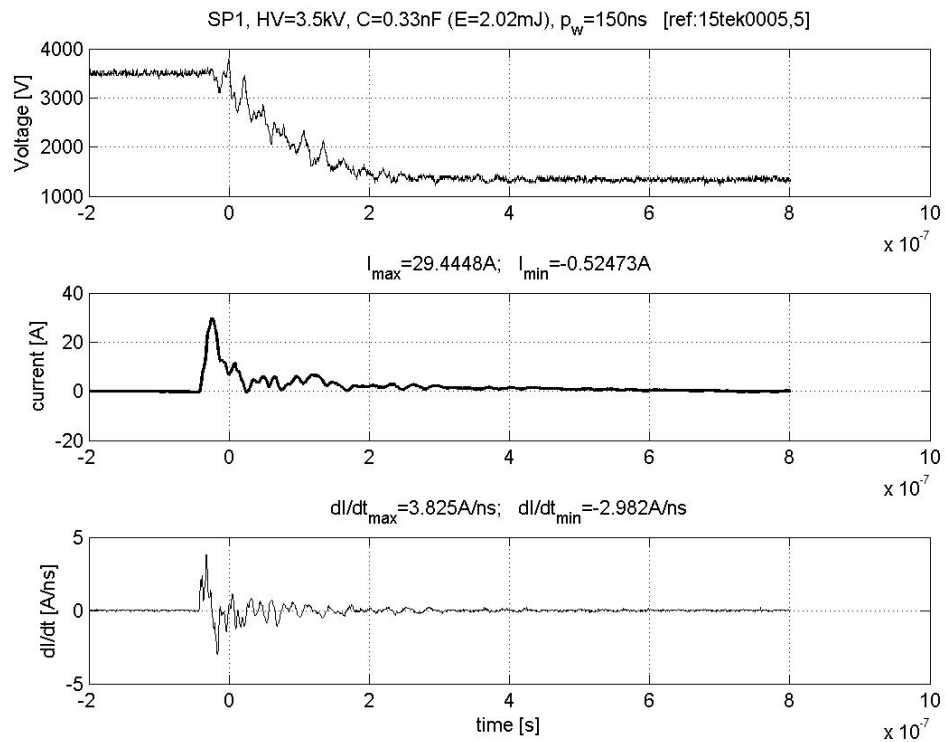
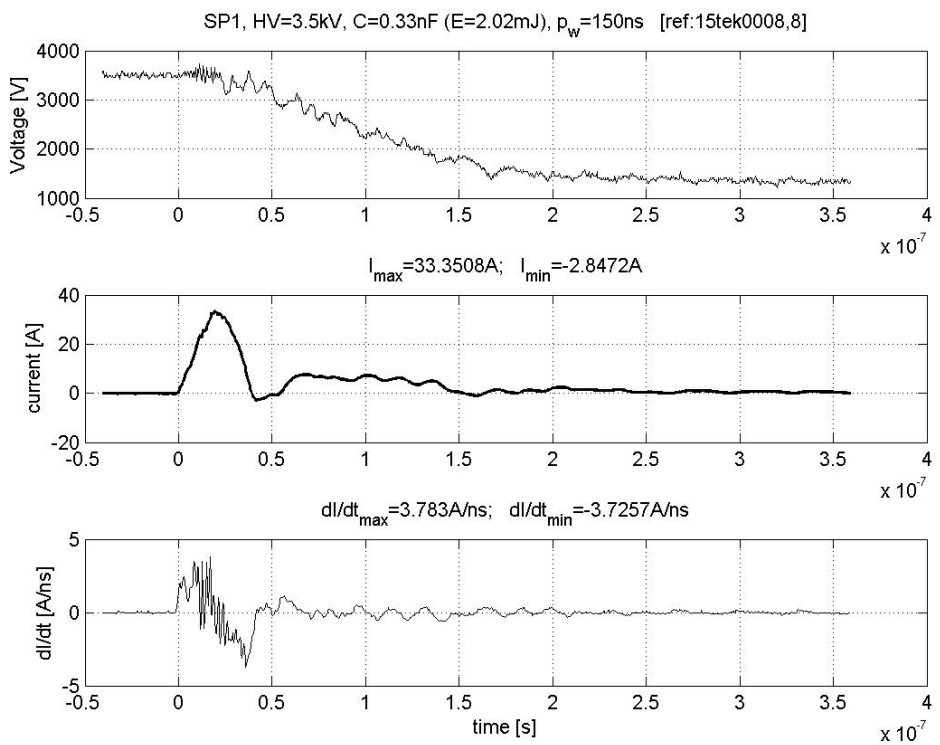
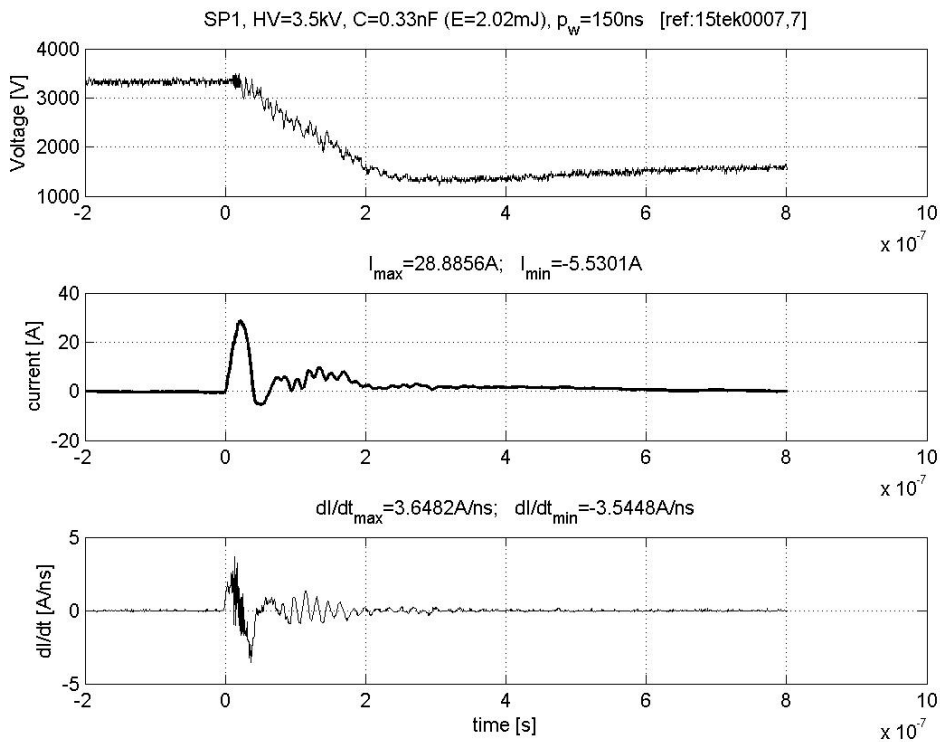


Figure A.3: MIC, SP1 breakdown tests ( $p_w = 150ns$ )







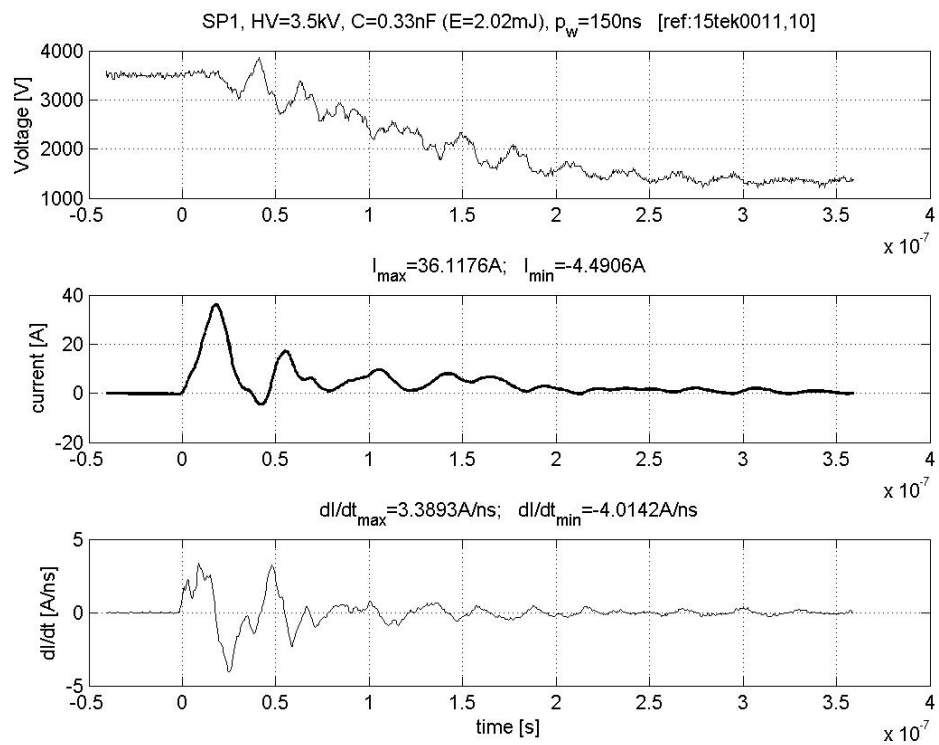
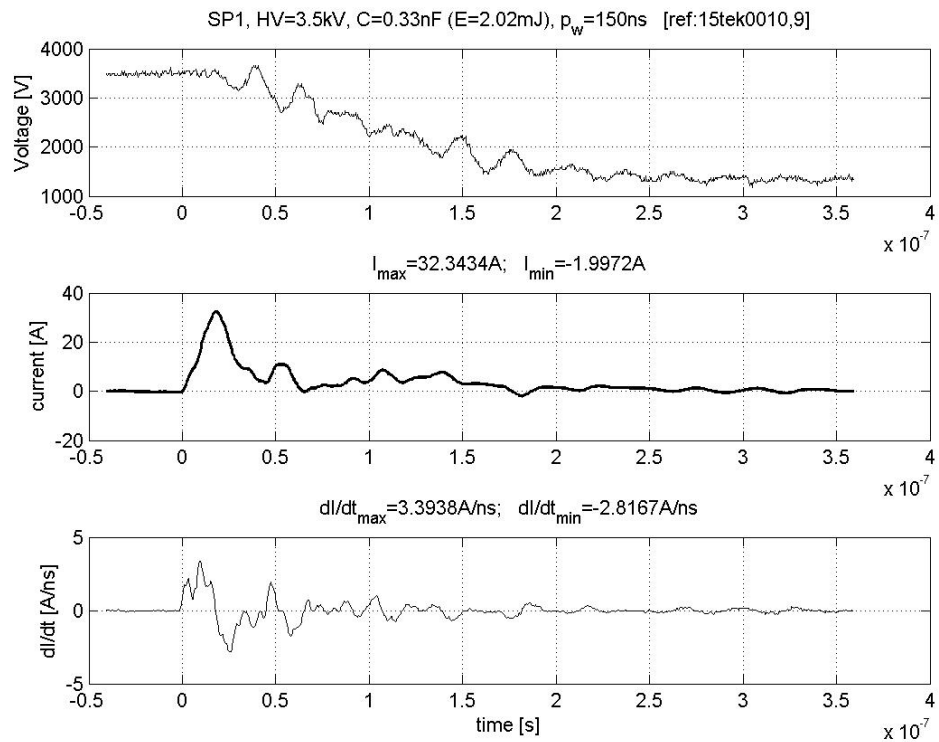
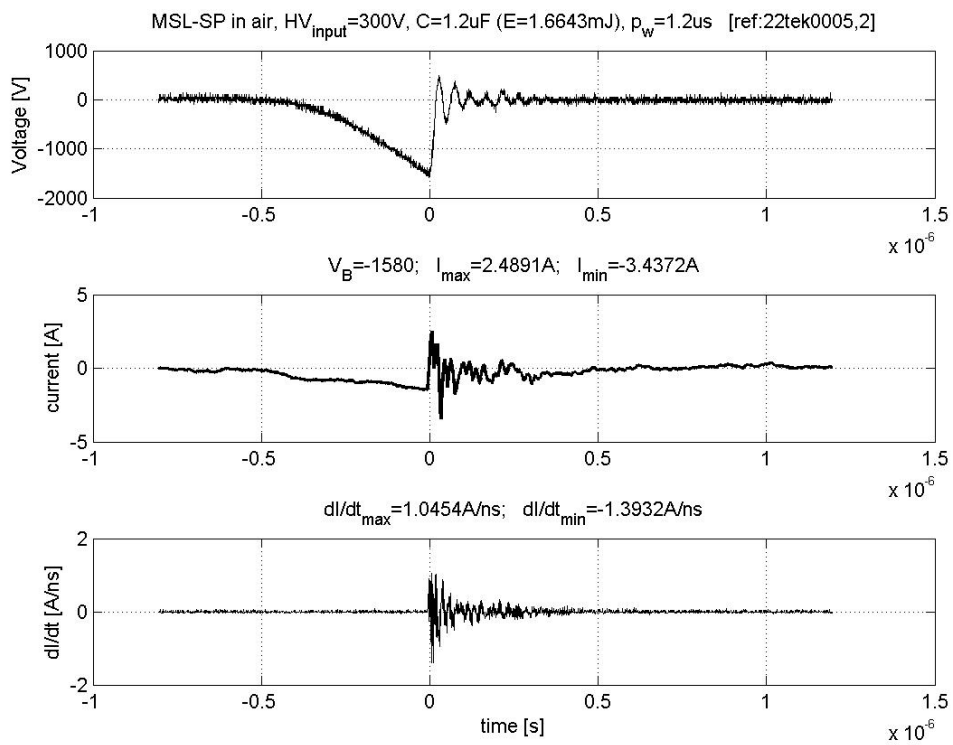
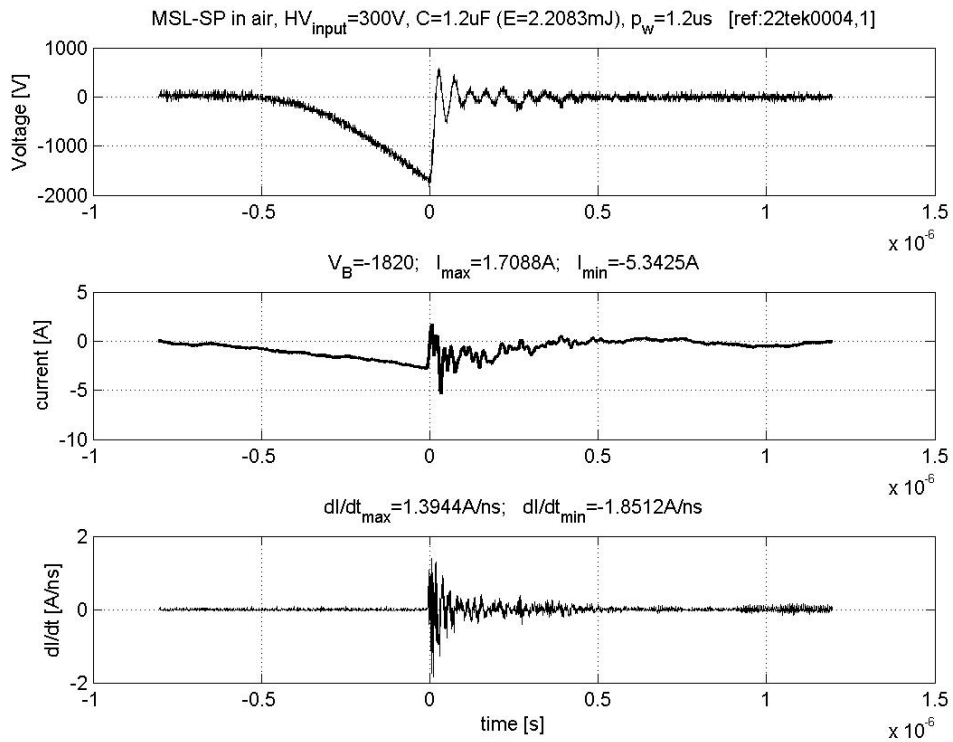


Figure A.4: TIC, MSL-SP breakdown tests in air



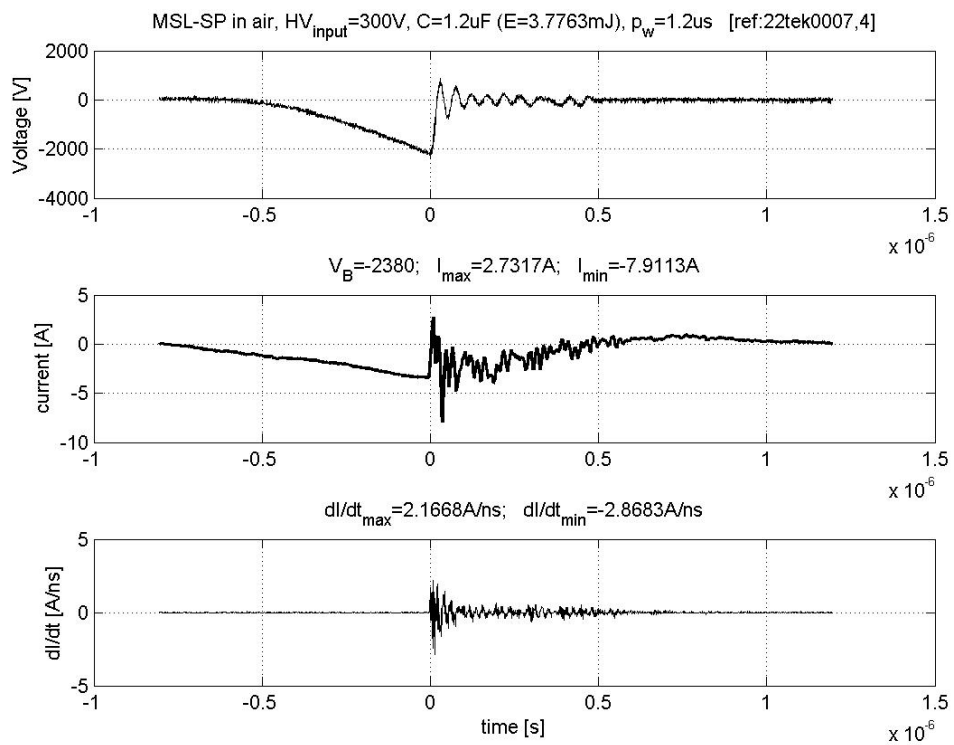
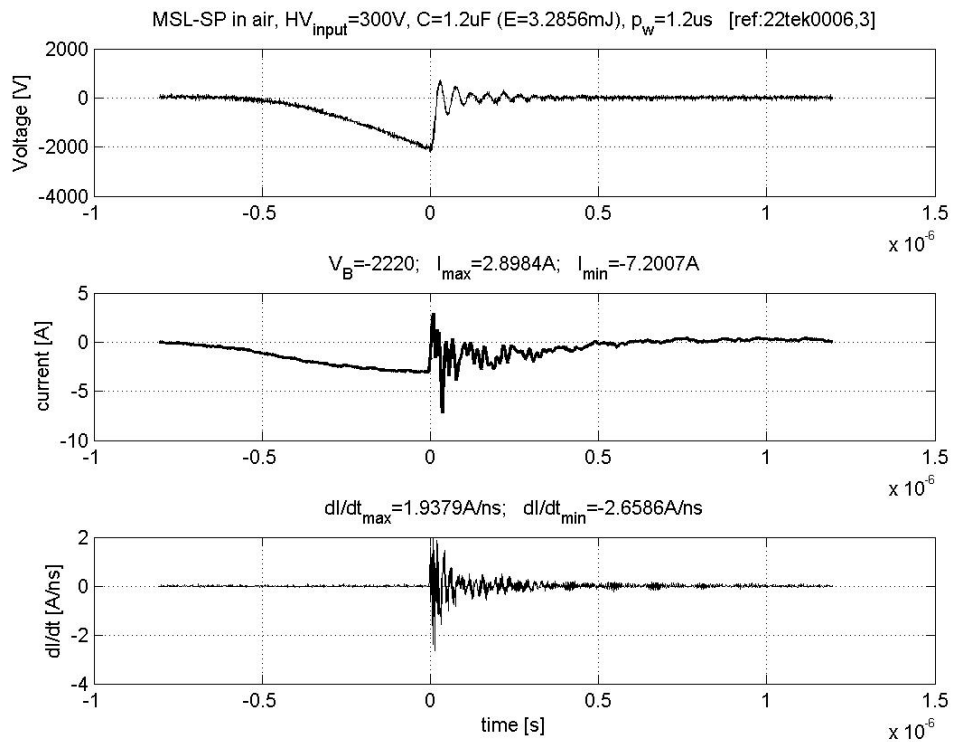
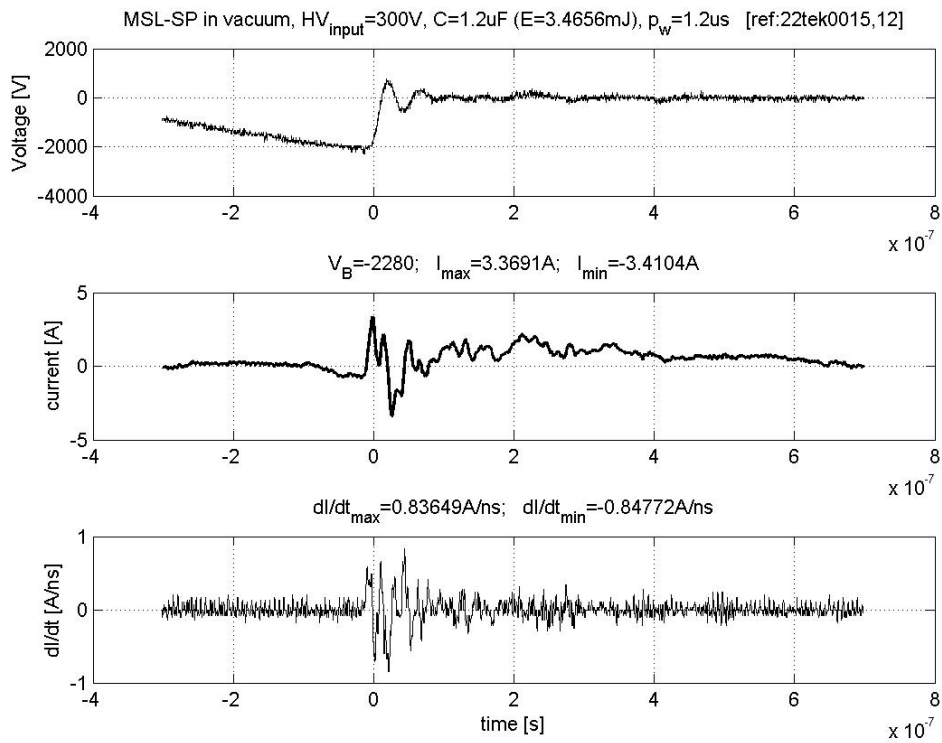
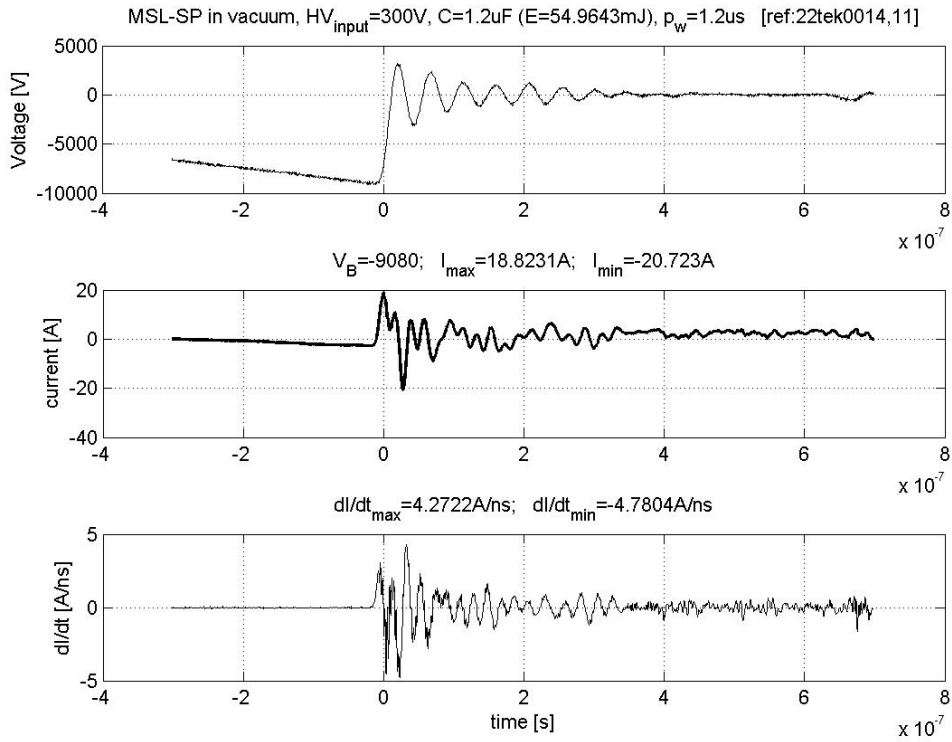


Figure A.5: TIC, MSL-SP breakdown tests in vacuum



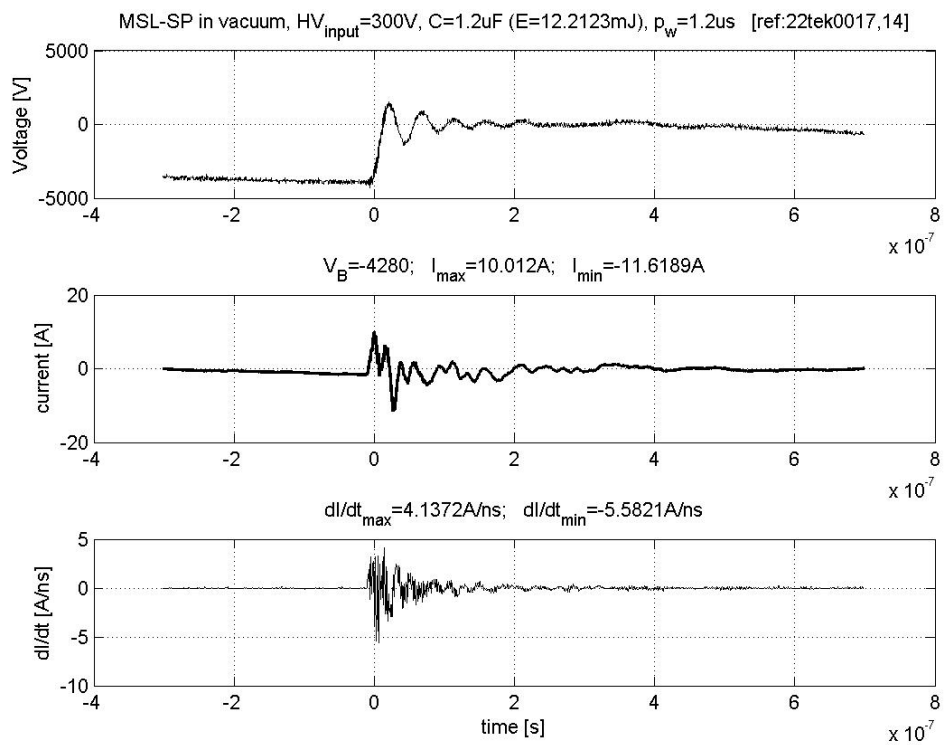
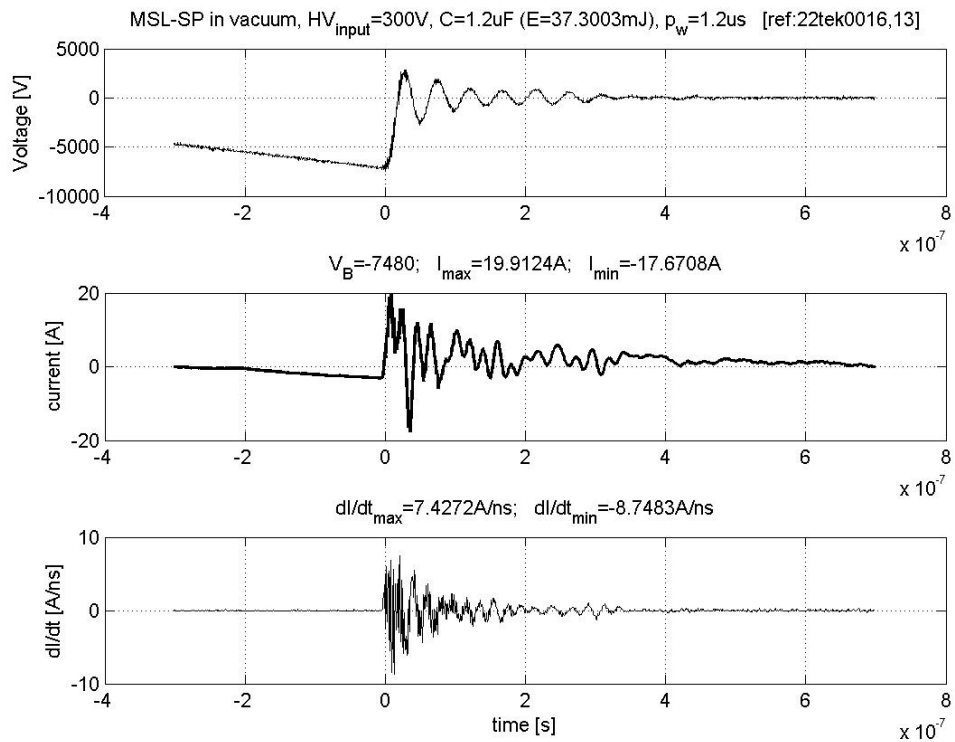
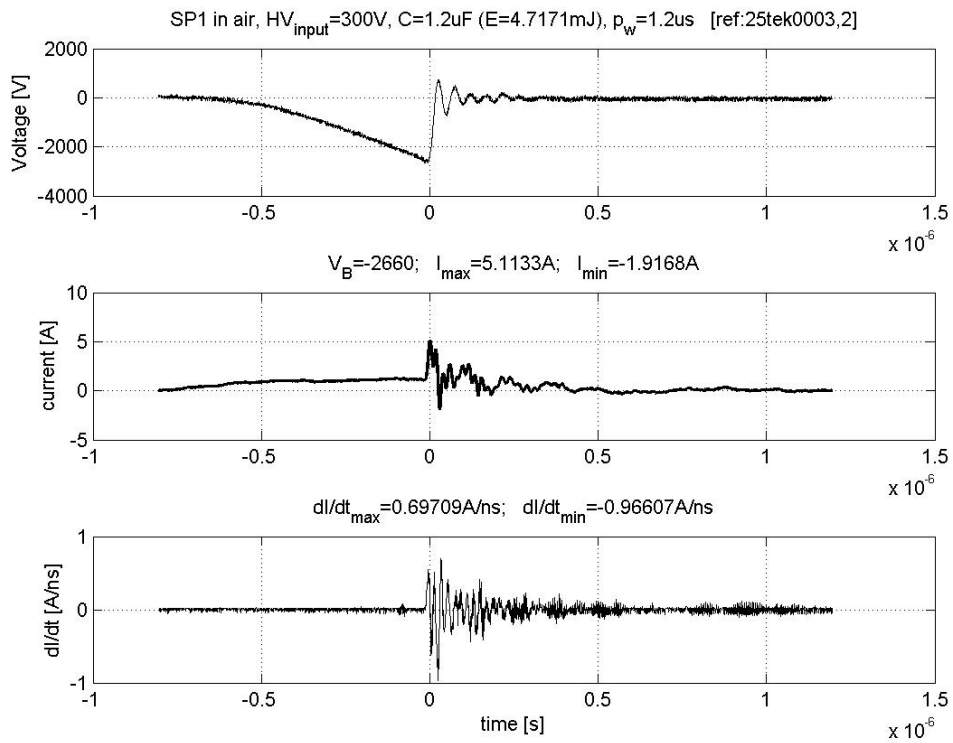
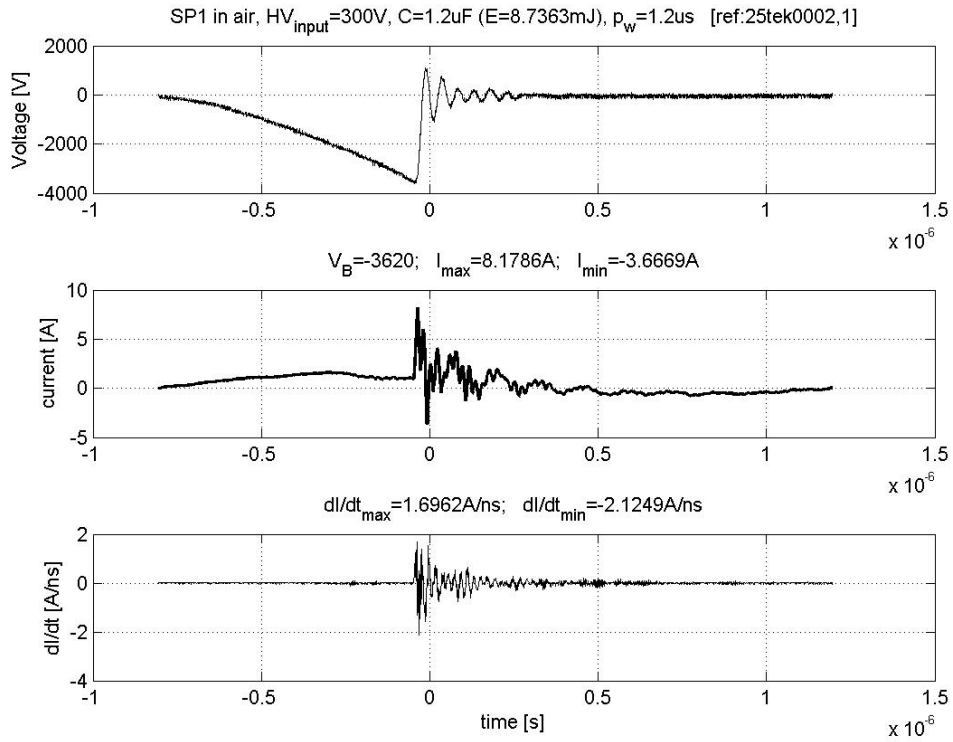


Figure A.6: TIC, SP1 breakdown tests in air



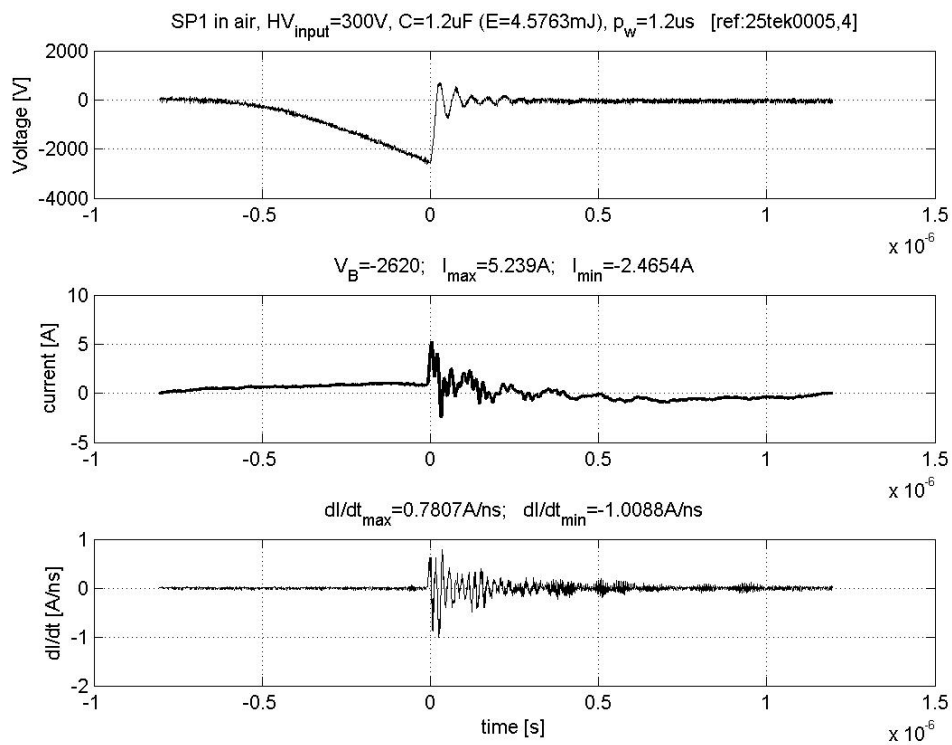
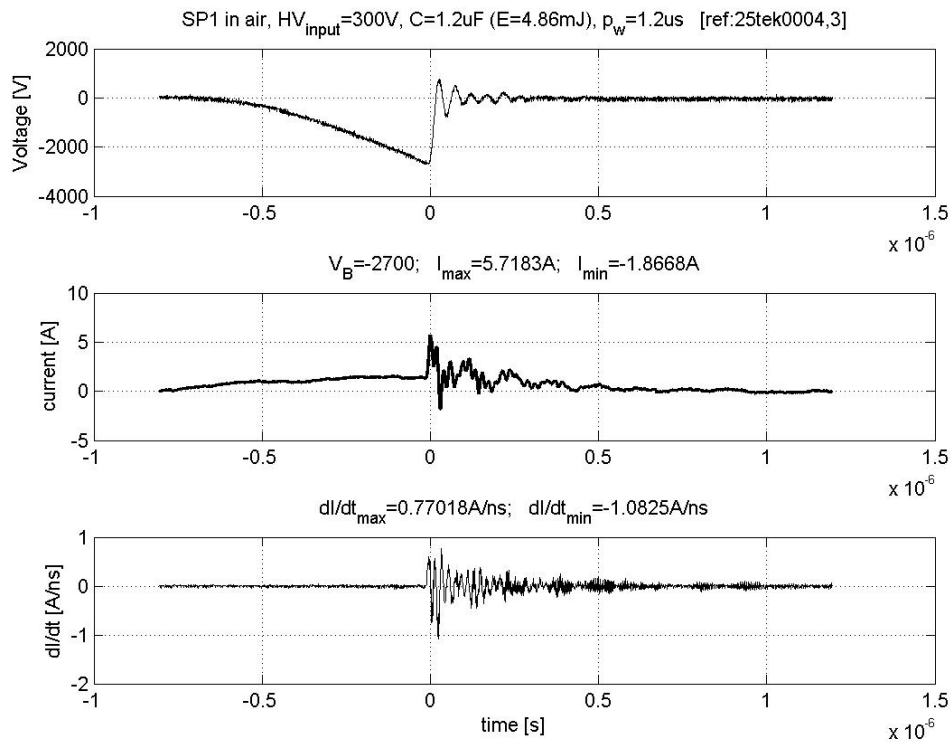
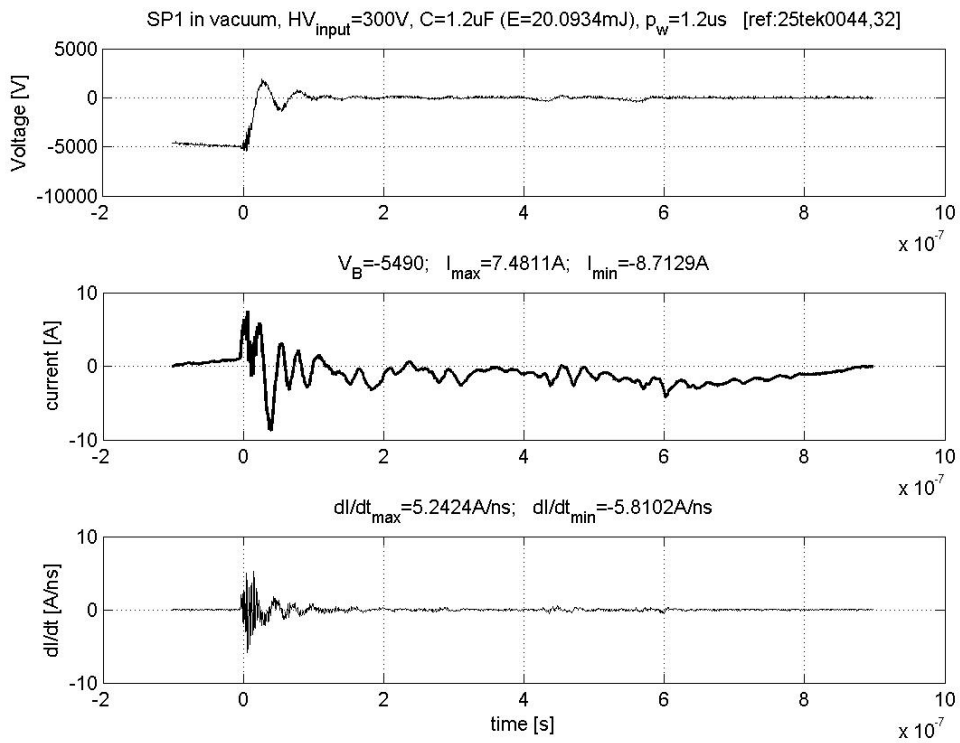
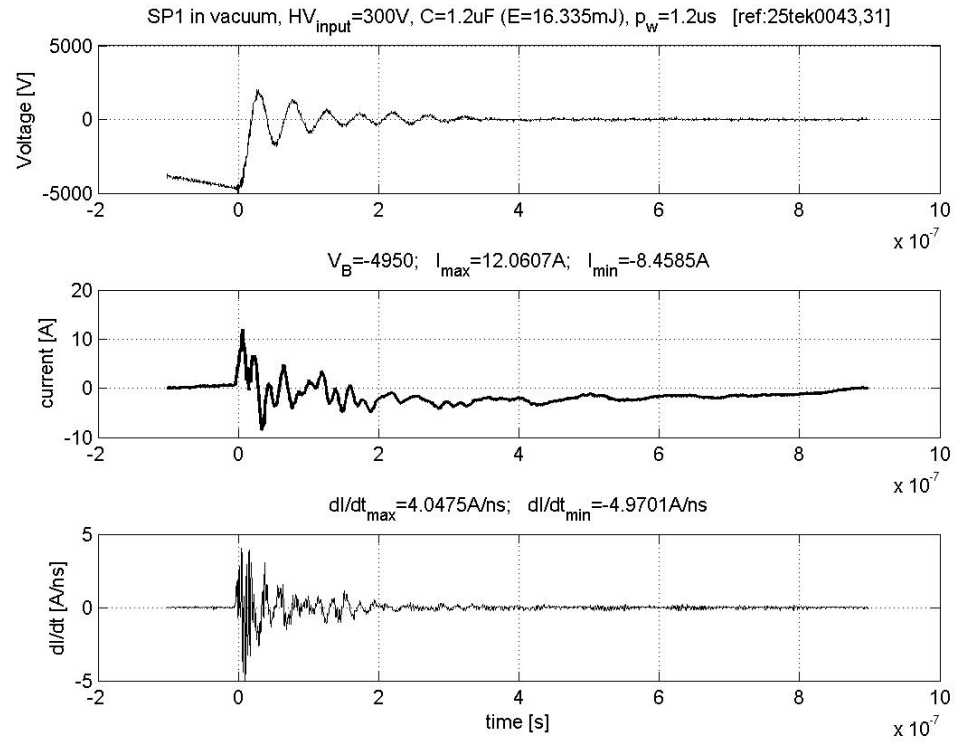


Figure A.7: TIC, SP1 breakdown tests in vacuum



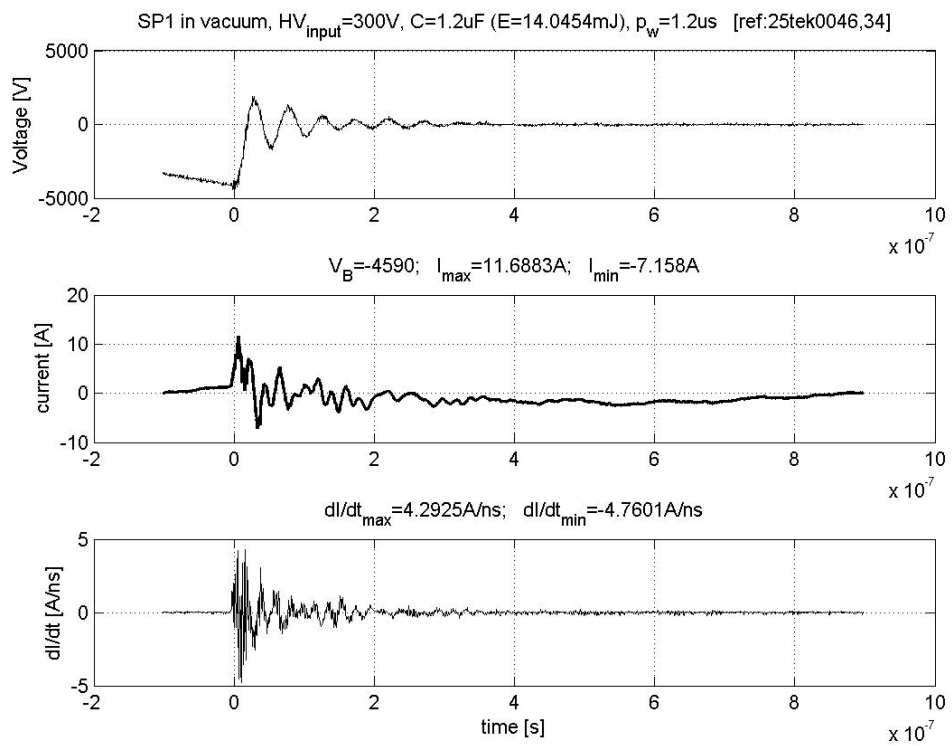
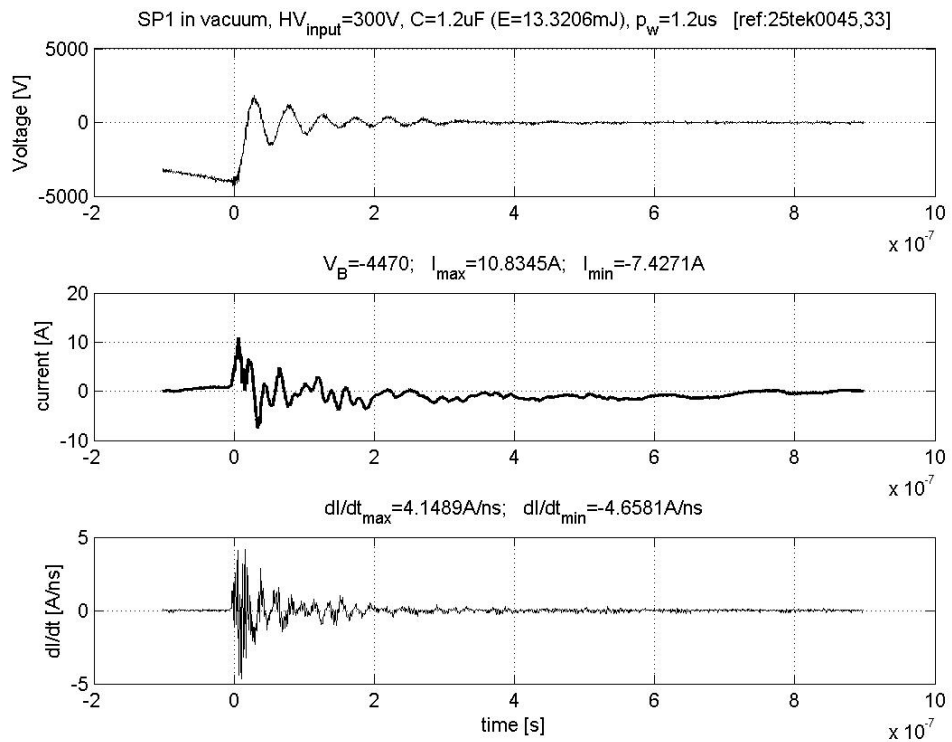
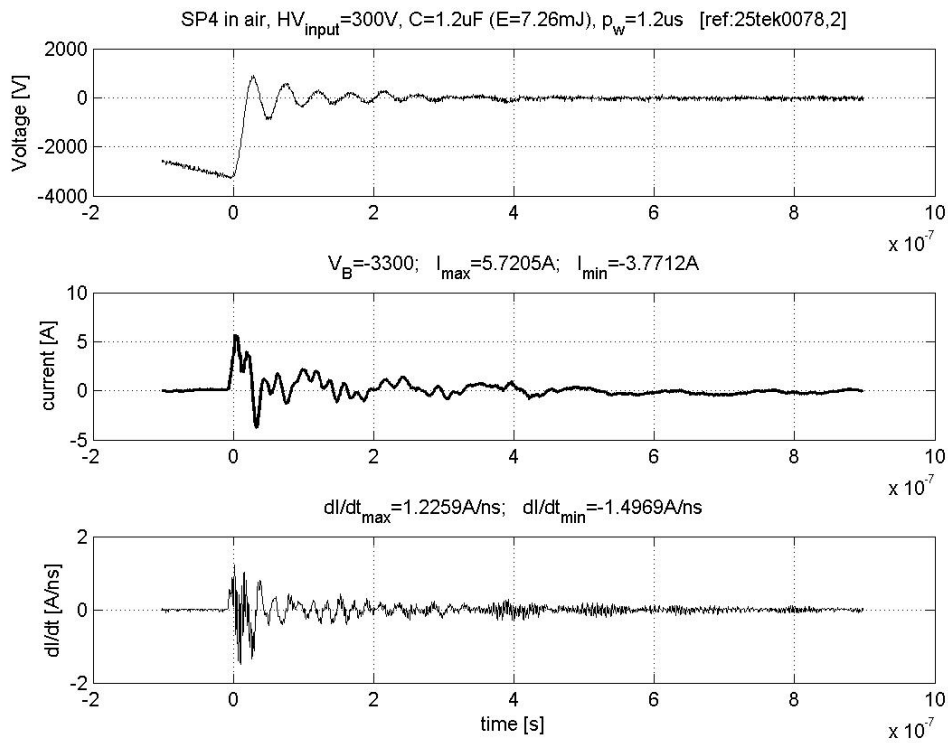
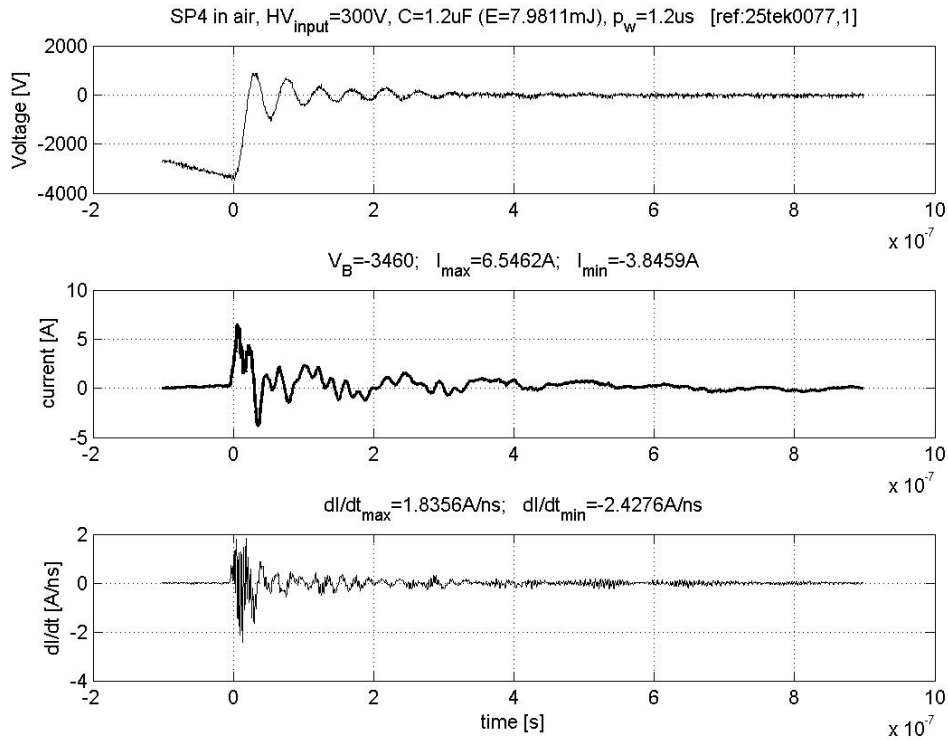
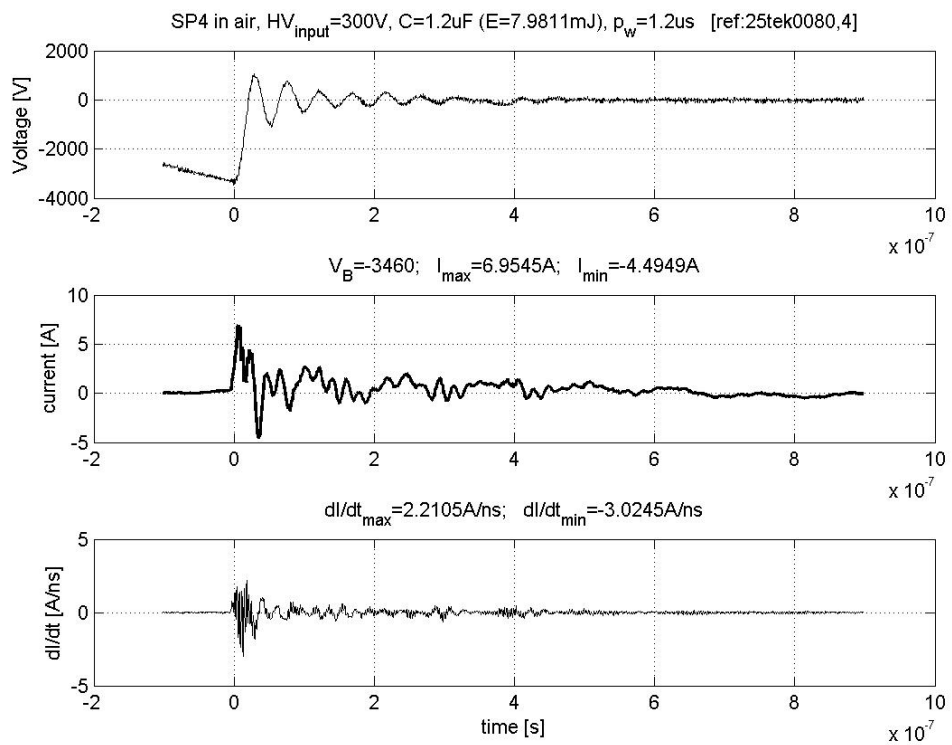
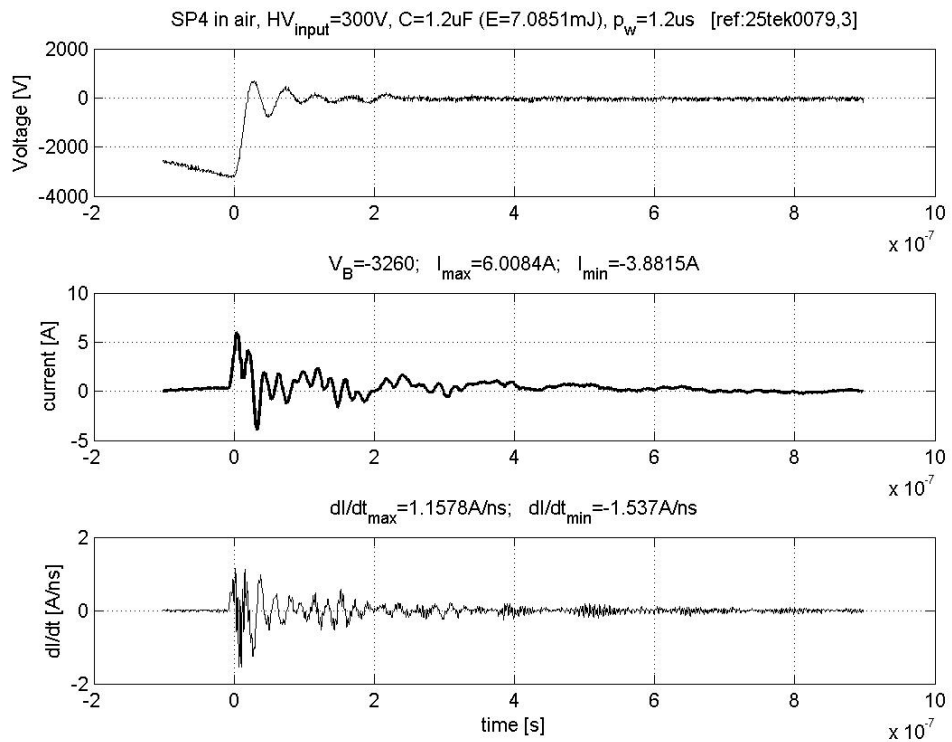


Figure A.8: TIC, SP4 breakdown tests in air





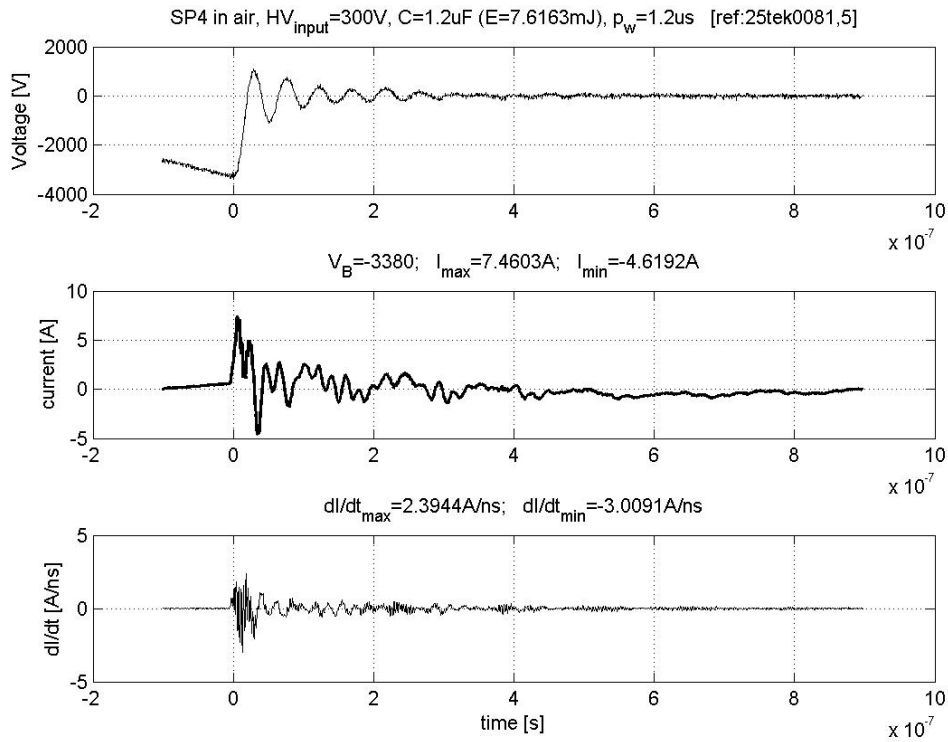


Figure A.9: TIC SP4 breakdown tests in vacuum

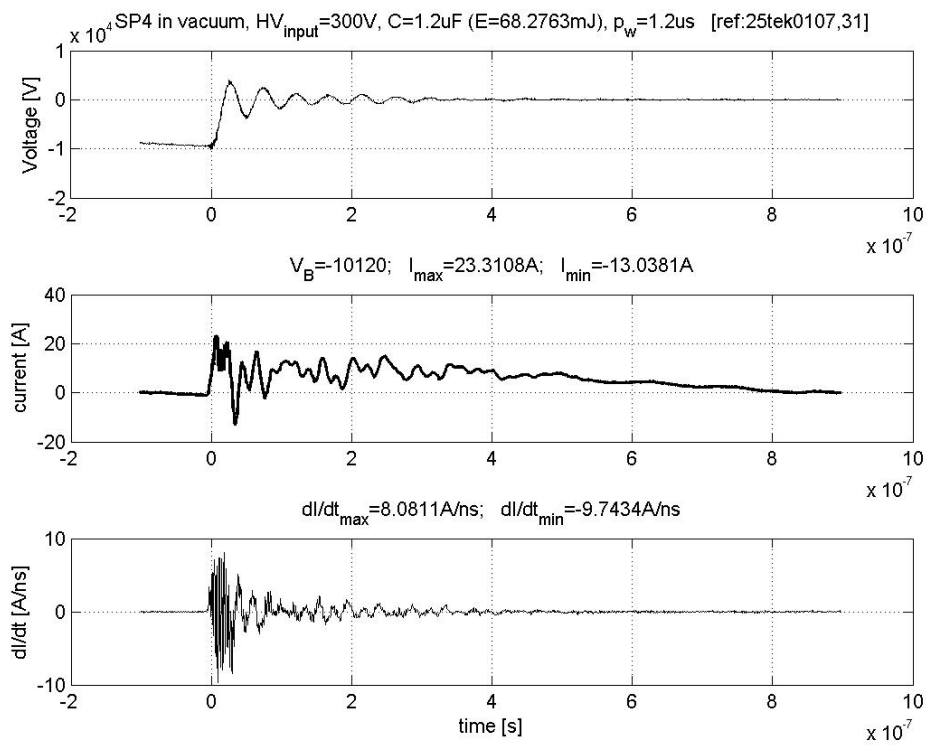
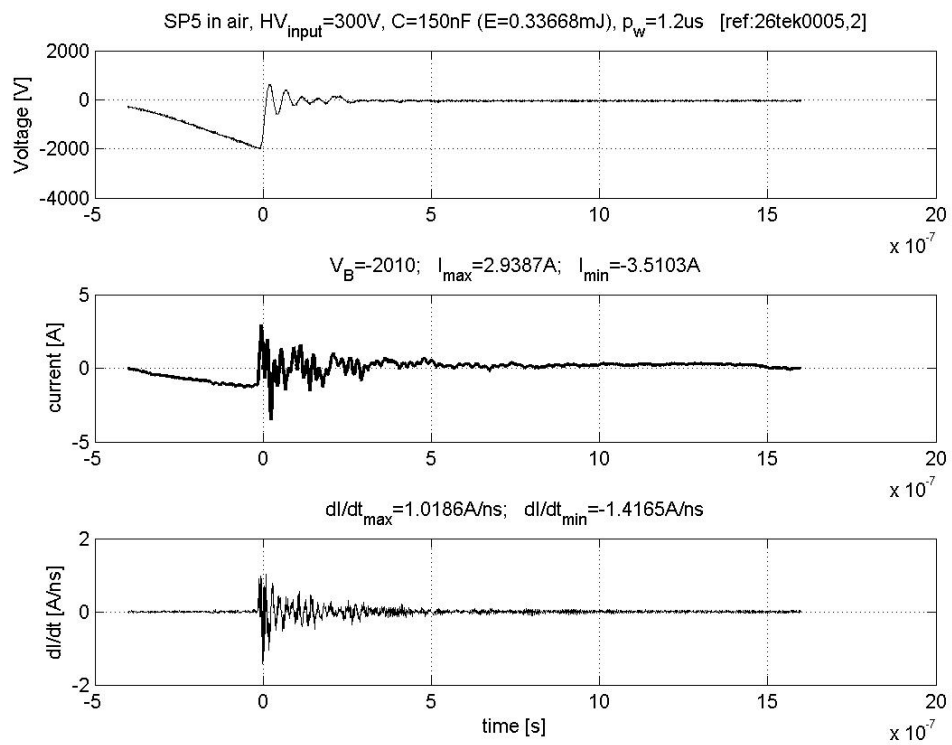
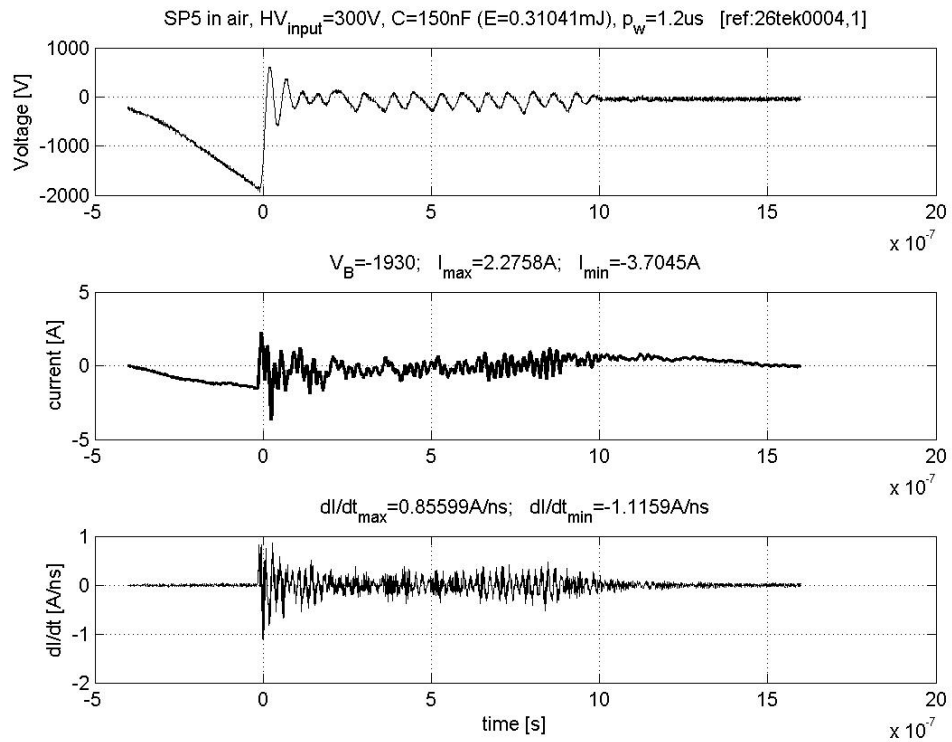


Figure A.10: TIC, SP5 breakdown tests in air



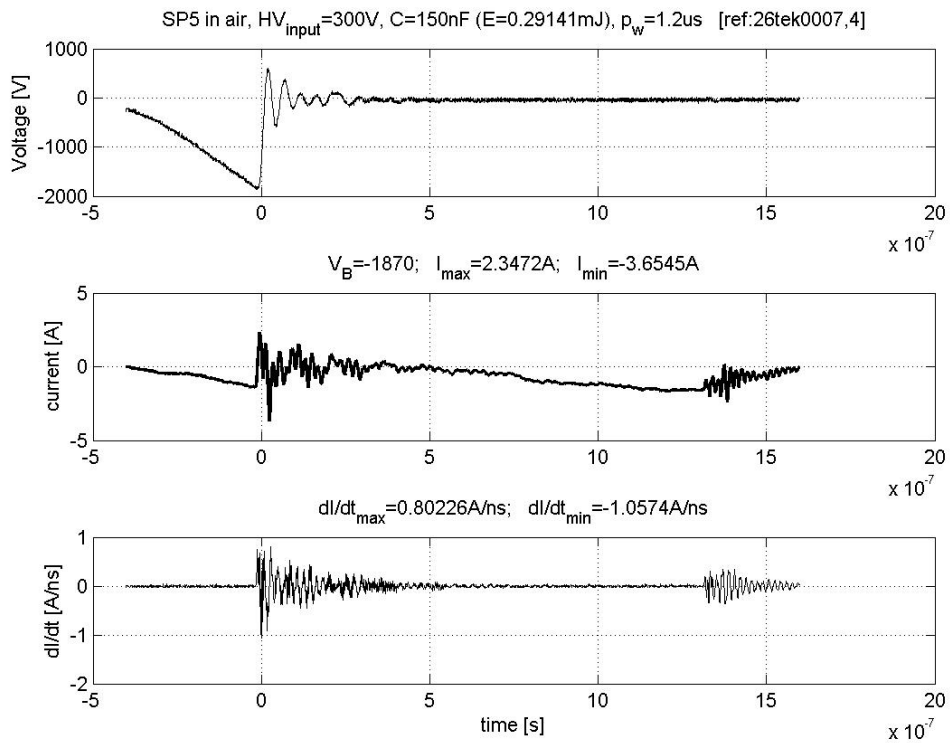
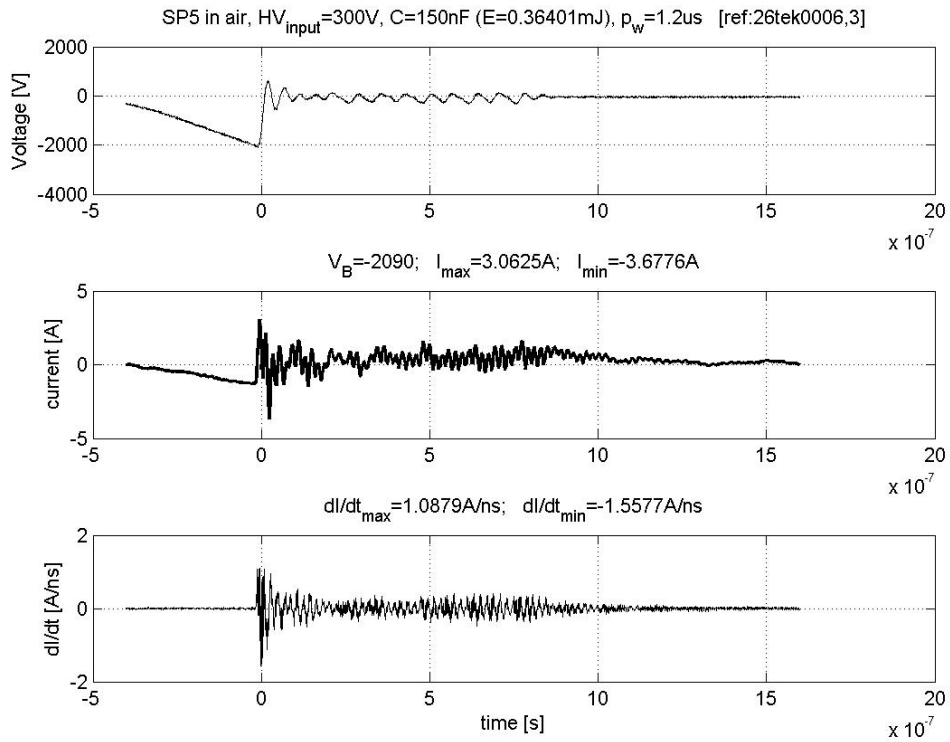
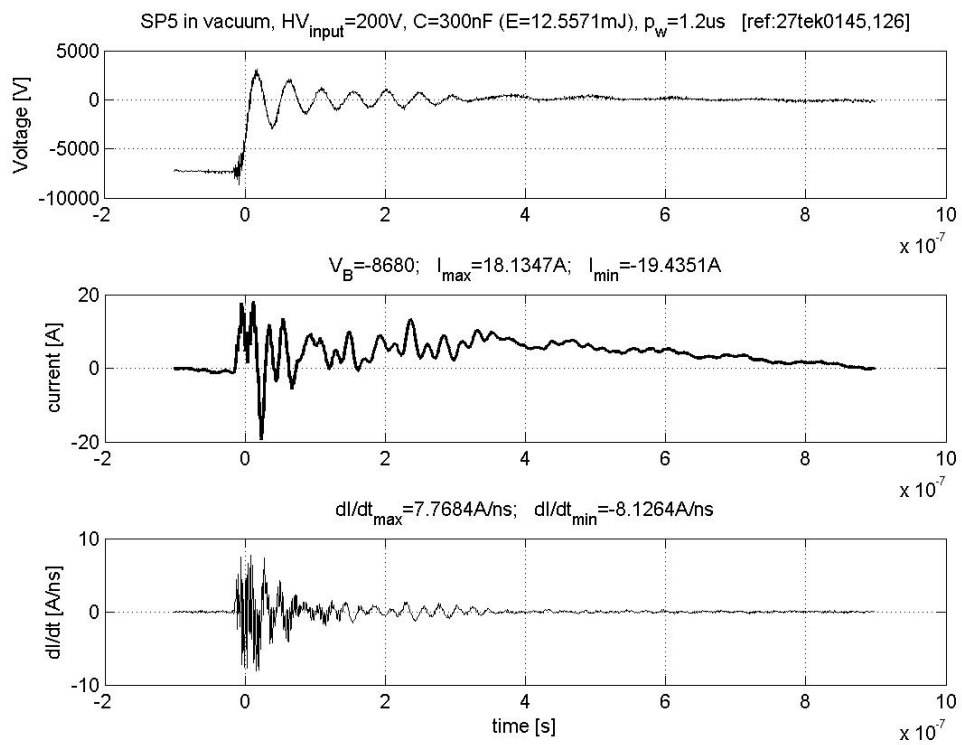
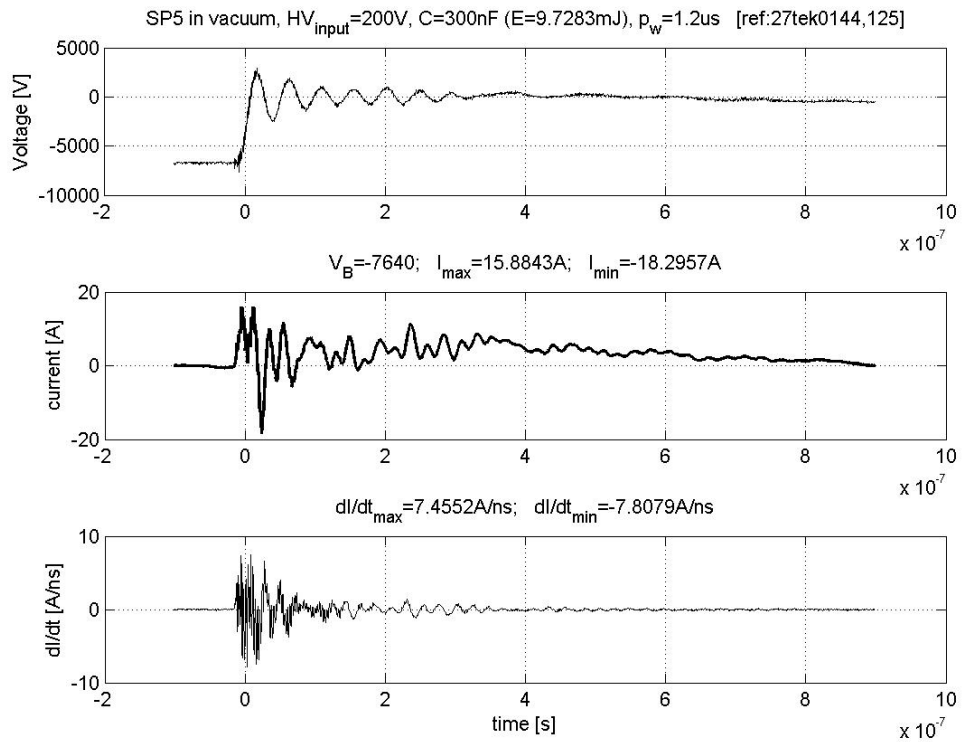
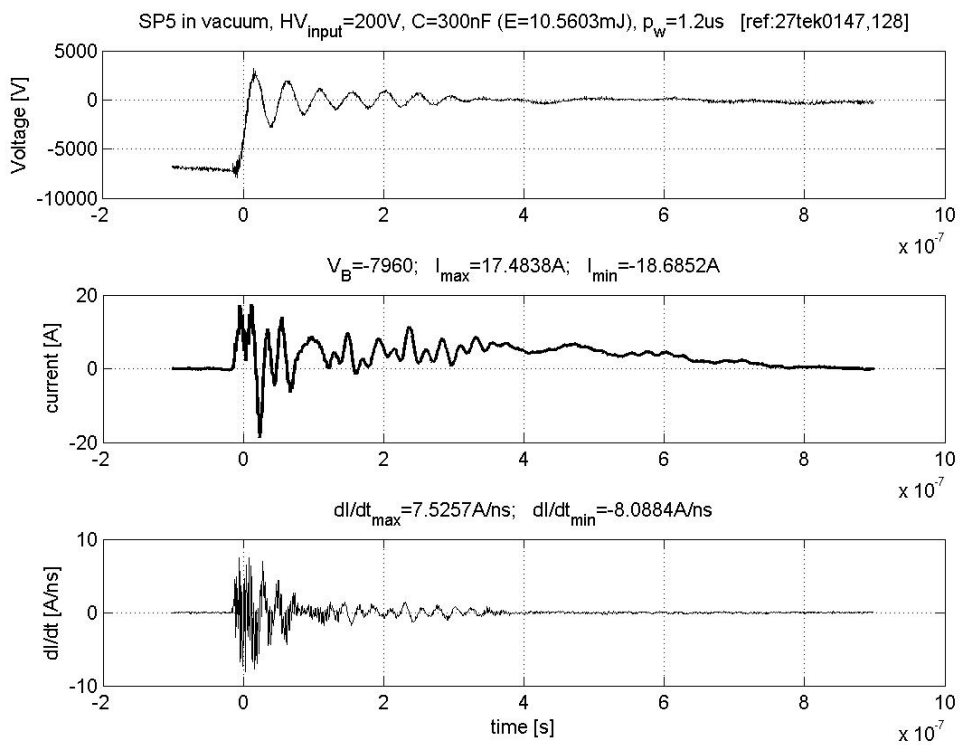
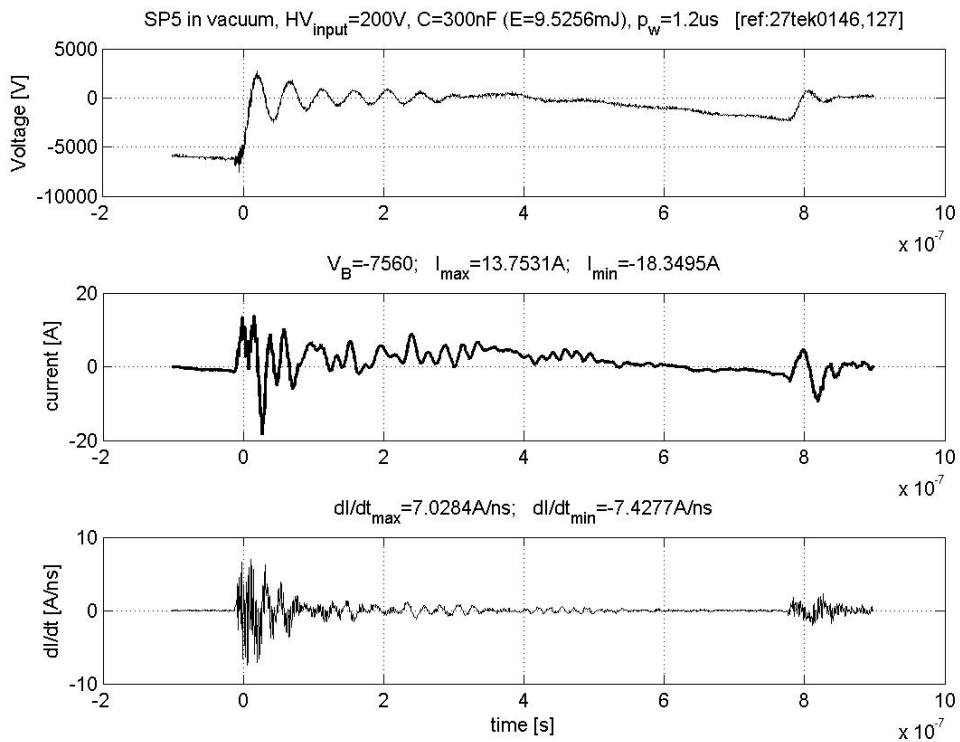


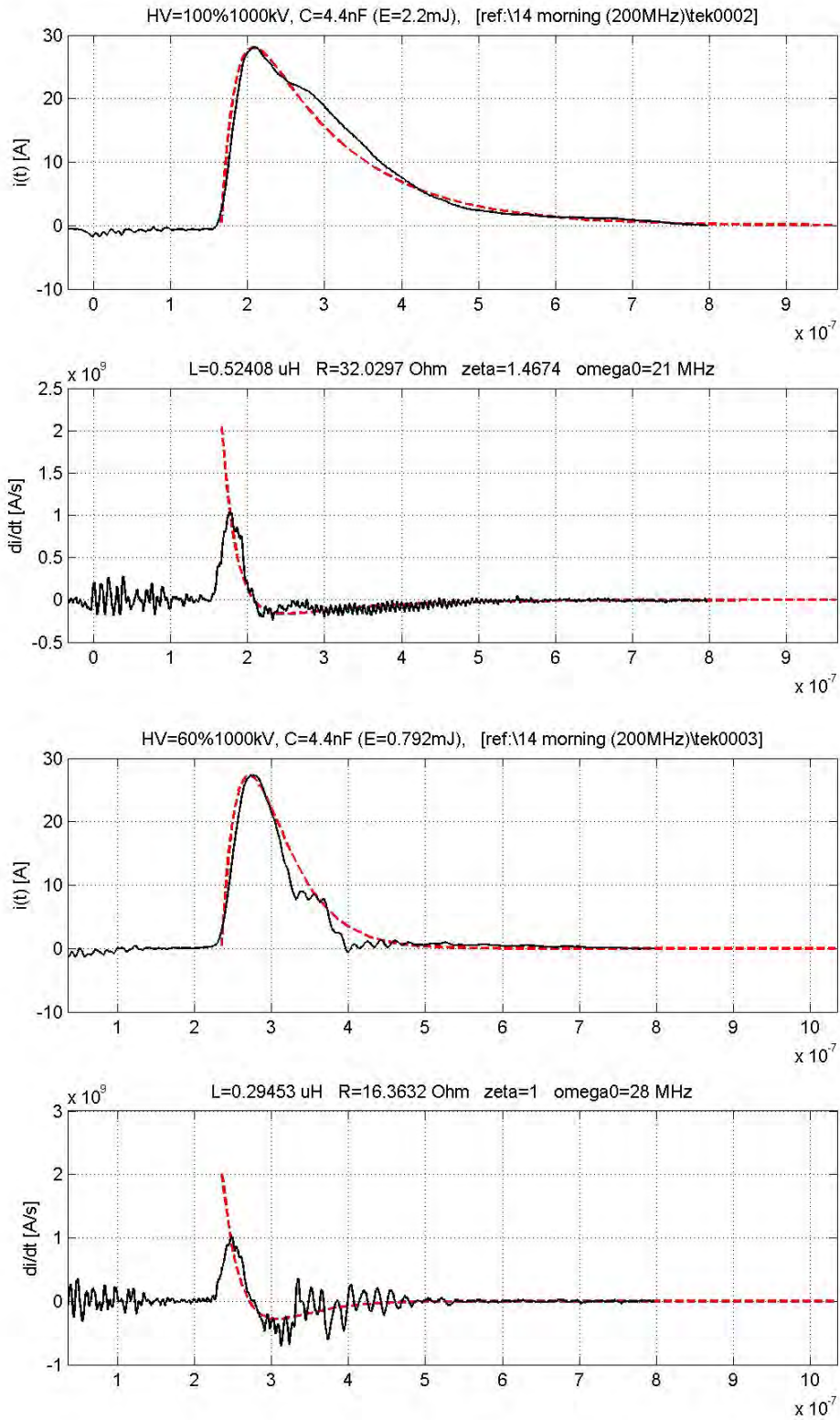
Figure A.11: TIC, SP5 breakdown tests in vacuum

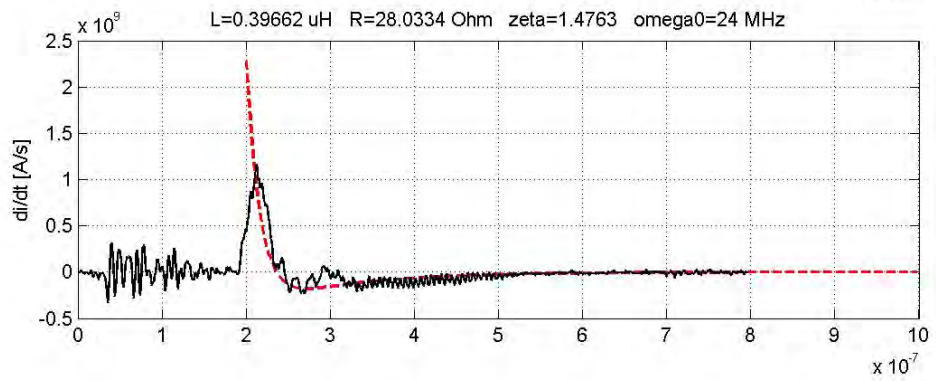
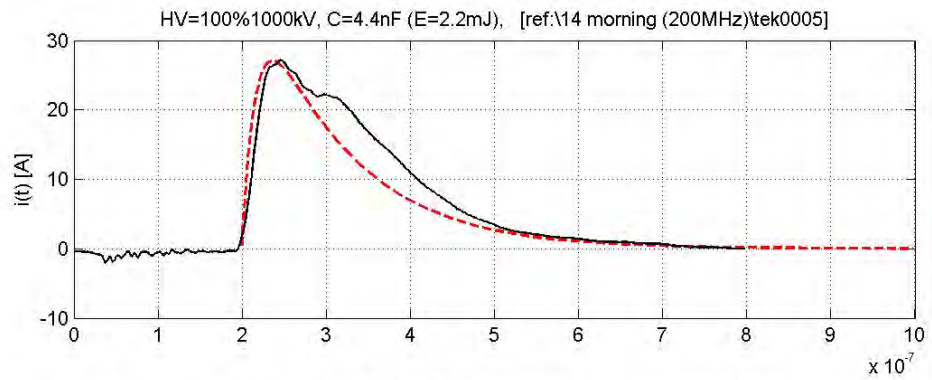
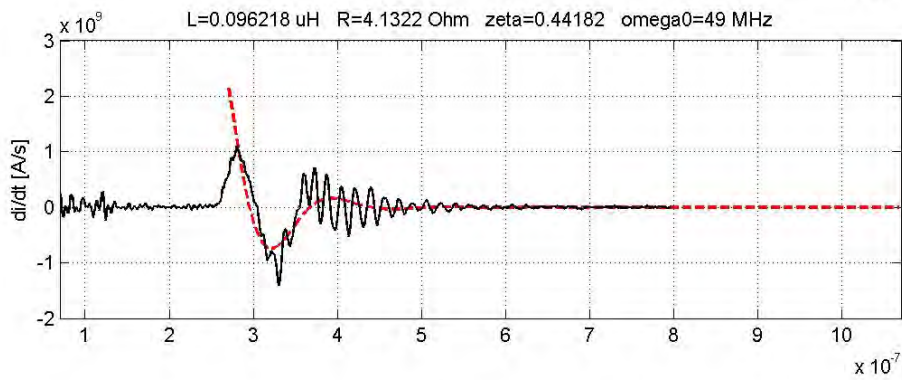
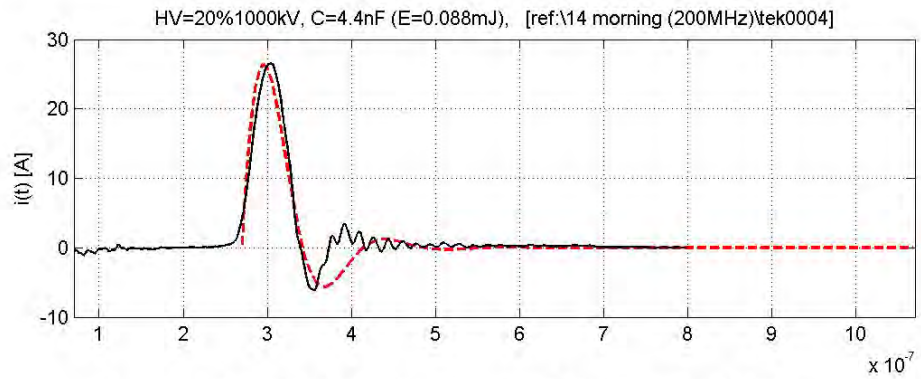


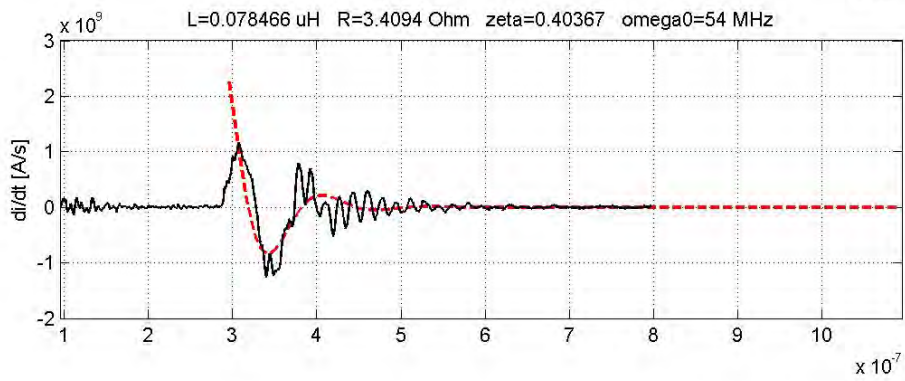
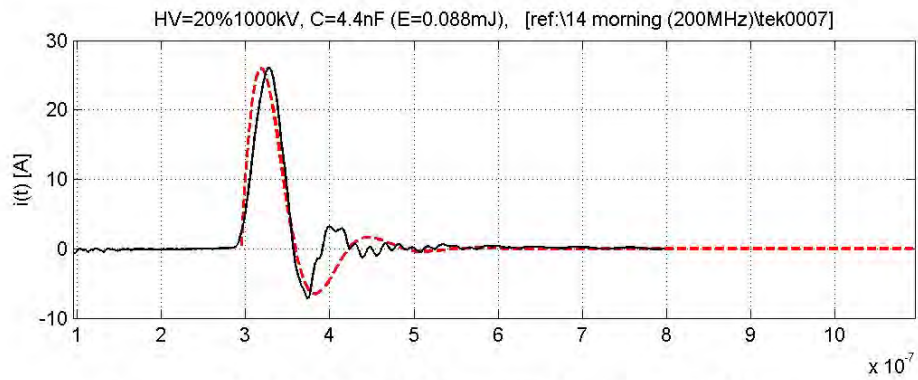
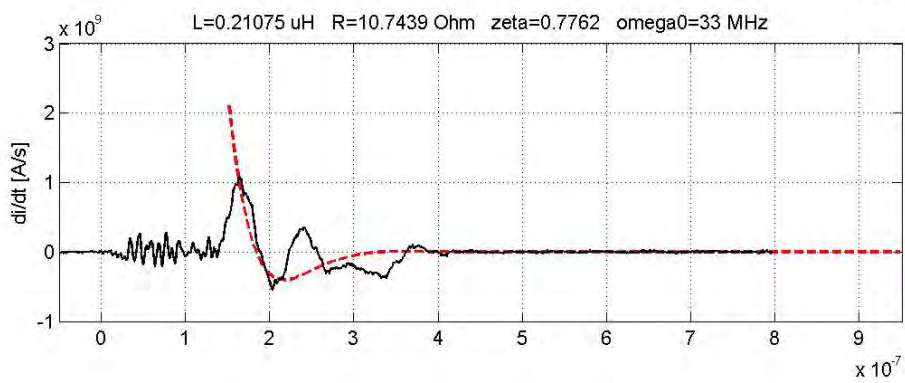
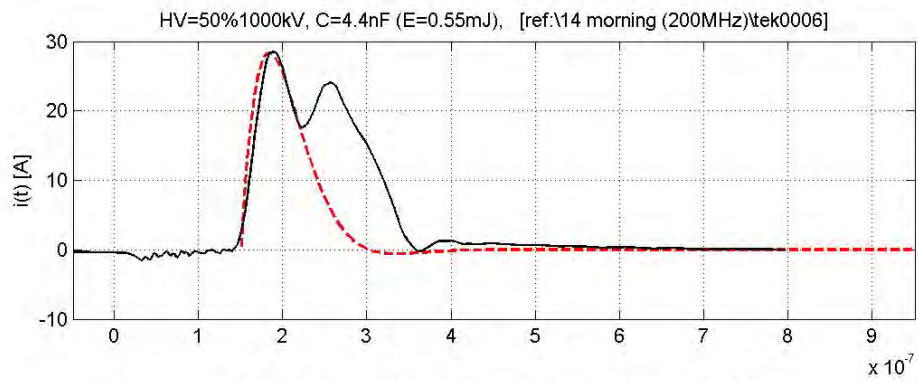


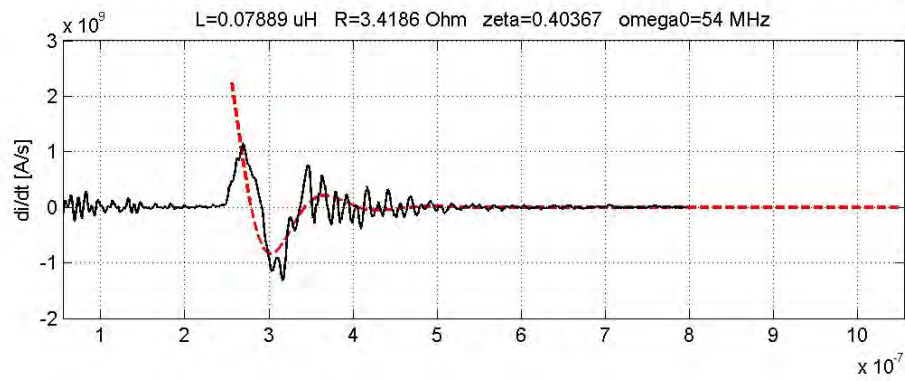
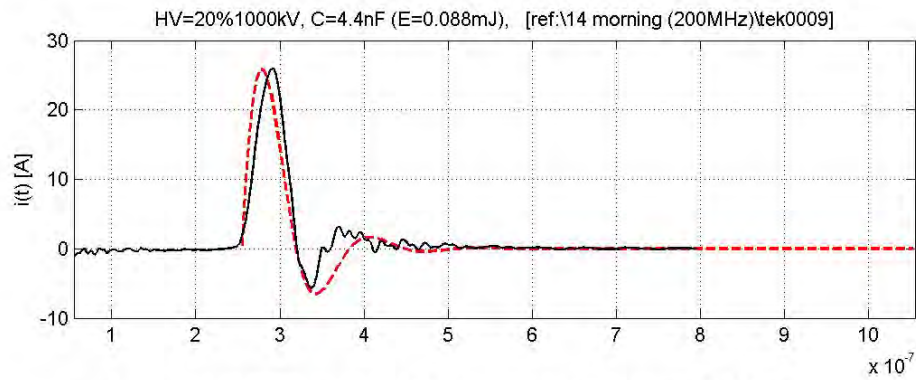
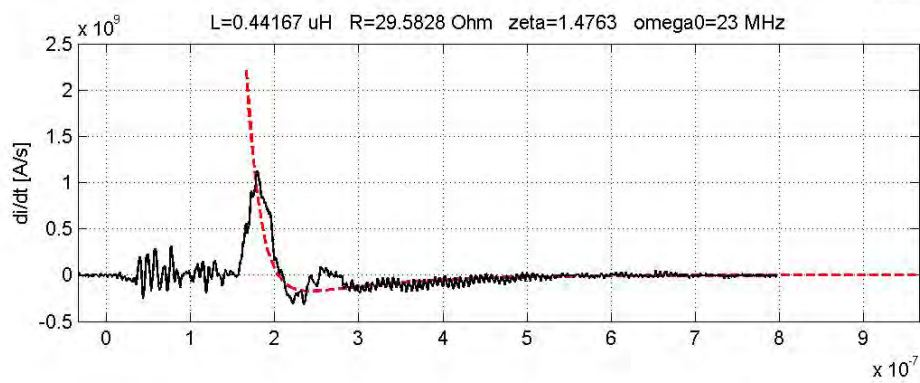
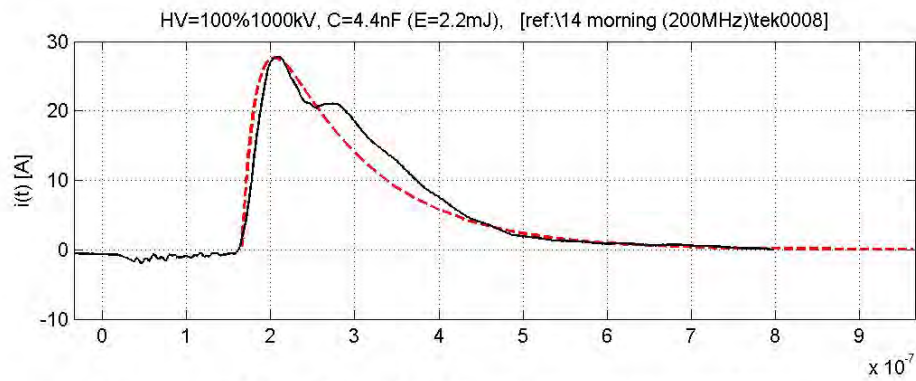
## A.2 RLC Series Modeling Examples

Figure A.12: RLC series modeling of spark plug breakdown for MIC,  $HV = 1kV$









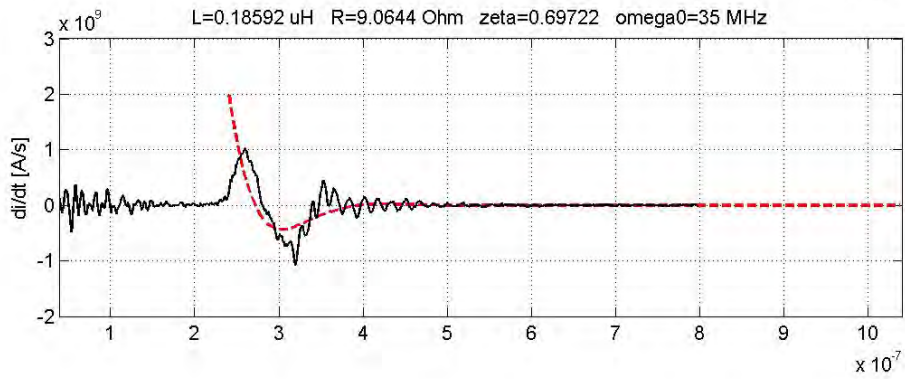
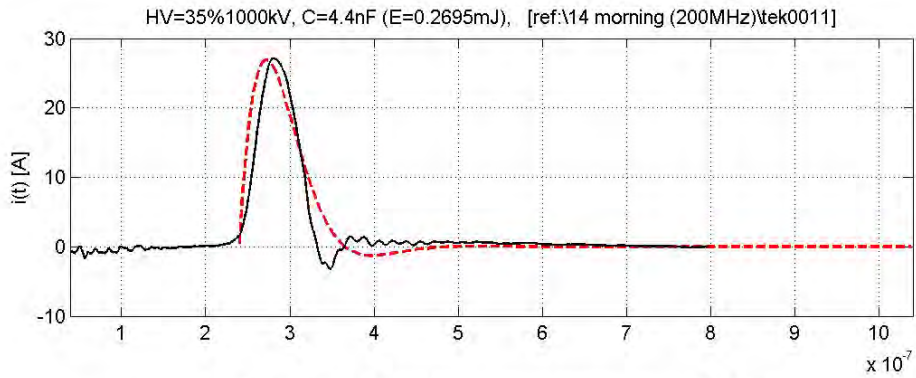
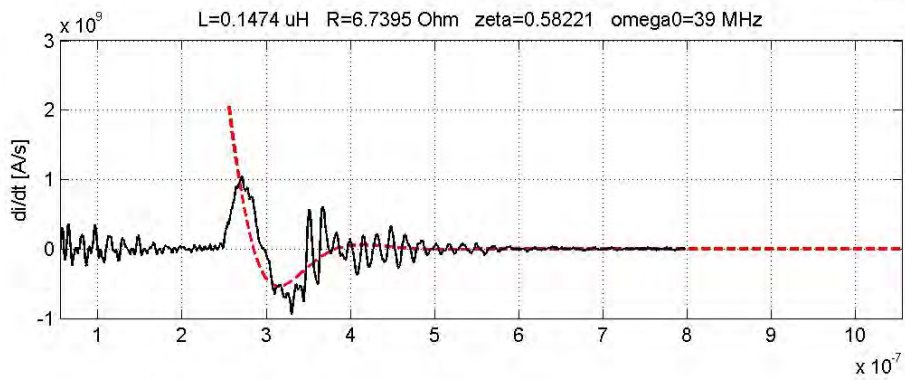
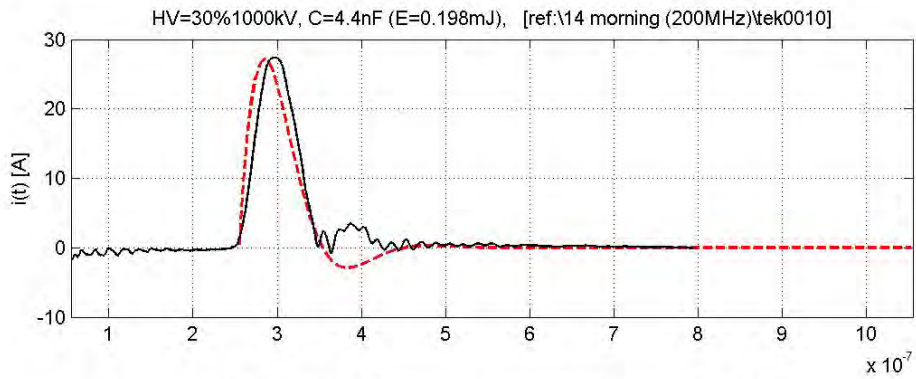
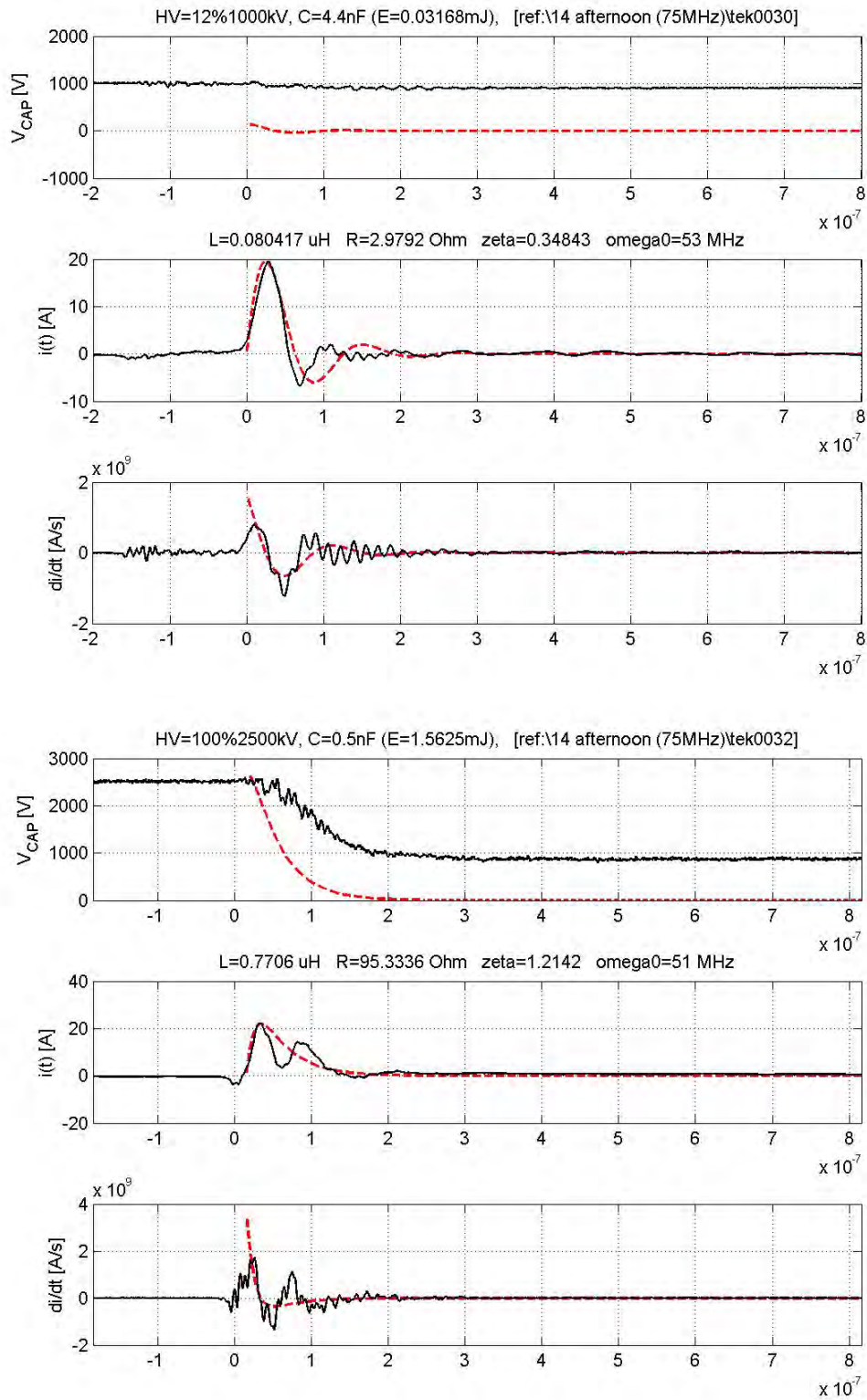
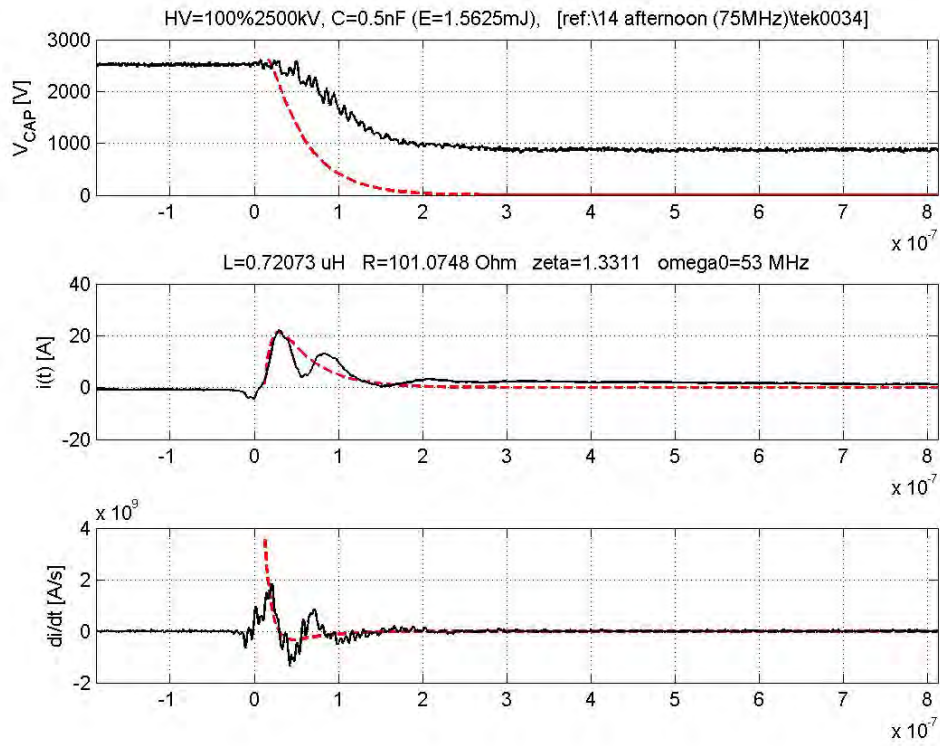
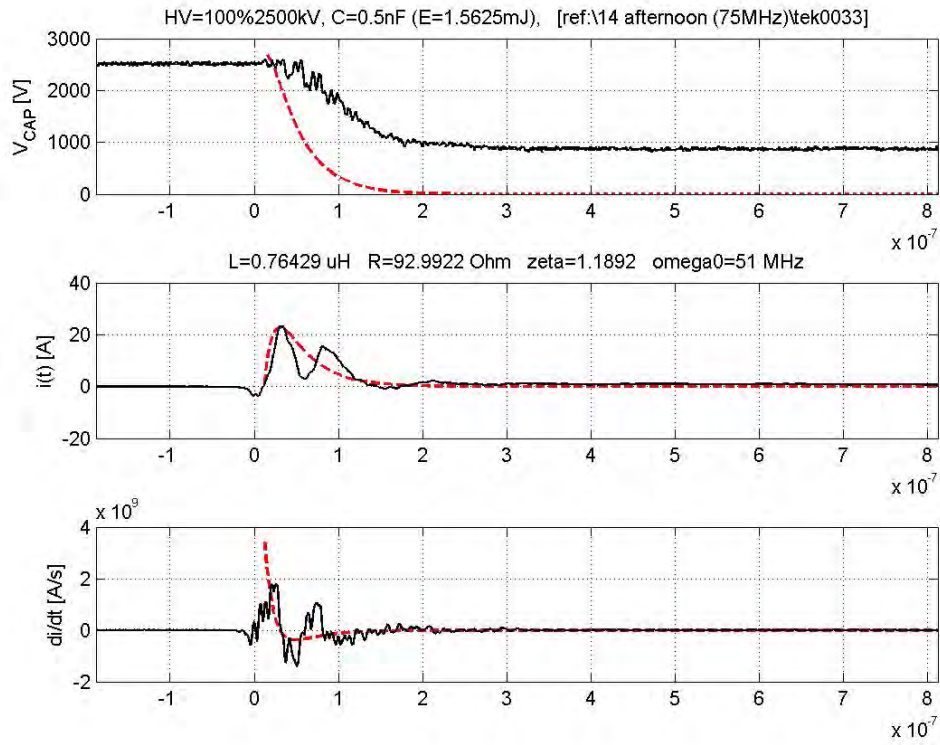


Figure A.13: RLC series modeling of spark plug breakdown for MIC,  $HV = 2.5kV$





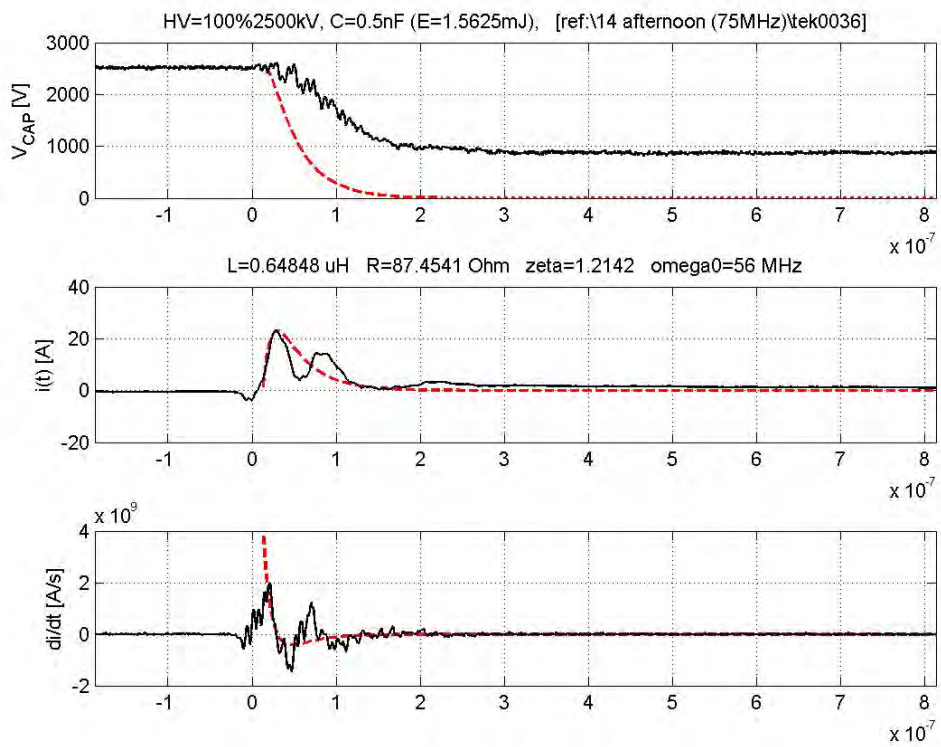
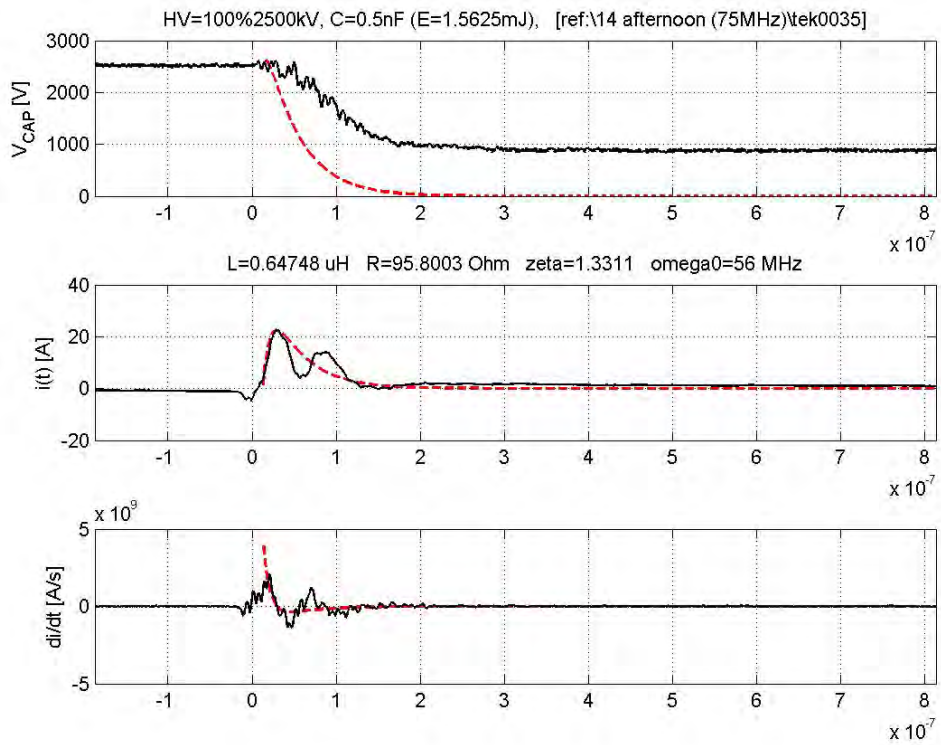
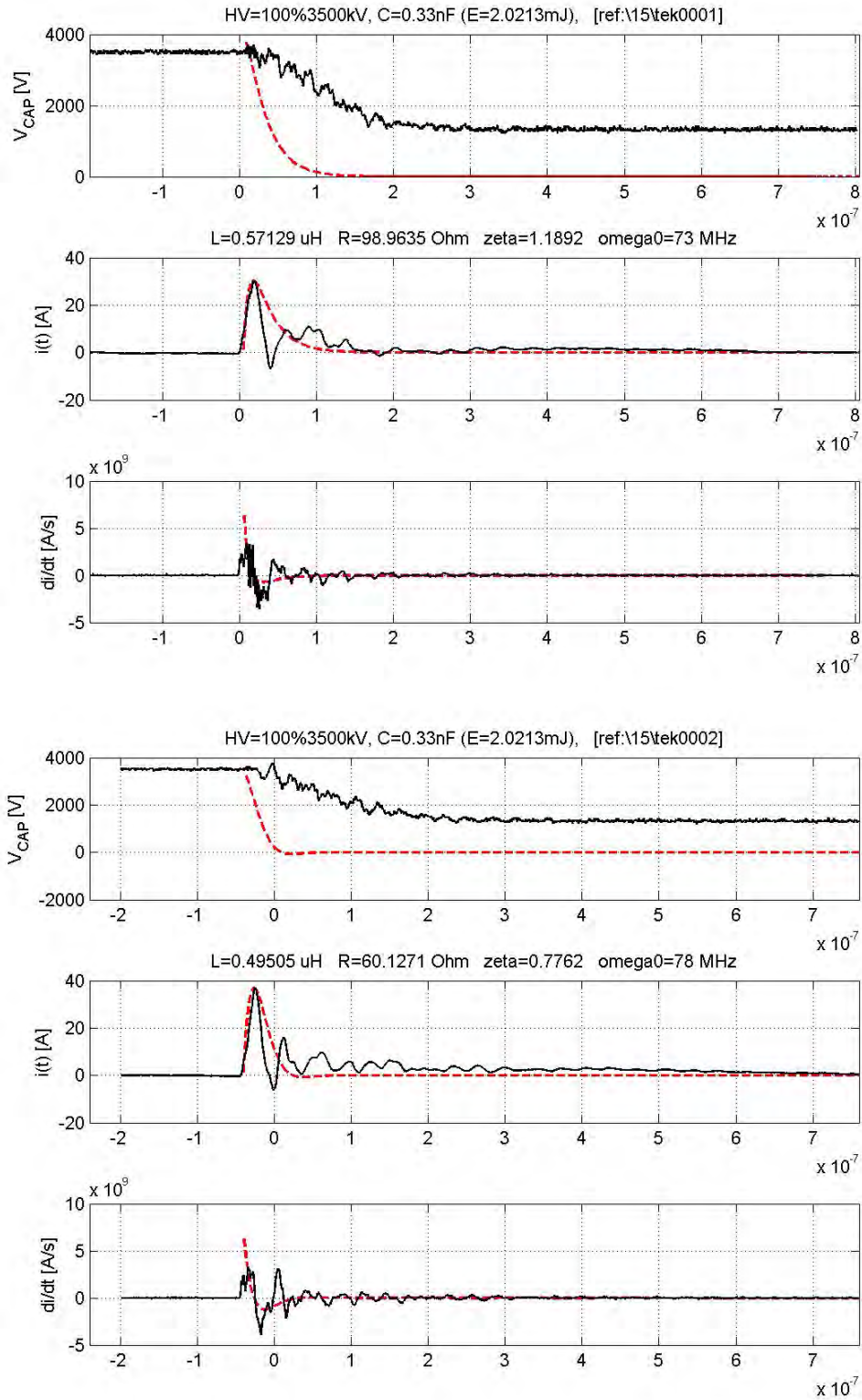
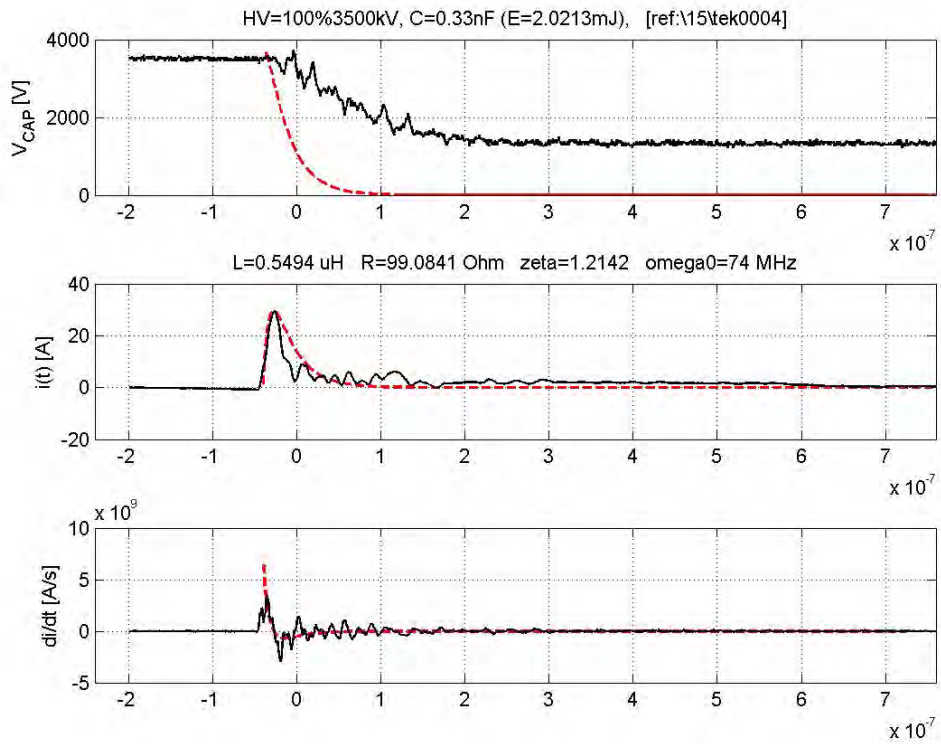
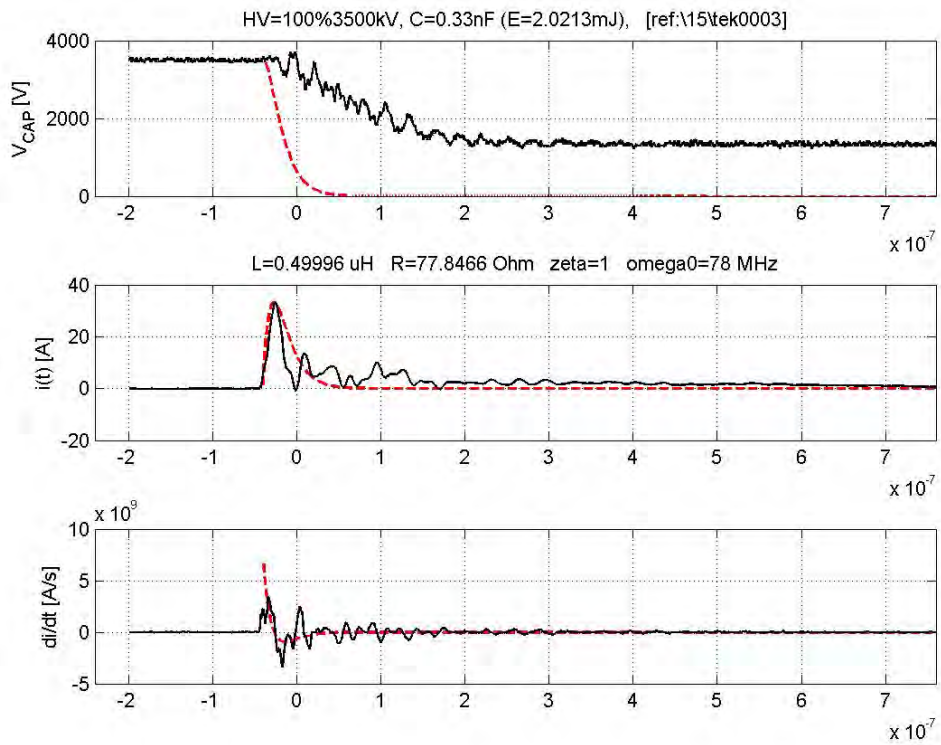


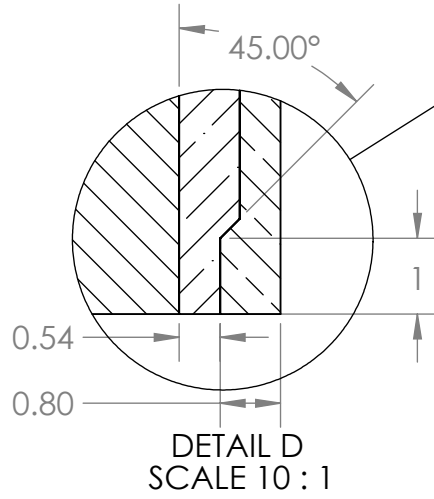
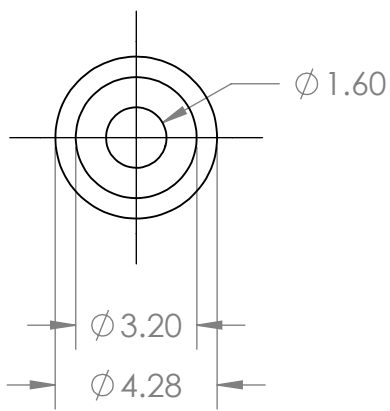
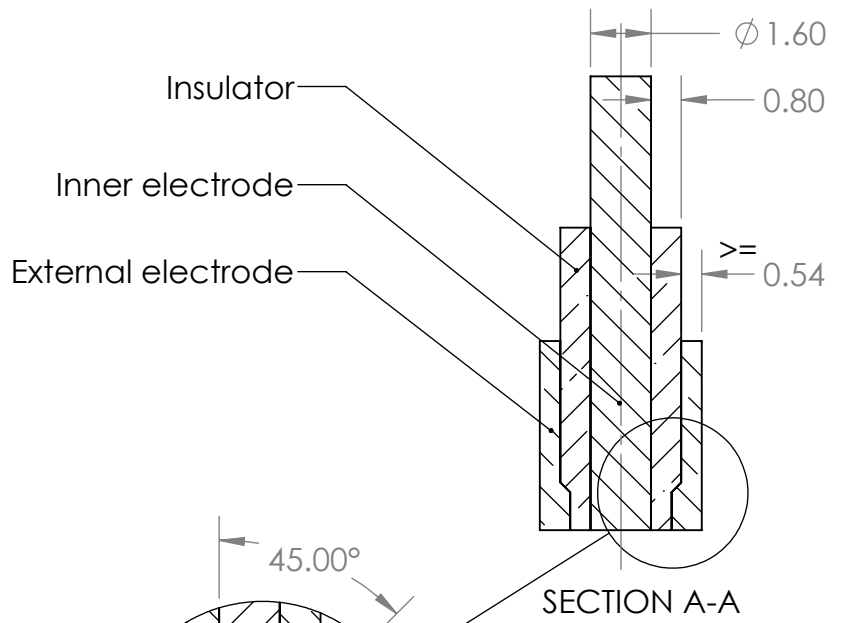
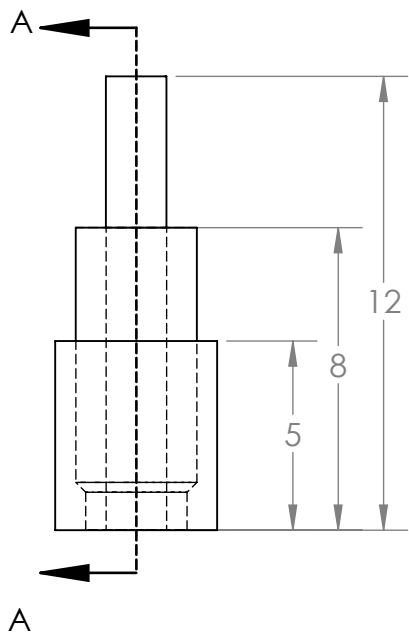
Figure A.14: RLC series modeling of spark plug breakdown for MIC,  $HV = 3.5kV$



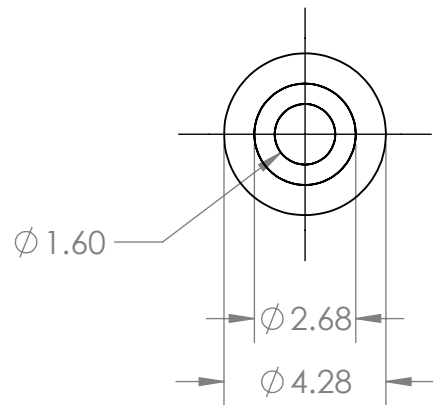
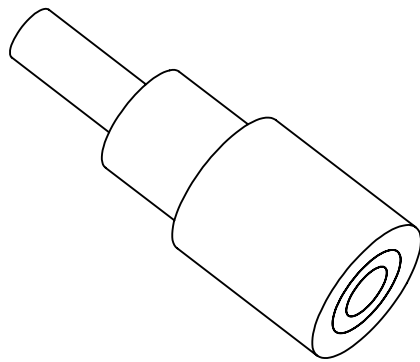


## Appendix B

# Spark Plug Design



Sparkplug top face



UNLESS OTHERWISE SPECIFIED:  
DIMENSIONS ARE IN MILLIMETERS  
SURFACE FINISH:  
TOLERANCES:  
LINEAR:  
ANGULAR:

FINISH:

DEBUR AND  
BREAK SHARP  
EDGES

DO NOT SCALE DRAWING

REVISION 2.0

**Federico Romei**

NAME	SIGNATURE	DATE			
DRAWN					
CHK'D					
APPV'D					
MFG					
Q.A				MATERIAL:	
				WEIGHT:	

TITLE:

DWG NO.

**Sparkplug design**

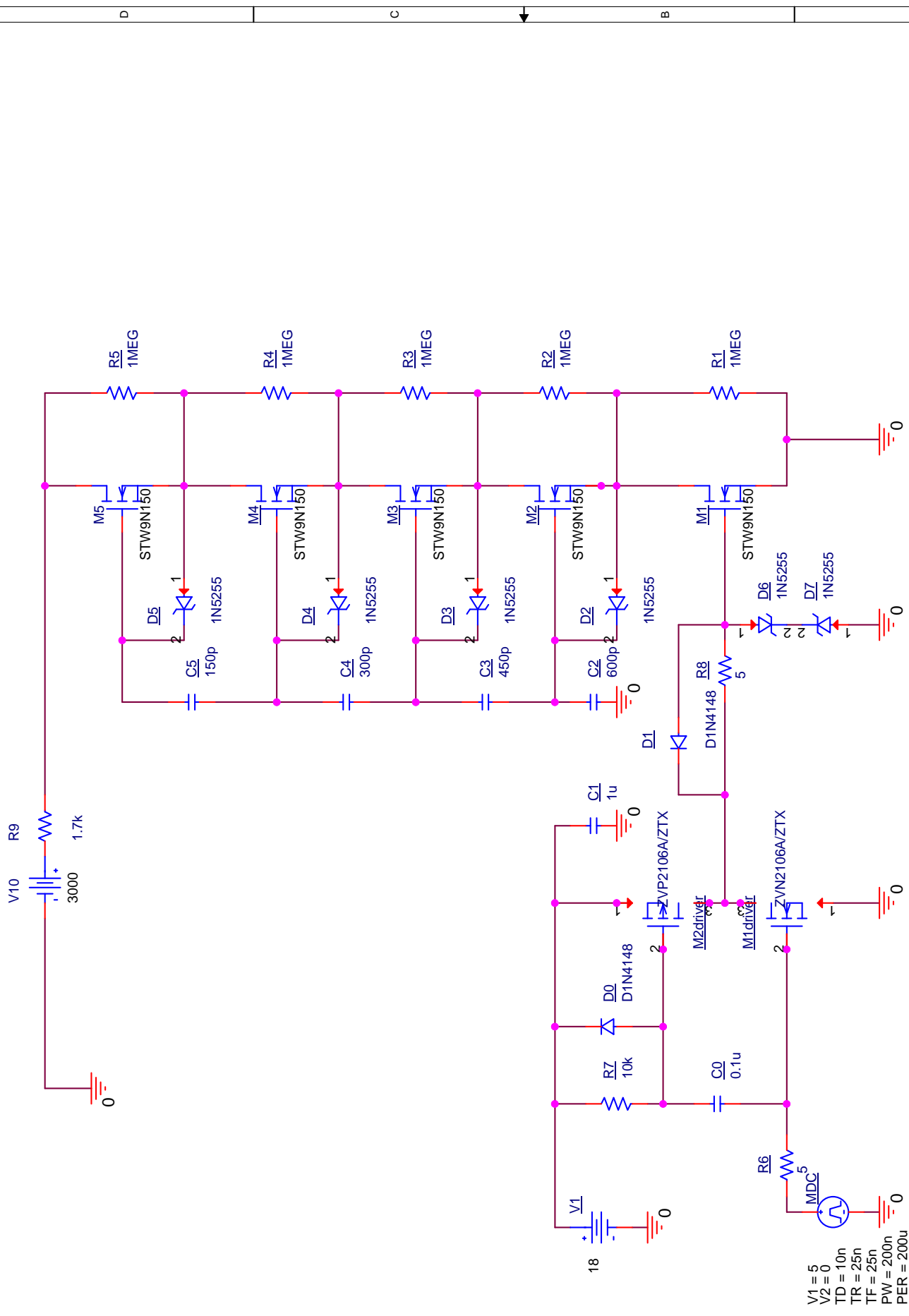
A4

SCALE:5:1

SHEET 1 OF 1

## Appendix C

# MOSFETs Ignition Circuit Design



V1 = 5  
 V2 = 0  
 TD = 10n  
 TR = 25n  
 TF = 25n  
 PW = 200n  
 PER = 200u

Title		Series MOSFETs Power Switch	
Size	A	Document Number	<Doc>
Date:		Sheet	1 of 1
Rev	1.0		

# Bibliography

- [1] S.-M. An and H.-J. Wu. Mdt-2a teflon pulsed plasma thruster. *Journal of Spacecraft and Rockets*, 19(5):385–386, 1982.
- [2] A. Anders, I. G. Brown, MacGill R. A., and M. R. Dickinson. Triggerless triggering of vacuum arcs. *Journal of Physics D: Applied Physics*, 31: 584–587, 1997.
- [3] G. Aston and L. C. Pless. Ignitor plug operation in a pulsed plasma thruster. *Journal of Spacecraft and Rockets*, 19(3):250–256, 1982.
- [4] S. W. Benson, L.A. Arrington, W. A. Hoskins, and N. J. Meckel. Development of a ppt for the eo-1 spacecraft. In *American Institute of Aeronautics and Astronautics*, Los Angeles, California, June 20-24, 1999. 35th Joint Propulsion Conference and Exhibit.
- [5] R. L. Boxman, D. M. Sanders, and P. J. Martin. *Handbook of Vacuum Arc Science and Technology - Fundamentals and Application*. Noyes Publication, Park Ridge, New Jersey, U.S.A., 1995.
- [6] M.E. Brady and G. Aston. Pulsed plasma thruster ignitor plug ignition characteristics. *Journal of Spacecraft and Rockets*, 20(5):450–451, Sept.-Oct. 1983.
- [7] R. L. Burton and P. J. Turchi. Pulsed plasma thruster. *Journal of Propulsion and Power*, 14(5):716–735, 1998.
- [8] L. H. Hess and R. J Baker. Transformerless capacitive coupling of gate signals for series operation of power mos devices. *IEEE Transactions on Power Electronics*, 15(5):923–930, September 2000.

- [9] *CoolMOS Power Transistor*. Infineon technologies AG, Jan. 2008. IPW60R045CP datasheet, Rev. 2.2.
- [10] H. C. Miller and E. J. Edward. The effect of mn/ti surface treatment on voltage holdoff performance of alumina insulator in vacuum. *Journal of Applied Physics*, 49(11):5416–5420, Nov. 1978.
- [11] A. Pourzaki and H. Mirzaee. New high voltage pulse generators. *Recent Patents on Electrical Engineering*, 2(1):65–76, 2009.
- [12] A. I. Rudikov, N. N. Antropov, and G. A. Popov. Pulsed plasma thruster of the erosion type for a geostationary artificial earth satellites. *Acta Astronautica*, 35(9-11):585–590, May-June 1995.
- [13] Sch<sup>’</sup>0nherr. *Investigation of Performances and Plasma Dynamics of the Pulsed Plasma SIMP-LEX*. PhD thesis, The University of Tokyo, 2011.
- [14] P. Shaw and V. Lappas. Modeling of a pulsed plasma thruster. simple design, complex matter. In *Space Propulsion Conference*, San Sebastian, Spain, 2010.
- [15] P. W. Shaw. *Pulsed Plasma Thrusters for Small Satellites*. PhD thesis, University of Surrey, June 2011.
- [16] *N-channel 1500V - very high voltage PowerMESH Power MOSFET*. STMicroelectronics, Jan. 2008. STW9N150 datasheet, Rev. 2.
- [17] *Power MOSFET*. Vishay Siliconix, Mar. 2011. IRFPG50, SiHFPG50, S11-0441-Rev. B.
- [18] R. J. Vondra and K. Thomassen. Flight qualified pulsed electric thruster for satellite control. *Journal of Spacecraft and Rockets*, 11(9):613–617, 1974.
- [19] F. Xue-Zhang and W. Han-Ji. Spark plug for pulsed plasma thruster. In *American Institute of Aeronautics and Astronautics*, Colorado Springs, CO, U.S.A., 1987. 19th International Electric Propulsion Conference.